MATERNAL HEPATIC ADAPTATIONS TO PREGNANCY

by

Shashank Manohar Nambiar

A Dissertation

Submitted to the Faculty of Purdue University

In Partial Fulfillment of the Requirements for the degree of

Doctor of Philosophy

Department of Biology at IUPUI

Indianapolis, Indiana

August 2021

THE PURDUE UNIVERSITY GRADUATE SCHOOL
STATEMENT OF COMMITTEE APPROVAL

Dr. Guoli Dai, Chair

Department of Biology

Dr. Teri Belecky-Adams

Department of Biology

Dr. Anthony Baucum II

Department of Biology

Dr. X. Charlie Dong

Department of Biochemistry and Molecular Biology

Approved by:

Dr. Theodore Cummins

Dedicated to Amma, Achan, Vishaka & Ankita

ACKNOWLEDGMENTS

First and foremost, I would like to thank Dr. Guoli Dai for his mentorship and guidance all throughout my thesis work. I would also like to thank you for your understanding and kindness you have always extended my way as well as the multiple chances to get back on my feet after faltering on my mistakes. If not for your support and encouragement, I may have not been able to make it so far.

Secondly, I would like to thank all the members of my committee namely, Dr. Teri Belecky-Adams, Dr. Charlie Dong, and Dr. A.J. Baucum for all their constructive critiques and even more valuable suggestions on my research project.

Thirdly, I would like to thank all my lab members, Dr. Joonyong Lee, Veronica, Jennifer, Dr. Huaizhou Jiang, and Dr. Yuhong Zou, for teaching me various experimental techniques, answering my numerous queries, and helping me during some of my experiments.

Next, I would like to thank all the staff members of the Biology Department Office namely, Shari, Sue, Laura, Anita, and Leslie for their help with completing various administrative formalities.

Last, but certainly not the least, I would like to thank my family for all their love as well as emotional and moral support during my Ph.D journey.

TABLE OF CONTENTS

LIST OF TABLES 8

LIST OF FIGURES 9

ABBREVIATIONS 10

ABSTRACT 13

CHAPTER 1 INTRODUCTION 15

1.1 The Liver 15

1.2 Pregnancy-induced maternal adaptations 21

1.3 Pregnancy-induced maternal liver adaptations 23

1.4 Endoreplication 24

1.5 Axin2-expressing hepatocytes 27

1.6 Hepatoblasts and their molecular markers 28

1.6.1 CD133 29

1.6.2 Alpha-fetoprotein (AFP) 30

1.6.3 Epithelial cell adhesion molecule (EPCAM) 31

1.7 Hippo signaling pathway 33

CHAPTER 2 MATERIALS AND METHODS 36

2.1 Animal care and "timed pregnancy" generation 36

2.2 Mouse models 36

2.2.1 C57BL/6J mice 36

2.2.2 B6.129X1-*Gt(ROSA)Sor*^{tm1EYFPcos}/J mice 36

2.2.3 B6.129S4-Gt(ROSA)26Sor^{tm1Sor}/J mice 37

2.2.4 B6.129(Cg)-Axin2$^{tm1(cre/ERT2)Rnu}$/J mice 38

2.2.5 YAP1$^{tm1.1Dupa}$/J mice 39

2.2.6 *RS26*$^{floxstopLacZ/\ floxstopLacZ}$; *Axin2*$^{wt/CreERT2}$ mice 40

2.3 Genotyping of mouse strains 40

2.4 5-Bromo-2'-deoxyuridine (BrdU) administration 41

2.5 Adeno-associated virus 8 (AAV8) administration 42
2.6 Tamoxifen (TMX) preparation and administration 42
2.7 Two-thirds partial hepatectomy (2/3rd PHx) 42
2.8 Tissue sample collection 43
2.9 Real-Time Quantitative Polymerase Chain Reaction (RT-qPCR) assay 43
2.10 In-situ hybridization (ISH) 45
2.11 Western blotting assay (WB) 46
2.12 Immunohistochemistry (IHC) 48
2.13 Serum collection and liver function test 51
2.14 Statistical Analysis 52
CHAPTER 3 RESULTS 53
3.1 Maternal organs exhibit differential gravimetric responses during pregnancy 53
3.2 Pregnancy-induced maternal organ growth is accompanied by large-scale cellular DNA synthesis activity 55
3.3 During pregnancy, maternal hepatocytes exhibit endoreplication instead of cell division following completion of S-phase 59
3.4 Examination of the proliferative activity of Axin2^{+} hepatocytes during pregnancy and other physiological conditions 62
3.5 Pregnancy induces dynamic expression of various hepatoblast protein markers in the maternal hepatocytes by post-transcriptional regulation 66
3.6 Metabolic zonation pattern of maternal livers does not undergo overt and permanent changes during the course of gestation 75
3.7 Activity status of hippo pathway remains unchanged during pregnancy-induced maternal liver growth 78
3.8 Effects of maternal hepatocyte specific YAP1 deletion on various aspects of pregnancy-induced maternal liver adaptations and physiology 84
3.8.1 Mid-gestational maternal hepatocyte specific YAP1 deletion does not affect pregnancy-induced maternal liver enlargement 84
3.8.2 Maternal hepatocyte specific YAP1 deletion leads to inhibition of CD133 expression without affecting AFP and EPCAM expression. 88

3.8.3 Mid-gestational maternal hepatocyte specific YAP1 deletion does not affect the maternal hepatic metabolic zonation patterns 92
3.8.4 Effects of YAP1 mid-gestational maternal hepatocyte specific YAP1 deletion on the biosynthetic metabolic processes of the maternal liver 95
CHAPTER 4 DISCUSSION 97
REFERENCES 103

LIST OF TABLES

Table 1: List of primers and primer Sequences used for Polymerase Chain Reaction (PCR)..... 41

Table 2: List of primers used for Real Time Quantitative Polymerase Chain Reaction (RT-qPCR) 45

Table 3: List of primary antibodies (1^{o}Abs), their dilutions, and applications..... 50

Table 4: List of secondary antibodies (2^{o}Abs), their dilutions, and applications 51

LIST OF FIGURES

Figure 1: Types of hepatic cells and their location within the liver. 18

Figure 2: Diagrammatic representation of the hepatic lobule. 19

Figure 3: Diagrammatic representation of hepatic metabolic zonation in the liver. 21

Figure 4: Gravimetric responses of maternal organs during pregnancy. 54

Figure 5: 5-Bromo-2'-deoxyuridine (BrdU) incorporation in maternal organs. 57

Figure 6: Efficacy of hepatocyte labeling, and different cellular units used to quantify and determine maternal hepatocyte proliferation during pregnancy. 61

Figure 7: Determining maternal hepatocyte rate of cell division. 62

Figure 8: Axin2^{+} hepatocytes did not exhibit expansion by cellular proliferation during pregnancy, 2/3rd partial hepatectomy, and homeostasis. 65

Figure 9: Characterization of *Cd133* gene expression in non-pregnant (NP) and pregnant maternal livers. 69

Figure 10: Characterization of *Afp* gene expression in non-pregnant (NP) and pregnant maternal livers. 71

Figure 11: Characterization of *Epcam* gene expression in non-pregnant (NP) and pregnant maternal livers. 73

Figure 12: Changes in the maternal hepatic metabolic zonation patterns during gestation. 77

Figure 13: Activation status of the cytoplasmic components of hippo pathway. 80

Figure 14: Activation status of nuclear components of the hippo pathway. 82

Figure 15: Validation of maternal hepatocyte specific *Yap1* gene deletion. 86

Figure 16: Effect of maternal hepatocyte specific *Yap1* gene deletion on pregnancy-induced maternal organ growth. 87

Figure 17 : Effects of maternal hepatocyte specific *Yap1* gene deletion on expression of YAP1, CD133, AFP, and EPCAM. 90

Figure 18: Effects of mid-gestational maternal hepatocyte specific YAP1 deletion on the maternal hepatic metabolic zonation. 94

Figure 19: Effects of maternal hepatocyte specific *Yap1* gene deletion on liver function test. 96

ABBREVIATIONS

AAV8 – Adeno-associated virus 8

ADAM17 – α-disintegrin and metalloproteinase 17

AFP – Alpha-fetoprotein

ago – Archipalego

ALAS2 – 5'-aminolevulinate synthase 2

ALB – Albumin

ALP – Alkaline phosphatase

ALT – Alanine aminotransferase

AST – Aspartate aminotransferase

BECs – Biliary epithelial cells

BrdU – 5-Bromo-2'-deoxyuridine

CCH – Compensatory cellular hyperplasia

CCH – Compensatory cellular hypertrophy

CCL_4 – Carbon tetrachloride

Cdk – Cyclin-dependent kinase

Chol – Cholesterol

Cki(s) – Cyclin-dependent kinase inhibitor(s)

CPS1 – Carbamoyl-phosphate synthase 1

Cre – Cre-recombinase enzyme

Ctgf – Connective tissue growth factor

CV – Central vein

Cyc – Cyclin

DAB – 3-3'-Diaminobenzamide

EAC – Ehrlich ascite carcinoma

EGFP – Enhanced green fluorescent protein

EGFR – Epithelial growth factor receptor

EKLF1 – Erythroid-Kripple-like factor 1

EPCAM – Epithelial cell adhesion molecule

EpEx – EPCAM extracellular domain fragment

EpICD – EPCAM intracellular domain fragment

ERT2 – Estrogen receptor 2

EYFP – Enhanced yellow fluorescent protein

FFPE – Formalin-fixed paraffin embedded

FHL2 – Four-and-a-half LIM domain protein 2

Gd(s) – Gestation day(s)

Glb – Globulin

Glu – Glucose

GOI – Genes of interest

GS – Glutamine synthetase

H-22 – Hepatoma 22

HCC – Hepatocellular carcinoma

HSCs – Hepatic stellate cells

HTVi – Hydrodynamic tail vein injection

IGF1 – Insulin-like growth factor 1

IHC – Immunohistochemistry

ISH – *In situ* hybridization

KO – Knockout

LacZ – β-galactosidase

LATS1/2 – Large tumor suppressor kinase 1/2

MAPK – Mitogen-activated protein kinase

MOB1A/2A (MOB1/2) – Mps one binding kinase 1A/2A

MST1/2 – Mammalian STE20-like kinase 1/2

mTOR – Mechanistic target of rapamycin

NP – Non-pregnant

PCR – Polymerase chain reaction

PHx – Partial hepatectomy

PT – Portal triad

RAS – Ras GTPase

RIP – Regulated intramembrane proteolysis

RT – Room temperature

RT-qPCR – Real-time quantitative PCR

SAV1 – Salvadore 1

SECs – Sinusoidal endothelial cells

TAZ – Tafazzin

TBG – Thyroxine binding globulin

TEAD – TEA-domain binding protein

TG/Trig - Triglyceride

TGCs – Trophoblast giant cells

TROP2 – Trophoblast cell-surface antigen 2

WB – Western blotting

wt – wildtype

YAP1 – Yes-associated protein 1

ABSTRACT

During gestation, the maternal liver undergoes various adaptive changes to cope with the increasing physiological and metabolic demands from both maternal and fetal compartments. Among these changes are robust growth and changes in transcriptome profile. However, how these events happen, and other aspects of this physiological phenomenon remains unexplored. Therefore, we aimed at further understanding how maternal liver responds to pregnancy. We used BrdU labeling combined with a virus-based tracing approach to quantify the percentage of maternal hepatocytes undergoing DNA synthesis and division over the course of gestation in mice.

We found that ~50% maternal hepatocytes entered S-phase but, unexpectedly, did not undergo cytokinesis. This strongly suggests that maternal hepatocytes in fact undergo endoreplication instead of hyperplasia, as believed previously. Pericentral Axin2^{+} hepatocytes were reported to behave as liver stem cells responsible for liver homeostasis and turnover. We generated an *in vivo* fate-tracing mouse model to monitor the behavior of these cells in the maternal liver. Our results showed that they did not proliferate during pregnancy, homeostasis, and following partial hepatectomy. Curiously, we uncovered that, hepatocytes exhibit developmental phenotypes at mRNA level pre-pregnancy and at both mRNA and protein level during pregnancy. In the non-pregnant state, hepatocytes reserved mRNA expression of liver progenitor marker genes *Cd133* and *Afp*, which are localized in the nuclei, without protein translation. During gestation, maternal hepatocytes displayed cytoplasmic translocation of *Cd133* and *Afp* transcripts, concomitant with corresponding protein expression.

Overall, all maternal hepatocytes became CD133^{+}, and a subset of them express AFP. Additionally, in non-pregnant livers, mRNA of *Epcam*, another liver progenitor marker, was expressed within majority of hepatocytes, whereas its protein was solely translated in the pericentral region. In contrast, by end-gestation, EPCAM protein expression switched to the periportal region. These observations indicate that maternal hepatocytes exhibit heterogeneous developmental phenotypes, partially resembling fetal hepatocytes. It is intriguing why mature hepatocytes dedifferentiate into a progenitor state in response to pregnancy. AFP is considered to be produced primarily from fetal liver and thus is used to evaluate fetal development health.

A potential clinical relevance of our data is that we identified maternal liver as a new source of AFP. The hippo signaling pathway has been shown to potently control liver growth and hepatocyte heterogenicity. Surprisingly, we found that pregnancy neither altered the expression nor activities of the components of this pathway and its effector YAP1/TAZ. This finding indicates that pregnancy-induced maternal liver growth is not driven by hippo-YAP1 pathway. However, we demonstrate that the presence of YAP1 is essential for CD133 protein expression in maternal hepatocytes. Collectively, we revealed that, as pregnancy advances, maternal hepatocytes likely undergo endoreplication and display developmental phenotypes. Mechanistically, YAP1 dictates the expression of CD133, contributing to the pregnancy-dependent phenotypic changes of maternal hepatocytes.

Keywords: Pregnancy, maternal liver, endoreplication, Axin2, developmental phenotypes, and hippo pathway.

CHAPTER 1. INTRODUCTION

1.1 The Liver

The mammalian liver is a multilobed organ that can be identified by its characteristic reddish-brown color. Typically, the liver is located in the abdominal cavity, just beneath the diaphragm, and adjacent to the stomach. In terms of its weight, the liver is the second largest organ and the largest gland of an organism. Functionally, the liver is one of the most versatile and efficient organs. The primary function of the liver is that it serves as a major center for the metabolism of proteins, carbohydrates, and lipids. Due to this, the liver is also known as the "metabolic hub" of an organism. It is the primary storage site of glycogen and, in addition, also serves as a secondary storage site for lipids, various vitamins (A, B12, D) as well as a few minerals [Copper (Cu) and Iron (Fe)] [1, 2]. The liver is responsible for the synthesis of important biological compounds. It produces bile that is critical for the emulsification and digestion of fat. It synthesizes and secretes various plasma proteins such as, albumin (ALB) [3], alpha-fetoprotein (AFP) [4], alanine transaminase (AST), aspartate aminotransferase (ASP) etc., in order to maintain blood homeostasis. Being a gland, the liver synthesizes hormones such as insulin-like growth factor 1 (IGF1) [5], angiotensinogen [6], and thrombopoietin [7]. Lastly, the liver also detoxifies the body by neutralizing most of the unwanted xenobiotic substances ingested by the organism. Considering its functional diversity as well as the nature of its functions, one could conclude that the liver is certainly one of the most, if not the most, important organs in an organism. The liver's functional multiplicity can be attributed to two key factors, that includes, its cellular composition and structural design.

The liver is formed by a diverse group of cells that are together known as the hepatic cells. Specifically, there are five different types of hepatic cells: 1) hepatocytes, 2) biliary epithelial cells (BECs) or cholangiocytes, 3) sinusoidal endothelial cells (SECs), 4) Kupffer cells, and 5) hepatic stellate cells (HSCs). Based on their abundance and the number of functions they perform; hepatic cells are broadly divided into two types: parenchymal and non-parenchymal cells. Parenchymal cells represent the predominant cell type of the liver, in terms of both abundance and functionality, and therefore comprise of only one cell type - the hepatocytes. The hepatocyte is the basic cellular unit of the liver. These cells occupy most of the parenchymal region of the liver tissue (Fig.1). Morphologically, hepatocytes are shaped like an irregular hexagon, have a cross-sectional

thickness of 25-30µm, and displace a volume of 5000-6000µm^3 [8]. Hepatocyte's make-up approximately 60% of the total liver mass [9]. A majority of the metabolic and biosynthetic functions, discussed earlier, are performed by the hepatocytes. Non-parenchymal cells represent the auxiliary cell type of the liver and comprise the remaining hepatic cells, that includes, BECs, SECs, Kupffer cells, and HSCs. Despite being an auxiliary component of the liver, non-parenchymal cells are equally important to the structural architecture and functioning of the organ. BECs, also referred to as cholangiocytes, are cells that form the bile ducts in the liver (Fig. 1). These cells contribute to 1% of the total hepatic cell population [10]. BECs help in the formation and transport of bile [11]; and to enable this, the luminal surface of their plasma membrane consists of microvilli and stereocilia [12]. SECs are specialized endothelial cells that line the walls of the hepatic sinusoids (Fig. 1). Hepatic sinusoids are narrow passageways that facilitate the passage of blood from the portal system, through the parenchyma, and into the central vein (described below). SECs comprise roughly 3% of the total liver mass [9]. SECs are specialized endothelial cells because their plasma membrane is highly fenestrated (small openings) [13, 14]. These fenestrations provide hepatocytes access to the blood while simultaneously filtering out the blood cells and large effete particles (cell debris and large molecular complexes). Furthermore, the pinocytic nature of SECs also help clear the incoming blood of various effete particles, albeit only to a limited extent. Kupffer cells are commonly referred to as the resident macrophages of the liver. These cells constitute approximately 2% of the total liver mass [15]. Kupffer cells reside within the hepatic sinusoids and in close proximity to the SECs (Fig. 1). Being phagocytic in nature, the main function of the Kupffer cells is to phagocytize the majority of unwanted particulate matter present in the blood. This includes materials such as cellular (red and white blood cells, hepatocytes, etc.) and bacterial debris, large molecular complexes, and other colloidal particles [16]. The fourth and last hepatic non-parenchymal cell type is the HSC. HSCs get their name due to the presence of multiple, long cell body processes that gives them a characteristic star-shaped appearance. These cells are located in small spaces created between the hepatic sinusoids and adjoining hepatocytes formally called the "Space of Disse" (Fig. 1). HSCs make up only 1.5% of total hepatic mass and their primary function is to metabolize and store vitamin A [9, 17]. The hepatic parenchymal and non-parenchymal cells work in close coordination with each other to achieve the liver's fullest functional potential.

In addition to its cellular versatility, another important factor responsible for the liver's functional diversity and efficiency is its unique structural design. Despite there being slight differences in opinion on the specific details, the most widely accepted model describing the liver's structural architecture is the "hepatic lobule" model (Fig. 2). According to this model, the entire three-dimensional mass of the liver is essentially made of an arrangement of hexagonally shaped columns that are termed the hepatic lobules. Hence, the hepatic lobule is the basic structural unit of the liver. The hepatic lobule, in turn, is made up of three important components: the central vein (CV), the hepatic parenchymal region, and the portal triad (PT) (Fig. 2). The CV is a blood vessel that is located at the center of the hepatic lobule and is formed by the endothelial cells. Radiating out from the central vein towards the periphery of the hepatic lobule are files of hepatocytes in an arrangement crudely resembling the 'spokes of a wheel'. Each file of hepatocytes ('spoke') is made of several hepatocytes that are packed tightly, one behind the other, in a line. The narrow gap between two adjacent files of hepatocytes forms the hepatic sinusoid which acts as a conduit for blood to drain from the portal triads into the central vein. Hepatic sinusoids are formed by the SECs. The region between the central vein and the periphery of the hepatic lobule, predominantly composed of hepatocytes (parenchymal cells) and the sinusoids, is called the - parenchymal region. The PT's are located at, and represent, the vertices of the hexagonal hepatic lobule. Thus, each hepatic lobule comprises of six PTs. The PT comprises of three structures: the hepatic artery; the hepatic vein; and the bile duct. The hepatic artery brings oxygenated blood from the heart to the liver. Hepatic veins are part of the hepatic portal system and brings nutrient-rich blood from the gastrointestinal system. The hepatic artery and vein are both formed from endothelial cells as well. The bile duct acts as a passageway to transport bile to the gall bladder and is lined by BECs.

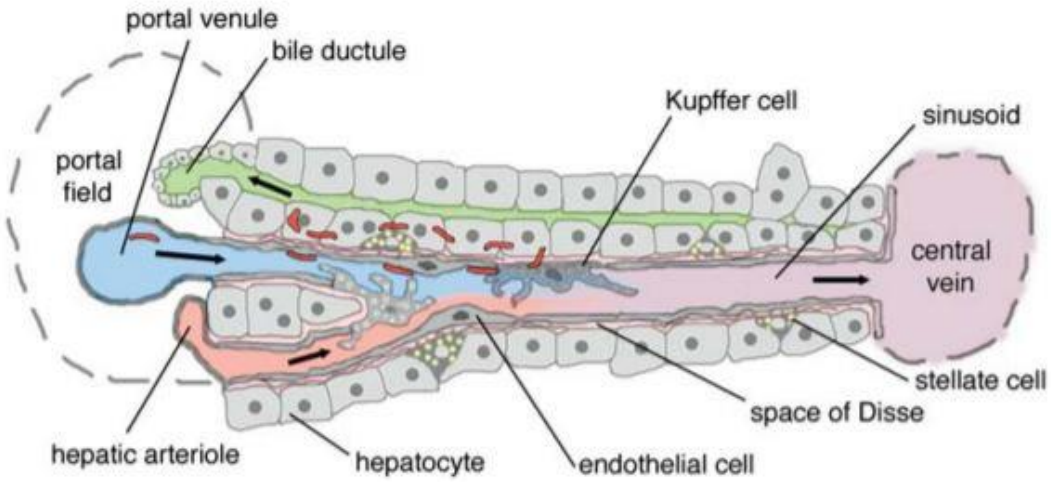

Figure 1: Types of hepatic cells and their location within the liver.

The above figure represents a cross-sectional view of the hepatic lobule, along the portal triad-to-central vein axis, to highlight the identity and location of the major hepatic cells of the liver. The liver is made of five major cell types: hepatocytes; biliary epithelial cells (BECs); endothelial cells; hepatic stellate cells; and Kupffer cells. Hepatocytes are the primary epithelial cell type (in terms of number and function) that occupies most of the parenchymal region of the liver. BECs, also known as cholangiocytes, are the secondary epithelial cell type of the liver. BECs are responsible for the formation of the bile ducts. Endothelial cells line the walls of the various blood vessels (hepatic artery, hepatic portal vein, and central vein) and the sinusoidal spaces of the liver. Hepatic stellate cells are star-shaped cells that are located in the regions between the hepatic sinusoids and the rows of hepatocytes, called the "Space of Disse". Kupffer cells are the resident macrophage of the liver and are mostly found inside the sinusoids. Picture credit: Frevert et. al (2005) [18].

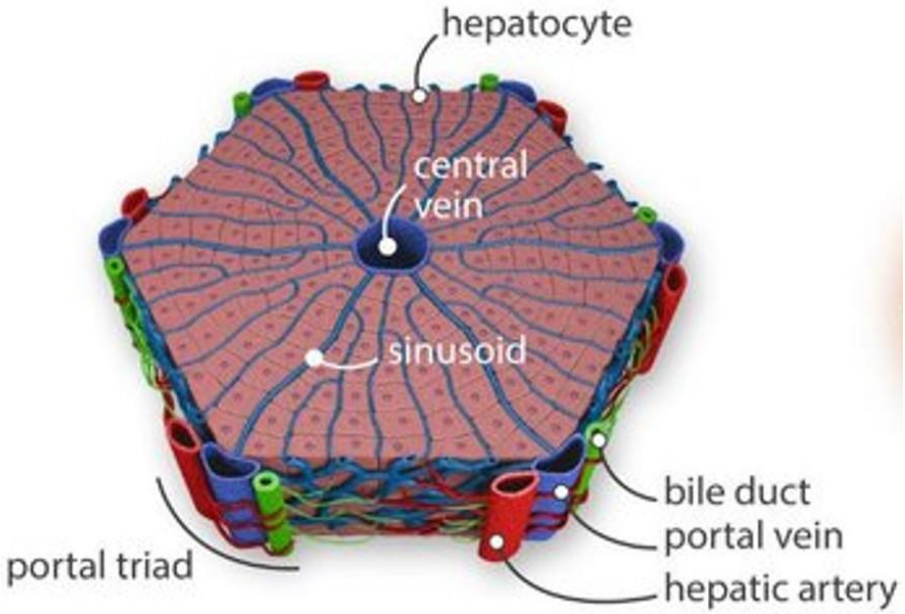

Figure 2: Diagrammatic representation of the hepatic lobule.

The hepatic lobule is a multi-component, hexagonally shaped column and is regarded as the basic "structural unit" of the liver. The entire liver is made of a tightly packed arrangement of multiple hepatic lobules. Each hepatic lobule is comprised of three main components that includes, the portal triad, the parenchymal region, and the central vein. The portal triad represents the vertices of the hexagonal hepatic lobule and in turn is comprised of the hepatic artery, the hepatic portal vein, and the bile duct. The parenchymal region represents the space between the portal triads and the central vein and is comprised of hepatocytes and the hepatic sinusoids. Lastly, the central vein is located at the center of the hepatic lobule and collects the blood that unidirectionally drains from the hepatic artery and portal veins of the portal triad and through the sinusoids. Picture credit: Leo A van Gruvensven (2017) [19].

Hepatic metabolic zonation is a unique phenomenon exhibited by the liver and that can be attributed to its structural design (Fig. 3). The hepatic metabolic zonation can be described as the regional sub-division of the hepatic lobule along the PT-to-CV (porto-central) axis. Each regional subunit is termed as a 'Zone' and the hepatic lobule is divided into three such zones. The regions surrounding the PT and CV are designated as Zone 1 (periportal) and Zone 2 (pericentral), respectively; and the remaining, mid-parenchymal region between Zones-1 and 3 is designated as Zone 2. In addition to the physical space, each zone is also represented by the sub-population of hepatocytes that populates the region and are accordingly designated as Zone 1, Zone 2, and Zone 3 hepatocytes. The regional sub-division of the hepatic lobule is based on the organically occurring separation of the myriad of hepatic metabolic processes along the porto-central axis. For example,

metabolic processes such as oxidative phosphorylation, gluconeogenesis, and ureagenesis occurs more efficiently within the Zone 1 region and decreases along the porto-central axis, whereas processes such as glycolysis and lipogenesis are carried out more efficiently within the Zone 3 region [20, 21]. Furthermore, the separation of the metabolic processes in turn is a manifestation of the zonal heterogeneity of hepatocytes that arises because of the unidirectional flow of blood from the PT to the CV. It has been shown that the unidirectional blood flow along the porto-central axis results in a decreasing concentration gradient of various key factors such as oxygen, nutrient substrates, and hormones across the hepatic lobule[20, 21]. This is believed to create unique microenvironments, with subtle concentration differences of various factors, between each zone that in turn facilitates and predisposes specific zonal hepatocytes towards a specific set of metabolic processes. Consequently, each zonal sub-population of hepatocytes exhibit and express certain characteristic metabolic protein markers that reflects their metabolic capacities. For instance, E-cadherin is a well-known Zone 1 hepatocyte marker. Arginase 1 and Carbamoyl-phosphate synthase 1 (CPS1) are well known markers of Zone 1 and Zone 2 hepatocytes. CYP1A2, CYP2E1, and glutamine synthetase (GS) are Zone 3 hepatocyte markers [22].

Due to its functional importance and multiplicity as well as its innate regenerative ability, the liver is one of the most well studied organs. However, one aspect of liver physiology that still remains to be studied is the physiology of the liver during pregnancy. Therefore, in this research project, we try to further elucidate the various changes that occur in the maternal liver during the course of pregnancy.

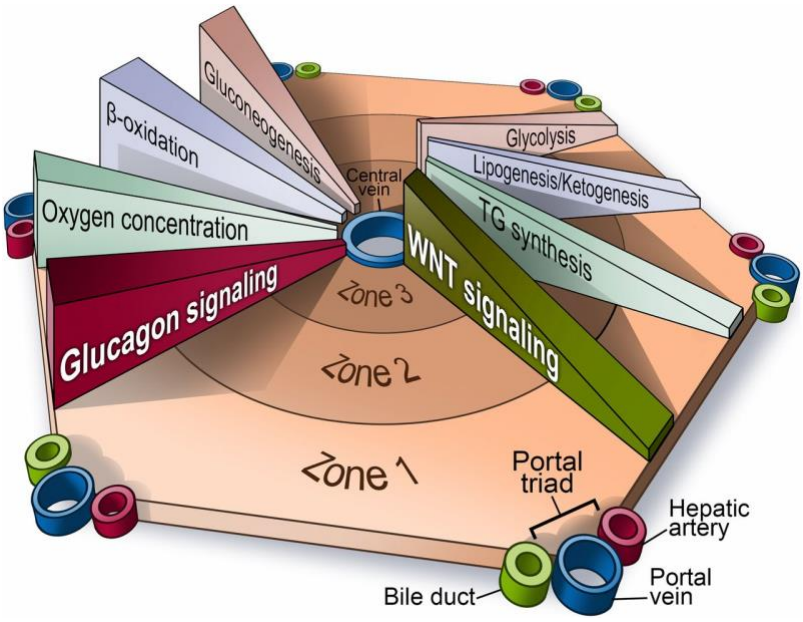

Figure 3: Diagrammatic representation of hepatic metabolic zonation in the liver.

Hepatic metabolic zonation is the regional sub-division of the hepatic lobule on the basis of the distribution and preferential allocation of the various hepatic metabolic processes. The region around the portal triad is designated as Zone 1. The region around the central vein is Zone 3. And the region between Zone 1 and Zone 3 is designated as Zone 2. Hepatic metabolic zonation is a consequence of the unidirectional blood flow that occurs between the portal triad-to-central vein axis (porto-central axis) and leads to a decreasing oxygen concentration across the axis. The decreasing oxygen gradient leads to hepatocyte heterogeneity between the different zonal regions. The hepatocyte heterogeneity is manifested in the propensity of different zonal hepatocyte sub-populations to carry different metabolic processes with varying rates of efficiency. Metabolic processes such as gluconeogenesis, β-oxidation, and glucagon signaling are carried out with decreasing efficiency along the porto-central axis whereas, processes such as glycolysis, lipogenesis/ketogenesis, and triglyceride (TG) synthesis occurs with increasing efficiency along the porto-central axis. The decreasing signaling strength of the Wnt-signaling pathway along the central vein-to-portal triad axis is one of the key factors responsible for the maintenance of hepatic metabolic zonation in the liver. Picture credit: Richard Howdy (Visually Medical) [23].

1.2 Pregnancy-induced maternal adaptations

During the course of pregnancy, the metabolic and physiological demands on various maternal organs increases dramatically. The increased demands result from the fact that in addition to meeting her own day-to-day nutritional and metabolic needs, the pregnant mother must also cater to the needs of her developing fetus(es). Therefore, in order to meet the day-to-day requirements of the pregnant mother and to facilitate the timely growth and development of her fetus(es), various maternal organs exhibit pregnancy-induced maternal adaptations. The nature and scope of the adaptations are not uniform and varies from one maternal organ to the other.

Most of our understanding of pregnancy-induced maternal adaptations comes from studies conducted primarily in rodents [24-33], and to a lesser extent in humans [34-38]. In rodents, pregnancy-induced maternal adaptations have been shown to be exhibited by the maternal brain [24], pancreas [25-27], heart [28, 29], spleen [30], and liver [31-33]. In the maternal brain of mice, studies have shown that pregnancy induces increased neurogenesis of olfactory interneurons in the maternal olfactory lobe [24]. In the mouse maternal pancreas, the period of late pregnancy stimulates an increase in the beta-cell mass by means of both, beta-cell hypertrophy (cell size increase) and hyperplasia (cell proliferation) [25-27]. It is well known that during gestation the maternal blood volume increases significantly [39, 40]. In order to cope with the resulting hemodynamic stresses, the mouse maternal heart is shown to exhibit "pregnancy-related cardiac hypertrophy" [28, 29]. "Pregnancy-related cardiac hypertrophy" refers to the increase in the maternal heart size during pregnancy and is a result of cardiomyocyte hypertrophy. In addition to the maternal heart, increase in blood volume also stimulates organ growth in the maternal spleen. The size of the rodent maternal spleen increases by almost three times (3X) that of its non-pregnant state during the second half of pregnancy. Furthermore, pregnancy also leads to an increased expression of several genes such as, erythroid-Krippel-like factor (EKLF), 5'-aminolevulinate synthase 2 (ALAS2), and β-major globin, that are involved in hemoglobin formation in the maternal spleen [30]. Another maternal organ that also undergoes dramatic changes in gene expression as well as pregnancy-induced organ enlargement is the liver. Comparison of pregnancy-induced maternal adaptations between humans and rodents has shown that many adaptive changes, for example the ones seen in the pancreas, heart, and spleen, are similar in both group of mammals. Due to this reason, pregnancy in rodents serves as a great animal model system to study pregnancy-induced maternal adaptations.

Despite the studies conducted so far, the area of pregnancy-induced maternal adaptations still remains mostly unexplored and underappreciated. Majority of the studies conducted in this field are observational and we are yet to fully understand the exact cellular and molecular mechanisms that orchestrate and regulate these adaptive changes. In our opinion, the realization that pregnancy-induces dramatic changes in various maternal organ systems raises many important questions that could have profound implications on our understanding of the female biology. For example, one important question that arises from our cognizance of the pregnancy-induced maternal adaptations pertains to whether these changes are permanent or temporary in nature? In a scenario where these

changes were permanent would imply that pregnancy could lead to various post-pregnancy sexual dimorphisms between the female and male sex. One area where this knowledge would be critical would be in designing therapeutic strategies and drugs.

1.3 Pregnancy-induced maternal liver adaptations

Pregnancy-induced maternal liver adaptations refer to the set of changes adopted specifically by the maternal liver during pregnancy. These adaptations allow the maternal liver to cope with the increased physiological demands and stresses of gestation. The idea that the maternal liver undergoes adaptive changes during pregnancy was first discovered in 1944 [41]. Most of our understanding of pregnancy-induced maternal liver adaptations comes from studies conducted primarily in rodents and to a lesser extent in humans, specifically, during the biochemical analysis of the maternal blood. But despite being discovered more that eighty years ago, this aspect of pregnancy-related liver biology still remains mostly unexplored.

Studies until now have shown that the maternal liver undertakes three main adaptive changes during the course of pregnancy. The first adaptive change is the increased biosynthetic and metabolic output of the maternal liver. During gestation, the volume of the maternal blood increases significantly. But, despite an increase in maternal blood volume, the concentration of most serum factors and metabolites synthesized by the liver either remains unchanged or increases compared to their levels in non-pregnant (NP) individuals. This strongly suggests that biosynthetic output of the maternal liver increases as a result of pregnancy. The second adaptive change is the dramatic differences in gene-expression patterns in pregnant maternal livers. Based on Illumina sequencing and DNA-microarray analysis, it has been found that the gene-expression pattern of maternal livers, at various gestation days (Gds), are markedly different from their NP counterparts [31, 33, 42, 43]. For example, compared to the NP livers, 115 and 123 genes were differentially expressed in Gd14 and Gd18 maternal livers, respectively [33]. Pathway analysis of the differentially expressed genes showed that many of these genes were associated with the metabolism of different nutritional molecules, embryonic development, cancer, and metabolic diseases [33]. But what is still not known is whether the differentially expressed genes returns to their NP state expression levels at the end of pregnancy. The third, and perhaps most striking adaptive change of the maternal liver, is the phenomenon of pregnancy-induced maternal liver

growth. Pregnancy-induced maternal liver growth can be defined as the robust but transient enlargement of the maternal liver during the course of gestation. In rodents, it has been observed that the total weight of the maternal liver increases to almost double that of the NP liver, in the second half of pregnancy [32, 33, 42]. Moreover, in addition to the total liver weight, the liver-to-body weight ratio also has been found to increase from ~4%, in the NP condition, to ~5% on Gd15, which provides further evidence to the idea that during pregnancy the functional capacity of the maternal liver increases. Studies conducted to determine the factors responsible for pregnancy-induced maternal liver growth revealed that this phenomenon was an outcome of both maternal hepatocyte hypertrophy and hyperplasia. However, while there is a strong consensus on the contribution of maternal hepatocyte hypertrophy towards maternal liver enlargement, the contribution of maternal hepatocyte hyperplasia remains contested [32, 33, 42].

In this report, we try to further elucidate the cellular and molecular mechanisms regulating pregnancy-induced maternal liver adaptations. Specifically, we focus on addressing three important aspects. First, using a direct experimental approach, we try to determine the proportion of maternal hepatocytes undergoing hyperplasia (cell division) during maternal liver enlargement. Second, we characterized the expression of AFP, CD133, and epithelial cell adhesion molecule (EPCAM) in the maternal liver. Pilot studies revealed that the maternal liver exhibits a dynamic expression of the three proteins during gestation and in the context of the liver, AFP, CD133, and EPCAM are important molecular markers of multi-potent hepatic stem cells called - Hepatoblasts. And third, we try to determine if the hippo signaling pathway is involved in regulating maternal liver growth. One of the main functions of the hippo pathway is to modulate organ size increase via cell proliferation and aberrations of the hippo pathway in the liver leads to uncontrolled cell proliferation and eventual development of hepatocellular carcinomas (HCCs).

1.4 Endoreplication

Endoreplication can be defined as a process by which a cell increases its ploidy number or genomic DNA content when subjected to an appropriate stimulus. These stimuli could either be natural, homeostatic, developmental signals, or signals produced under adverse environmental or physiological conditions. This process is particularly seen within the context of multicellular organisms that are made up of a multitude of different cell types. In the case of various

multicellular organisms, it has been commonly observed that certain types of cells, present in specific tissues, maintain a greater ploidy number than that of the organism itself. For example, ploidy number of human beings is diploid (2N). However, the hepatocytes that form the human liver exhibit a range of ploidy from some hepatocytes being diploid (2N), tetraploid (4N), hexaploid (6N), and in lesser frequency, octaploid (8N) [44]. The process by which cells increase their ploidy number is called endoreplication. The cells undergoing endoreplication do so by going through a special type of cell cycle, known as the endocycle. While the mitotic cell cycle comprises four phases namely, G1, S, G2, and M-phase, the endocycle comprises just the G-phase and the S-phase. As a result, a cell undergoing the endocycle undergoes one or more rounds of DNA replication (S-phase) without cell division (M-phase), hence resulting in endoreplication [45, 46].

Endoreplication is employed by different cells and tissues for a variety of functional reasons. It has been observed that cells that are involved in the large-scale production of various biomolecules, commonly exhibit endoreplication. By increasing their ploidy number through endoreplication, these cells in turn increase the copy number of the genes that are directly or indirectly involved in the synthesis of the particular biological substance(s). The ovarian follicular cells within the *Drosophila* egg [47-49] and the salivary gland cells of the *Drosophila* larva [50-52] are examples of such type of cells. In order to accommodate the extra chromosomal copies, cells that undergo endoreplication assume a larger size in comparison to their diploid counterparts. As a result, cells that are tasked with storage of various nutritional substances such as the cells of the endosperm tissue in developing plant embryos exhibit endoreplication [53-55]. Endoreplication is used by certain types of cells for their homeostatic development. For example, megakaryocytes [56, 57] and trophoblast giant cells (TGCs) (in mammals) [58] become terminally differentiated and demarcate their final phase of development by undergoing endoreplication and becoming polyploid. Endoreplication is also used as a mechanism of tissue repair and regeneration following an injury. The cells of certain tissues have evolved to undergo endoreplication to promptly increase their cell size (hypertrophy) in order to rapidly recover the lost tissue mass as a result of an injury. This process is called “compensatory cellular hypertrophy” (CCH). An example of CCH is seen in the case of hepatocytes following partial hepatectomy (PHx), a surgical procedure involving removal of three of the five liver lobes in rodents [59]. However, although most attributes of endoreplication are found to be advantageous and beneficial, endoreplication could also lead to certain undesirable consequences. The genomic instability caused within

endocycling cells [60] along with their susceptibility to incur chromosomal aberrations [61, 62] is believed to predispose cells undergoing endoreplication to eventually become cancerous [46].

Perhaps because of its involvement in tissue repair and regeneration as well as its role as a potential cancer-causing factor, the regulatory mechanisms underlying endoreplication have been widely studied and well characterized. The progression of cells into endoreplication takes place in two phases. The first phase involves the transition of the cells from the mitotic cell cycle to the endocycle. This transition phase is most commonly regulated by the activation of the notch signal transduction pathway within the cells destined for endoreplication [47, 63, 64]. Dysregulation of notch signaling pathway in follicle cells of drosophila and mouse TGCs resulted in failure of the cells to execute endoreplication. The activation of notch pathway would eventually culminate in the appropriate transcriptional activation or repression of various genes required for the endocycle. In addition to the notch pathway, more recent studies have shown that the mechanistic target of rapamycin (mTOR) [65] and epithelial growth factor receptor/RAS/mitogen-activated protein kinase (EGFR/RAS/MAPK) pathways [66] also induced endoreplication in the cells of the fat body and intestine of drosophila, respectively. The second phase entails the progression and maintenance of the endocycle. This is achieved through the repeated, cyclical oscillations of cyclin E (CycE) and cyclin-dependent kinase 2 (Cdk2) activity [50, 52, 58]. Cdk2 and its activating cyclin, CycE (together represented as CycE/Cdk2), are not only the G1-to-S-phase transition regulators of the regular cell cycle but also serve as the main regulatory factors of the endocycle. Their cyclical activation and inactivation cause the cell to undergo multiple rounds of G- and S-phase of the endocycle. The CycE/Cdk2 activity during the endocycle can be regulated in different ways and depends on the specific cell type. For example, the *Drosophila* follicle cells regulate CycE/Cdk2 activity by the timed degradation of CycE with the help of the Archipelago (ago) protein [67]. CycE levels are restored with the help of the E2F1 transcription factor that activates the transcription of the *CycE* gene [68-70]. TGCs in rodents inhibit Cdk2 activity with the help of cyclin dependent kinase inhibitor (Ckis) proteins such as p57 [71, 72].

In the case of pregnancy-induced maternal liver growth, the exact contribution of endoreplication towards maternal liver enlargement remains debated. Previous studies have shown that during the course of gestation a large sub-population of maternal hepatocytes undergo S-phase DNA synthesis. However, what is still uncertain is the percentage of maternal hepatocytes undergoing

endoreplication versus those that undergo cell division post DNA synthesis. In a report by Milona et. al, the authors concluded that all S-phase completing maternal hepatocytes undergo endoreplication [32] whereas, a recent report by Prince et. al and previous studies from our lab have found evidence of maternal hepatocyte proliferation during gestation [33, 42, 43]. Therefore, in this study we use a more targeted approach to quantify the percentage of maternal hepatocytes undergoing endoreplication versus cell division in order get an accurate idea of the contribution of endoreplication to the enlargement of the maternal liver during gestation.

1.5 Axin2-expressing hepatocytes

Until recently, one important question that still persisted in the field of hepatology was regarding the presence of a genuine sub-population of adult hepatic stem cells in the liver. However, during the initial period of this research, two landmark studies convincingly demonstrated that a special sub-population of hepatic cells namely, Axin2-expressing hepatocytes, exhibited all the characteristic behavioral traits shown by true adult stem cells [73, 74]. Both reports employed the lineage tracing approach to study the behavior of the Axin2-expressing hepatocytes, hereafter referred to as $Axin2^+$ hepatocytes, during adult liver injury and homeostasis. In the first report, Huch et. al showed that the $Axin2^+$ hepatocytes repopulated a significant portion of the adult liver following an injury induced using carbon tetrachloride (CCl_4) [73]. And in the second report, Wang et. al not only demonstrated the ability of the $Axin2^+$ hepatocytes for self-renewal but also demonstrated that $Axin2^+$ hepatocytes repopulated and replaced approximately 30% of pre-existing hepatocytes after a duration of one year under homeostatic conditions [74]. Together, both these studies showed that the $Axin2^+$ hepatocytes exhibited the three key features that are characteristic of adult stem cells which are, capacity for constant self-renewal, replacing pre-existing cells during homeostasis, and participating in regeneration following injury.

The $Axin2^+$ hepatocytes are a sub-population of pericentral or Zone 3 hepatocytes [22, 73]. More precisely, these hepatocytes occupy an approximately three to four cell layer thick concentric region surrounding the central vein and are situated immediately adjoining the endothelial cells, that comprise the central vein. As their name suggests, the $Axin2^+$ hepatocytes are characterized by the expression of the *Axin2* gene. The constitutive expression of *Axin2* in this sub-population of hepatocytes is a consequence of the decreasing Wnt-ligand concentration gradient across the

CV-to-PT axis of the hepatic lobule [22, 75]. The *Axin2* gene is one of the targets of the Wnt-signal transduction pathway and encodes the AXIN2 protein which, under homeostatic conditions, is involved in the degradation of β-catenin and, therefore, a negative regulator of the Wnt pathway [76-79]. Furthermore, in the context of tissues strongly influenced by the Wnt-signaling pathway, for example different epithelial tissue, AXIN2 has been shown to be a stem cell marker [80, 81]. In addition to the expression of the *Axin2* gene, other important characteristic features of the $Axin2^+$ hepatocytes include the co-expression of the transcription factor Tbx3 (another prominent hepatoblast marker) [82], ability to self-renew, and having a diploid nucleus [74].

In this study we evaluate the behavior and response of the maternal $Axin2^+$ hepatocytes during the course of gestation. More specifically, we were interested to determine the contribution of the $Axin2^+$ hepatocytes to the process of pregnancy-induced maternal liver enlargement by means of cellular hyperplasia (cell division). The results obtained in our study could further validate the stemness of the $Axin2^+$ hepatocyte population. In the context of the liver, it has been frequently observed in numerous prior studies that the hepatic stem cell compartment is activated only under conditions of immense stress. And we believe that the duration of pregnancy represents one of those high-stress states within the maternal liver that is ripe for stimulating the activity of its resident stem cell population, that is $Axin2^+$ hepatocytes.

1.6 Hepatoblasts and their molecular markers

Hepatoblasts are the primary hepatic stem cells that originate from the foregut endodermal cells and are responsible for the organogenesis of the liver [83-86]. Specifically, these cells are bipotent progenitor cells that are committed towards the hepatic lineage and, by means of differentiation, give rise to both hepatocytes and BECs in the liver. In rodents, hepatoblasts appear along with the formation of the liver diverticulum, also known as the liver bud, around embryonic day 9 (E9). Formation of the liver bud demarcates the initiation of liver organogenesis. Following this, between E9 to E13.5, hepatoblasts undergo a phase of rapid expansion by means of cell proliferation and thereafter, post E13.5, begin the process of differentiation and maturation of hepatocytes and BECs [84, 86]. Being a stem cell, hepatoblasts are characterized by their expression of various stem cell marker proteins like CD133 (Prominin 1) [87-91], alpha-fetoprotein (AFP) [92-97], and epithelial cell adhesion molecule (EPCAM) [98-104]. It should

also be noted that the hepatoblasts express these different markers in different combinations depending on the developmental stage and lineage commitment, either towards hepatocytes or BECs. Therefore, in the context of the liver, the concurrent expression of CD133, AFP, and EPCAM is seen to occur during development within hepatoblasts which represent a cellular state that is under active cell proliferation.

1.6.1 CD133

The CD133 protein is an evolutionarily conserved penta-spanning transmembrane glycoprotein. This protein was first discovered in the year 1997; found embedded in the plasma membrane of mouse neuroepithelial stem cells [105]. In mice, the gene encoding the CD133 protein is located at the 5 B3 genetic loci of chromosome 5 and contains a total of 34 exons [106]. Whereas, in humans, the Cd133 gene is located at the 4p15.33 loci of chromosome 4 and contains 37 exons [106]. Yet, despite differing exon numbers between mice and humans, the CD133 protein is translated by a similar size mRNA transcript with approximately 4.4 kilobases (kb). An interesting feature of the *Cd133* gene is that it contains five distinct promoters distributed throughout the gene. Different promoters regulate the expression of different isoforms of CD133, for example the recently discovered CD133-2 isoform, in a tissue-specific manner. During the course of fetal development, CD133 is expressed by different types of stem- and progenitor cells such as fetal brain stem cells [107], embryonic epithelial stem cells [105, 108], and hepatoblasts [87-91]. In adults, the expression of *Cd133* gene products occurs in a unique manner. It has been found that while the Cd133 transcript is expressed by many somatic cells, CD133 protein expression occurs only in a subset of those cells such as hematopoietic stem cells [105], myogenic stem cells [109] and differentiated epithelial cells of the intestine, lung, kidney, etc. [110-112]

CD133 has been shown to be associated with multiple biological functions. However, despite there being sufficient research done on the protein, the exact mechanism by which CD133 influences its functionality or the identity of its common ligands (being a transmembrane protein) is still unknown. Initially, following its discovery, the CD133 protein was mostly recognized as a stem cell molecular marker. Shortly thereafter, it was found that, in addition to being a marker protein in normal and healthy stem cells, CD133 was also commonly expressed in a variety of cancers such as leukemia [113], retinoblastoma [114, 115], teratocarcinoma [115], and HCCs. As a result

of its significance as a stem- and cancer-cell marker, the CD133 antigen in concert with its antibody has been widely used for the isolation and clinical detection of a variety of stem cells and different types of cancers. It has commonly been observed that the $CD133^+$ sub-population of stems cells, separated by means of cell sorting, facilitate better rates of cellular and tissue regeneration compared to their $CD133^-$ counterparts. Examples of these include $CD133^+$ subpopulations isolated from human endothelial progenitor cells, peripheral blood cells, and bone-marrow stem cells. Recent studies have also revealed that CD133 is involved in the metabolism of cholesterol [116], transferrin (blood glycoprotein) [117], and glucose [118-120].

1.6.2 Alpha-fetoprotein (AFP)

AFP is a well-known oncofetal glycoprotein that is encoded by the *Afp* gene. Oncofetal proteins represent a group of proteins that are primarily expressed either during the course of early fetal development or in individuals who have been diagnosed with certain types of cancers. AFP is an evolutionarily conserved, blood-plasma protein, that belongs to the albuminoid gene superfamily of proteins [121]. Being a member of the albuminoid family of proteins, the tertiary molecular structure of AFP assumes a characteristic 'U-shaped' structure that is sub-divided into three domains [122, 123]. Domains-1 and 3 represent the 'arms' of the protein while Domain 2 represents the 'hinge' region that connects the two 'arms'. Since AFP is also rich in cysteine residues that are mostly located in Domains-1 and 3, both these domains in turn are comprised of multiple looped regions as a result of the disulfide linkages between the cysteine residues. Multiple studies in rodents and humans have revealed that organisms typically express at least three different genetic variants of AFP. These variants of AFP are translated from differently sized transcripts that are transcribed from the *Afp* gene. The transcript sizes of the three variants include a 2.2kb variant [124, 125], a 1.5kb variant [126], and a 1.35kb variant [127]. However, among the three versions, the most common and abundantly expressed form of AFP is encoded by the 2.2kb variant which translates into a 69 kilodalton (kDa) glycoprotein with 609 aa residues. In a healthy organism, AFP expression is seen mostly during the prenatal and perinatal periods of development. Initially, AFP is expressed by the cells of the yolk-sac but, shortly thereafter, the expression of AFP shifts primarily to the developing fetal hepatocytes and to a lesser extent in the fetal kidneys [128]. Following parturition, AFP expression decreases sharply, to the point of little to no expression, and is replaced by ALB. In adults, AFP is expressed in significant quantities during

various pathological conditions such as HCC, ovarian or testicular cancers, and during liver injury due to cirrhosis or hepatitis [129-132].

Within an organism, AFP has been shown to play two important functional roles. The first functional role of AFP is as a carrier/transport protein within the fetal blood. After its synthesis, AFP is released into the fetal blood stream where it can bind to different biomolecules and facilitate their transport. This function of AFP is akin to that of ALB in the adult blood. AFP has been shown to bind to various biomolecular and mineral substrates such as bilirubin [133], fatty-acids [134], estrogen [135, 136], copper [137], and zinc [137]. The second functional role of AFP is as a growth modulator. Depending on the context, AFP has been shown to both promote or inhibit growth in various cells and organs. For example, AFP was found to stimulate growth in placental cells and tumors such as hepatoma-22 (H-22) and Ehrlich ascites carcinoma (EAC) [138]. While, on the other hand, AFP was found to inhibit growth in glucocorticoid-induced splenic growth, during frog metamorphosis, and liver regrowth following PHx [139-141]. In addition to its functional roles, the properties of AFP have made it extremely useful in various clinical applications as well. Since AFP is a biomarker of HCCs, teratomas, and certain other tumors, its detection in blood samples is used to clinically diagnose cancer conditions in patients. It has been found that AFP has the ability to be conjugated with a variety of anti-cancer drugs such as doxirubricine, daunamycine, and mitomycin C [142-144]. Moreover, the potency and efficacy of various anti-cancer drugs increased significantly when used in combination with AFP versus being administered by itself [142-144]. As a result of this property, AFP is widely used in cancer therapy. AFP is also used as an indicator to monitor the health of pregnancy in humans. It is well known that during gestation the fetal AFP is detected in the maternal blood and amniotic fluid. In case of a healthy state of pregnancy, the level of fetal AFP stays within an expected range. However, aberrant fetal AFP levels in the maternal blood (or amniotic fluid) are a potential indicator of various fetal birth defects such as spina bifida, neural tube defects, hemolysis, and in severe cases intrauterine fetal death [145-147].

1.6.3 Epithelial cell adhesion molecule (EPCAM)

EPCAM is a single-span transmembrane protein that is commonly expressed in the plasma membrane of various epithelial cells. The human EPCAM protein, which is the most well

characterized EPCAM homolog, is encoded by the *Epcam* gene that in located at the 2p21 locus of chromosome 2 [148-150]. The gene comprises of 9 exons of which; exons 1-6 form the extracellular domain; exon 7 forms the transmembrane domain; and exons 8 and 9 form the intracellular domain of the protein. The EPCAM protein is made of a total of 314 aa residues [151]. Out of the 314 aa residues, residues 1 to 266 make up the N-terminal extracellular domain; residues 267 to 288 makes up the transmembrane domain; and residues 289 to 314 makes up the C-terminal intracellular domain [148-151]. Being a glycoprotein, EPCAM contains three N-glycosylation sites, all of which are located in the extracellular domain of the protein [152, 153]. Furthermore, EPCAM also contains two important cleavage sites, one in the extracellular domain being a substrate for α-disintegrin and metalloproteinase 17 (ADAM17) and the other in the intracellular domain being a substrate for γ-secretase, that renders the protein as a signaling molecule [99]. Studies have also revealed that mammals comprise another paralog of EPCAM which is the trophoblast cell-surface antigen 2 (TROP2) [150, 154]. EPCAM is expressed by various stem cells during early development as well as in adult stem cells [98, 155, 156]. But in addition to stem cells EPCAM is also expressed by various types of differentiated epithelial cells, and specifically, of simple and pseudo-stratified epithelial types [157-161].

Functionally, EPCAM is a versatile protein. One prominent function of EPCAM, as evident from its name, is in facilitating intercellular adhesion interactions through homophilic dimerization. More precisely, EPCAM promotes weak cell-cell interactions and due to its disruptive interaction with E-cadherin, enables a cell to control the strength of its cell-cell or cell-extracellular matrix interactions [162, 163]. In certain cellular contexts, EPCAM serves as a pro-proliferative factor. Multiple studies have shown that cells in a state of active proliferation are characterized by abundant EPCAM expression and ectopic downregulation of EPCAM in these cells lead to significant decrease in their rate of proliferation [99, 100, 164-166]. More recent studies have also revealed a novel function of EPCAM as an extracellular and intracellular signaling molecule. The mechanism responsible for initiating EPCAM signaling is called regulated intracellular membrane proteolysis (RIP). As touched upon above, RIP involves the timely proteolysis of the extracellular and intracellular domain of EPCAM by ADAM17 and γ-secretase, respectively [99]. The extracellular domain fragment, called “EpEx”, serves as an extracellular signaling molecule while the intracellular domain fragment, called “EpICD”, is used intracellularly. Free “EpICD” mediates intracellular signaling through the transcriptional regulation of its target genes such as c-Myc,

CycD1, and CycE (indirectly) [100, 164, 167]. It is hypothesized that "EpICD" first forms a heteromeric complex with four-and-a-half LIM domains protein 2 (FHL2) and β-Catenin in order to be translocated into the nucleus where it can then bring about transcriptional regulation of its target genes [99, 149].

Our particular interest in the three hepatoblast/fetal developmental markers namely, CD133, AFP, and EPCAM with regards to maternal liver adaptations was developed following certain preliminary studies. The results of our pilot studies revealed that pregnancy induced a dynamic expression of the three markers in the maternal liver. As these three factors are considered pro-proliferative markers, especially in the context of the liver, we were interested to determine if their expression was associated with the potential proliferation of maternal hepatocytes during pregnancy-induced maternal liver growth. Therefore, to make this determination, in our current study, we characterized the expression of Cd133, Afp, and Epcam at both mRNA and protein levels.

1.7 Hippo signaling pathway

The hippo pathway is a signal transduction pathway that is most widely known for its role in regulating organ growth and size. The inactivation of various components of the hippo pathway often leads to defects in maintaining organ size. It should be noted that under normal homeostatic conditions, an active hippo pathway negatively regulates the growth of an organ. The hippo pathway was first discovered in the *Drosophila melanogaster* [168, 169], however, further studies in *Caenorhabditis elegans* [170] and mammals revealed that this signaling pathway was evolutionarily conserved, which also underscores the importance of the hippo pathway.

In its essence, the hippo pathway is a 'kinase cascade' signal transduction pathway. In mammals, the canonical hippo pathway transduces its signal and regulates organ growth by the following mechanism. Under homeostatic conditions, the hippo pathway is maintained in its active or "ON" state and negatively regulates organ growth by preventing cell proliferation. In this state, an appropriate signal first leads to the phosphorylation and activation of the mammalian STE20-like kinase 1 (MST1), or its paralog MST2. MST1/2, a serine-threonine kinase, is the first core kinase of the hippo pathway [130, 171-174]. In addition to being phosphorylated, the complete activation of MST1/2 also requires heterodimerization of the kinase with its co-activator salvadore 1 (SAV1)

[175-177]. Activated MST1/2 then phosphorylates and activates the downstream second core kinase of the hippo pathway namely, large tumor suppressor kinase 1 (LATS1) or its paralog LATS2 [178]. And, similar to that of MST1/2, complete activation of LATS1/2 also requires its dimerization with another co-activator that is Mps one binder kinase activator-like 1A (MOB1A or its homolog MOB2A) [179, 180]. Activated LATS1/2 in turn leads to the phosphorylation and deactivation of the final effectors of the hippo pathway namely, yes-associated protein 1 (YAP1) or its homolog tafazzin (TAZ). YAP1 and TAZ are both transcriptional co-activators and in the phosphorylated (deactivated) state are unable to translocate into the nucleus to activate their pro-proliferative target genes. Instead, phosphorylated YAP1/TAZ is sequestered in the cytoplasm where it binds to 14-3-3 for degradation [181]. However, when the cell is signaled to undergo proliferation, an appropriate stimulus results in dephosphorylation of MST1/2 and LATS1/2 that in turn leads to dephosphorylation and activation of YAP (or TAZ). Active YAP (or TAZ) is then transported to the nucleus where it heterodimerizes with TEA-domain-containing family of proteins 1 to 4 (TEADs 1-4) and binds to their respective response elements [182-185]. Example of YAP1 target genes in the liver include connective tissue growth factor (*Ctgf*) [185] and *Notch2* [186].

Over the years, the hippo pathway has been shown to be involved in a variety of biological functions. Indeed, its most prominent role has been in the regulation of organ size. In mammals, the hippo pathway has been shown to regulate the growth of the heart [187, 188] and liver [174, 189]. Apart from growth, this signaling pathway is also crucial in the homeostatic development and maturation of various organs. Studies so far have shown that the hippo pathway influences organ development either by promoting cell-fate decisions through differentiation of stem cells or by maintaining stem cell sub-populations in adult organs. Timely modulation of hippo-YAP activity is required for neurogenesis of specific neuronal subtypes such as guidepost cells of corpus callosum [190, 191]. YAP/TAZ activity is important in maintaining the self-renewing capacity of the basal progenitor cells [192]. Within the liver, the hippo pathway is found to regulate fatty acid, cholesterol, and glucose metabolism [193-196]. Furthermore, it is also suspected that the hippo pathway may be important in the maintenance of hepatic metabolic zonation [186, 197]. Lastly, the hippo pathway is also a potent causative factor of cancers as aberration in the pathway that leads to YAP/TAZ overactivation causes different carcinomas such as HCC [198].

Pregnancy-induced maternal liver growth is one of the most striking adaptations of the maternal liver during gestation. Furthermore, previous studies have provided strong evidence that suggests that pregnancy-induced maternal liver growth is accompanied, at least partly, by the proliferation of maternal hepatocytes. Therefore, considering the importance of the hippo pathway in the regulation of organ growth, particularly by regulating cell proliferation, in this current study we investigate the role of the hippo pathway in regulating the process of pregnancy-induced maternal liver growth. Analyzing the activity of the hippo pathway in the maternal liver could help us further validate the contribution of maternal hepatocyte hyperplasia towards maternal liver growth.

CHAPTER 2. MATERIALS AND METHODS

2.1 Animal care and "timed pregnancy" generation

Protocol for the care and use of animals was prepared as per NIH guidelines and all animals were maintained in accordance with the regulations outlined by the Indiana University-Purdue University Indianapolis Animal Care and Use Committee (IACUC). Animals had ad libitum access to food and drinking water. Irrespective of their physiological state, that is NP or pregnant, all animals were fed 'regular chow'. Temperature and relative humidity of the animal rooms were maintained at 22±1^{o}C and 40-60% respectively. Lighting period comprised of a 12hr of light and 12hr dark cycle. To generate a timed pregnancy, a virgin female and male mouse, both aged between 3 to 3.5 months old, were housed together. Following day onwards, the female mouse was inspected for a seminal plug that indicated successful mating. Appearance of seminal plug was denoted as gestation day 1 (Gd1) and the male was separated from cage. Mouse strains used in this study have a gestational duration of 19 days.

2.2 Mouse models

Following is a listing along with a brief description of the different mouse strains used in this study. All mouse strains were purchased from 'The Jackson Laboratory', Maine, USA.

2.2.1 C57BL/6J mice

The C57BL/6J mouse strain, stock # - 000664, served as the "genetic pure line" of the study. We used this mouse strain as the genetic pure line as the C57BL/6J mouse strain is commonly used as a "genetic pure line" as its genetic make-up is devoid of any mutations and the strain. Data generated using this strain represented the foundational processes taking place during pregnancy-induced maternal liver growth.

2.2.2 B6.129X1-*Gt(ROSA)Sor^{tm1EYFPcos}*/J mice

The B6.129X1-*Gt(ROSA)Sor^{tm1EYFPcos}*/J mouse strain (henceforth referred as *RS26*$^{\text{floxstopEYFP/floxstopEYFP}}$ mice), stock # - 006148, is a reporter strain that was used to determine maternal hepatocyte proliferation during pregnancy. Mice in this strain were homozygous for the

Rosa26^{floxstopEYFP} (*RS26*^{floxstopEYFP}) transgene. The *RS26*^{floxstopEYFP} transgene comprises of three important components; 1) a ubiquitous RS26 promoter sequence; 2) a loxP STOP cassette sequence; and 3) an enhanced yellow fluorescent protein (EYFP) gene. This mouse strain was used in combination with the hepatocyte-specific adeno-associated virus 8-thyroxine binding globulin-Cre (AAV8-TBG-Cre) viral vector. Under regular conditions, the loxP STOP cassette, located upstream of the EYFP sequence, inhibits the transcription and expression of the EYFP protein. However, upon exposure to the Cre-recombinase protein (conditionally induced via the AAV8-TBG-Cre viral vector), the loxP STOP cassette is excised from the transgene leading to expression of EYFP in the hepatocytes transfected with the AAV8 vector. Using this mouse strain, AAV8 transfected hepatocytes and their progeny are, thus, permanently labelled with EYFP.

Mice were genotyped by the polymerase chain reaction (PCR) assay. Please refer to section 2.3 for a detailed description of the PCR protocol used for in this study. Following is a brief description of the genes amplified for genotyping, primers used for PCR, and DNA band sizes of the amplified gene products. Two genes were amplified to determine the appropriate genotype - 1) the wildtype (wt) *RS26*^{wt} allele and 2) the mutant *RS26*^{floxstopEYFP} allele, encoding the enhanced yellow fluorescent protein (EYFP). *RS26*^{wt} allele was amplified by the primers 21306 (forward primer) and 24500 (reverse primer). *RS26*^{floxstopEYFP} mutant allele was amplified by the primers 24951 (forward primer) and 24952 (reverse primer). Primer sequences are given in Table 1. The DNA band sizes of the RS26^{wt} allele and the *RS26*^{floxstopEYFP} allele were 142bp and 384bp respectively. Mice that were homozygous for the mutant allele were selected.

2.2.3 B6.129S4-Gt(ROSA)26Sor^{tm1Sor}/J mice

The B6.129S4-Gt(ROSA)26Sor^{tm1Sor}/J mouse strain (henceforth referred as RS26$^{floxstopLacZ/floxstopLacZ}$ mice), stock # - 003474, is another reporter strain used in this study. The *RS26*$^{floxstopLacZ/floxstopLacZ}$ mouse strain was used to trace the fate of the *Axin2*-expressing maternal hepatocytes during pregnancy. The genetic design of the *RS26*$^{floxstopLacZ/\ floxstopLacZ}$ reporter strain is very similar to the *RS26*$^{floxstopEYFP/\ floxstopEYFP}$ strain, with the only difference being the reporter protein on the transgene. Instead of the EYFP reporter, *RS26* $^{floxstopLacZ/\ floxstopLacZ}$ mice comprise the β-galactosidase (LacZ) enzyme. The *RS26* $^{floxstopLacZ/\ floxstopLacZ}$ mice are homozygous for the *RS26*^{floxstopLacZ} transgene. The *RS26*^{floxstopLacZ} transgene also comprises of three components; 1) a

ubiquitous RS26 promoter; 2) an upstream loxP-STOP cassette; and 3) a downstream, LacZ gene sequence. Under normal circumstances, LacZ expression is inhibited by the upstream loxP-STOP cassette sequence. However, ablation of the loxP-STOP cassette mediated by Cre-recombinase exposure will result in LacZ expression.

Mice were genotyped by the PCR assay. Please refer to section 2.3 for a detailed description of the PCR protocol used for this/in this study. Following is a brief description of, the genes amplified for genotyping, primers used for PCR, and DNA band sizes of the amplified gene products. Two genes were amplified to determine the appropriate genotype - 1) The wt *RS26*^{wt} and 2) The mutant *RS26*^{floxstopLacZ} transgenic allele, encoding the LacZ enzyme. *RS26*^{wt} allele was amplified by the primers oIMR8545 (forward primer) and oIMR8546 (reverse primer). *RS26*^{floxstopLacZ} mutant allele was amplified by the primers oIMR8545 (forward primer), common to the wt allele as well, and oIMR8052 (reverse primer). Primer sequences are given in Table 1. The DNA band sizes of the *RS26*^{wt} allele and the *RS26*^{floxstopEYFP} mutant allele were 650bp (approximately) and 340bp respectively. Mice that were homozygous for the mutant allele were selected.

2.2.4 B6.129(Cg)-Axin2$^{tm1(cre/ERT2)Rnu}$/J mice

The B6.129(Cg)-Axin2$^{tm1(cre/ERT2)Rnu}$/J mouse strain (henceforth referred as *Axin2*^{CreERT2} mice), stock # - 018867, was used to specifically and permanently label the Axin2-expressing subpopulation of hepatocytes with the LacZ reporter. We could therefore trace the fate of the *Axin2*-expressing hepatocytes during various physiological conditions, for example, pregnancy and partial hepatectomy. The Axin2$^{wt/CreERT2}$ mice are heterozygous for the *Axin2* gene. These mice have one wt *Axin2*^{wt} allele while the other allele, namely *Axin2*^{CreERT2}, is modified such that the AXIN2 protein coding sequence is replaced by a sequence encoding the chimeric Cre-ERT2 protein. Therefore, these mice have only one functional allele transcribing the AXIN2 protein. The Cre-ERT2 protein is a fusion protein comprising the Cre-recombinase enzyme (Cre) attached to the estrogen receptor (ERT2). In these mice, all the AXIN2-expressing cells express the Cre-ERT2 protein which is localized in the cell cytoplasm. As a result of being conjugated to the ERT2 protein, Cre-recombinase cannot enter the nucleus. Cre-ERT2 nuclear localization can occur only upon exposure of cells to tamoxifen, an estrogen analog.

Mice were genotyped by the PCR assay. Please refer to section 2.3 for a detailed description of the PCR protocol used for this/in this study. Following is a brief description of, the genes amplified for genotyping, primers used for PCR, and DNA band sizes of the amplified gene products. Two genes were amplified to determine the appropriate genotype - 1) The wt *Axin2*^{wt} allele and 2) The mutant *Axin2*^{CreERT2} allele, encoding the Cre-ERT2 chimeric protein. *Axin2*^{wt} allele was amplified by the primers 26423 (forward primer) and 26424 (reverse primer). *Axin2*^{CreERT2} mutant allele was amplified by the primers 26423 (forward primer), common to the wt allele as well, and 16774 (reverse primer). Primer sequences are given in Table 1. The DNA band sizes of the *Axin2*^{wt} allele and the *Axin2*^{CreERT2} mutant allele were 499bp and 328bp respectively. Mice that were heterozygous were selected.

2.2.5 YAP1$^{tm1.1Dupa}$/J mice

The YAP1$^{tm1.1Dupa}$/J mouse strain (henceforth referred as *Yap1*$^{flox/flox}$ mice), stock # - 027929, was used to study the effects of maternal hepatocyte-specific YAP1 deletion on pregnancy-induced maternal liver growth. Mice in this strain are homozygous for the *Yap1*^{flox} transgene. The *Yap1*^{flox} transgene is generated by modifying the wt YAP1 allele. In the *Yap1*^{flox} transgene, the coding region comprising exon 1 and exon 2 of the *Yap1*^{wt} allele is flanked by a loxp site on both sides. Despite the insertion of the loxP sites, the *Yap1*^{flox} transgene still translates the YAP1 protein. However, when exposed to the Cre-recombinase enzyme, the coding region comprising exons 1 and 2 is excised thereby inhibiting YAP1 expression. Hepatocyte specific YAP1 deletion was achieved by inoculating mice with the AAV8-TBG-Cre viral vector.

Mice were genotyped by the PCR assay. Please refer to section 2.3 for a detailed description of the PCR protocol used for this/in this study. Following is a brief description of, the gene amplified for genotyping, primers used for PCR, and DNA band size of the amplified gene product. Only one gene was amplified by the PCR assay since these mice were homozygous for the *Yap1*^{flox} allele. The *Yap1*^{flox} allele was the amplified by the primers 29878 (forward primer) and 29879 (reverse primer). Primer sequences are given in Table 1. The DNA band sizes of the *Yap1*^{wt} allele and the *Yap1*^{flox} mutant allele were 418bp and 300bp (approximately) respectively. Mice that were homozygous for the *Yap1*^{flox} allele were selected.

2.2.6 *RS26*$^{floxstopLacZ/\ floxstopLacZ}$; *Axin2*$^{wt/CreERT2}$ mice

The *RS26*$^{floxstopLacZ/\ floxstopLacZ}$; *Axin2*$^{wt/CreERT2}$ mouse strain is a bi-transgenic strain that was generated by crossbreeding the *RS26*$^{floxstopLacZ/\ floxstopLacZ}$ and the *Axin2*$^{wt/CreERT2}$ mouse strains. This mouse strain was used to label and trace the fate of Axin2-expressing maternal hepatocytes during pregnancy. In this strain, under homeostatic conditions, all Axin2-expressing cells express the CreERT2 chimeric protein. The CreERT2 protein is made by fusing the Cre-recombinase enzyme with a modified version of the estrogen receptor protein (ERT2). Cre-recombinase is unable to translocate into the nucleus due to its fusion to ERT2. However, when these mice are injected with tamoxifen (an ERT2 ligand and an analog of estrogen), Cre-recombinase is transported into the nucleus where it excises the loxP STOP sequence on the *RS26*^{floxstopLacZ} allele and facilitates LacZ reporter expression. Therefore, using this mouse strain, the fate of AXIN2-expressing maternal hepatocytes could be traced during pregnancy.

2.3 Genotyping of mouse strains

Mice with the appropriate genetic make-up were selected by means of genotyping. The genotypes of mice were determined by PCR. DNA samples were extracted from ear snips and mice were simultaneously ear tagged for identification. To isolate DNA from ear snips, samples were boiled in DNA extraction buffer (25Mm NaOH, 0.2mM EDTA) for 1 hr at 98^{o}C. After 1 hr, 150 µl Tris-HCl (40mM) was added to the DNA extracts to neutralize the sample mixture. DNA samples were centrifuged at 5000 rpm for 3 mins and stored at -20^{o}C until further use.

The PCR reactions for each mouse strain was performed as per the instructions of the vendor (The Jackson Laboratory). The PCR master mix solution was prepared using reagents from the Kapa Taq PCR kit (Kapa Biosystems Inc., Wilmington, MA, USA) and the respective primers, all of which were purchased from Integrated DNA Technologies (Coralville, IA, USA). PCR was performed to amplify specific genes of interest (GOI). Following gene amplification, PCR products were resolved by DNA gel electrophoresis. Gel composition for electrophoresis was 1.5% agarose (#DSA20090-500, Dot Scientific) with adequate ethidium bromide (#IB40075, IBI Scientific). A UV transilluminator was used to visualize the separated gene products (DNA bands). For band sizes of specific GOI, please refer to the respective mouse strain description above. For primer details please refer to Table 1.

Table 1: List of primers and primer Sequences used for Polymerase Chain Reaction (PCR)

Serial No.	Primer	Primer type	5'->3' Primer sequence
1	21306	Wildtype Forward	CTGGCTTCTGAGGACCG
2	24500	Wildtype Reverse	CAGGACAACGCCCACACA
3	24951	Mutant Forward	AGGGCGAGGAGCTGTTCA
4	24952	Mutant Reverse	TGAAGTCGATGCCCTTCAG
5	oIMR8545	Common Forward	AAAGTCGCTCGTAGTTGTTAT
6	oIMR8546	Wildtype Reverse	GGAGCGGGAGAAAGTGATATG
7	oIMR8052	Mutant Reverse	GCGAAGAGTTTGTCCTCAACC
8	26423	Common Forward	CTTTCCAGAGAGGAGGCTCA
9	26424	Wildtype Reverse	GCCTGAACCCATTACAAGCA
10	16774	Mutant Reverse	CATCGACCGGTAATGCAG
11	29897	Forward	AGGACAGCCAGGACTACACAG
12	29898	Reverse	CACCAGCCTTTAAATTGAGAAC

2.4 5-Bromo-2'-deoxyuridine (BrdU) administration

In this study, the C57BL/6J and *RS26*$^{\text{floxstopEYFP/floxstopEYFP}}$ mouse strains were administered BrdU. Mice were chronically exposed to BrdU via drinking water and the drinking water was refreshed every two days. The concentration of BrdU in drinking water for the first two days was 0.2mg/ml and thereafter was increased to 0.3 mg/ml. Pregnant mice were exposed to BrdU from Gd1 upto the day of sacrifice (Gds-10, 14, or 18) while NP mice were exposed to BrdU for 18 days. Drinking water bottles were covered with aluminum foil to prevent BrdU photodegradation.

2.5 Adeno-associated virus 8 (AAV8) administration

The AAV8 viral vector was administered to the *RS26*$^{floxstopEYFP/floxstopEYFP}$ and *Yap1*$^{flox/flox}$ mouse strains to determine maternal hepatocyte proliferation and effects of YAP1 deletion on maternal liver enlargement, respectively. The AAV8.TBG.PI.Cre.rBG (hereafter referred as AAV8-TBG-Cre) and AAV8.TBG.PI.Cre.rBG (referred to as AAV8-TBG-Null) viral vectors were purchased from the Penn Vector Core, Perelman School of Medicine, University of Pennsylvania, PA, USA. AAV8-TBG-Cre consists of a transgene that contains the Cre-recombinase gene coding sequence driven by the hepatocyte specific TBG promoter. Before inoculation, an appropriate volume of viral particles was reconstituted in chilled, sterile saline (#RL-2099, Aqualite® System). Mice were administered AAV8 by hydrodynamic tail vein injection (HTVi). The *RS26*$^{floxstopEYFP/floxstopEYFP}$ mice were administered a low viral dose of $2.5x10^{10}$ GC/mouse in order to label only a small representative sub-population of hepatocytes. On the other hand, the *Yap1*$^{flox/flox}$ mice were administered a high viral dose of $1x10^{12}$ GC/mouse in order transfect and delete *Yap1* gene from every hepatocyte.

2.6 Tamoxifen (TMX) preparation and administration

Mice were administered TMX using a 24 mg/ml TMX working solution. TMX working solution was prepared by dissolving appropriate amount of TMX (#T5648-1G; Sigma Aldrich) in a solvent containing 10% (v/v) ethanol (#BP2818; Fischer Scientific) and sesame oil (#S3547-1L; Sigma Aldrich). The working solution was incubated overnight at 37^{o}C with constant mixing to facilitate complete TMX dissolution. All mice were administered TMX intraperitoneally.

2.7 Two-thirds partial hepatectomy (2/3rd PHx)

2/3rd PHx was performed on 3-3.5 months-old virgin female and male mice. Mice were sedated using isoflurane and placed on a heating pad throughout the surgical procedure. An abdominal incision was made to expose the liver lobes. Amongst the five liver lobes, we resected the left-lateral lobe and the left- and right-median lobes. A ligature was applied at the root of each lobe before its resection. The peritoneum and skin were closed by a continuous suture. Immediately post-surgery, partially hepatectomized mice were subcutaneously injected 3 ml sterile saline to replenish fluid loss during surgery and placed under a warming light for 15 mins to facilitate

recovery. Recovery of partially hepatectomized mice was further monitored for two more days. 25 days post 2/3rd PHx, mice were sacrificed by cervical dislocation, livers were harvested, and processed for performing LacZ staining.

2.8 Tissue sample collection

Mice were sacrificed by cervical dislocation at the appropriate time. Different weight measurements, namely, total body weight, total maternal organ weights, fetus weight, and placenta weight, were recorded to determine gravimetric (weight related) responses during pregnancy. Maternal organs (tissue samples) were dissected and apportioned for various assays. Tissue samples for real-time quantitative polymerase chain reaction (RT-qPCR) and western blotting analysis (WB) were flash frozen in liquid nitrogen. For LacZ staining assay, tissues were frozen in Optimal Cutting Temperature (OCT) medium (#4583 Tissue Tek, Sakura) and stored at -80^{o}C (for at least 48 hrs) until sectioning. LacZ staining was performed using 16 µm thick frozen tissue sections which were sectioned using a microtome (Leica). For in-situ hybridization (ISH) and immunohistochemistry (IHC), tissue samples were fixed in 4% neutral buffered formalin (4% NBF) for ~96 hrs. Following fixation, 5 µm thick formalin fixed paraffin embedded (FFPE) tissue sections were prepared for performing ISH and IHC assays.

2.9 Real-Time Quantitative Polymerase Chain Reaction (RT-qPCR) assay

RT-qPCR assay was used to measure the change in relative mRNA expression of the *Cd133*, *Afp* (Alpha-fetoprotein), *Epcam*, *Ctgf* (Connective tissue growth factor), *Notch2*, and *Yap1* (Yes-associated protein 1) genes during pregnancy. To perform RT-qPCR, mRNA was first extracted from liver tissue samples, followed by cDNA generation, and RT-qPCR was performed using the cDNA samples. The following is a brief description of the RT-qPCR protocol.

Total mRNA extraction: For each sample, mRNA was extracted from approximately 80-100 mg whole liver tissue. mRNA was extracted using the "trizol-chloroform extraction method". Briefly, tissue samples were homogenized in 1 ml trizol reagent (#15596026, Thermo Fischer Scientific). Due to the nature of mRNA, care was taken to avoid contamination and mRNA degradation. Tissue homogenates were then transferred to RNase free Eppendorf tubes (#609-GMT, Dot Scientific)

and mixed with chloroform. The two phases were separated by centrifuging tissue homogenates at 12,000 xg for 15 mins at 4^{o}C and then transferring the upper aqueous phase, containing mRNA, to fresh RNase free tubes. The RNA extracts were further purified by mixing the extracts with isopropyl alcohol followed by centrifugation at 12,000 xg for 10 mins at 4^{o}C. Following centrifugation, the supernatant was discarded, the RNA pellet was washed, dried, and dissolved in molecular biology grade water (#786-72C, G Biosciences). RNA concentration and purity were measured using the NanoDrop 2000 Spectrophotometer (Thermo Scientific, Rockford, IL). For cDNA generation, 0.2 µg/ml RNA samples were prepared in molecular biology grade water.

Generation of cDNA: To generate cDNA, we used the Verso cDNA Synthesis Kit (#AB-1453/B, Thermo Fischer Scientific) and followed the vendor's protocol. Briefly, a master mix solution was prepared using the reagents provided in the kit. The master mix solution contained the following components, cDNA synthesis buffer, dNTPs mix, anchored oligo-Dt RNA primer, reverse transcriptase enhancer, and Verso enzyme mix. The volume of master mix solution prepared depended on the number of cDNA samples being generated. Reverse transcriptase-PCR reactions were carried out in 96 well plates (#951-PCR, Dot Scientific). Each well comprised of 15 µl of master mix solution and 5 µl (1 µg) of RNA sample (0.2 µg/µl concentration). The plates were centrifuged briefly, and the reverse transcriptase-PCR reaction was carried out using the Eppendorf Mastercycler® Pro S 6325 Thermal Cycler (Eppendorf; Enfield; CT). The RT-PCR reaction comprised of the following conditions in sequence; 1) 1 cycle at 25^{o}C for 10 mins; 2) 1 cycle at 42^{o}C for 60 mins; 3) 1 cycle at 95^{o}C for 2 mins; and 4) End cycle at 4^{o}C. Following the reverse transcriptase-PCR reaction, the cDNA samples were diluted by a ratio of 1:4 by adding 60 µl of molecular biology grade water (#786-72C, G Biosciences) to the newly generated 20 µl cDNA samples. cDNA samples were stored at -20^{o}C until further use for RT-qPCR assay.

RT-qPCR: The RT-qPCR assay was performed using the 7300 Real Time PCR System (Applied Biosystems, Foster City, CA). The RT-qPCR reaction mixture was made using the prepared cDNA, 2X Taqman Gene Expression Master Mix (#4369016; Applied Biosystems), and the Taqman gene expression assay probes (Applied Biosystems). Taqman probes used for RT-qPCR are listed in Table 2. 20 µl reaction mixtures were added to a 96 well plate (#N8010560, Applied

Biosystems) and the RT-qPCR assay was run using the instrument mentioned above. Albumin (*Alb*) gene was used as an endogenous control.

Table 2: List of primers used for Real Time Quantitative Polymerase Chain Reaction (RT-qPCR)

Sr. No:	Gene Name	Assay ID	Catalog No.	Gene Type
1	*Afp*	Mm00431715_m1	4331182	Target
2	*Cd133*	Mm00477115_m1	4331182	Target
3	*Epcam*	Mm00493214_m1	4331182	Target
4	*Ctgf*	Mm00515790_m1	4331182	Target
5	*Notch2*	Mm00803077_m1	4331182	Target
6	*Yap1*	Mm00494236_m1	4351372	Target
7	*Albumin*	Mm00802090_m1	4331182	Endogenous Control

2.10 In-situ hybridization (ISH)

ISH was performed by following the instructions of the RNAscope® 2.5 HD Detection Kit (Brown) developed by Advanced Cell Diagnostics Inc. (USA). Following is a brief description of the ISH protocol. 5 µm thick formalin fixed paraffin embedded (FFPE) liver tissue sections were baked for 1 hr at 60^{o}C in a dry oven. Tissue sections were then deparaffinized by incubating the slides twice in xylene (#64111-04, Electron Microscopy Sciences), for 5 mins each, followed by incubating the slides twice in 100% ethanol, for 1 min each. Next, tissue sections were air dried at room temperature (RT) for 5 mins to remove excess ethanol. After air drying, tissue sections were treated with hydrogen peroxide (provided by vendor) for 10 mins at RT to quench the endogenous peroxidase enzyme activity of tissues samples. Subsequently, tissue sections were placed on a slide-rack and rinsed in distilled water (DW). Tissue sections were rinsed by dipping the slide-rack 3-5 times in the appropriate rinsing solution. Following the DW rinse, tissue sections were boiled in 500 ml of 1X Target Retrieval Solution (provided by vendor) for 30 mins using a hot plate. To clear tissue sections of excess target retrieval solution, slides were rinsed sequentially in DW and then 100% ethanol. Tissue sections were air dried to remove excess ethanol. Next, using the Immedge™ Pen (#H-4000, Vector Laboratories), tissue sections were encircled with a

hydrophobic boundary to contain the various reagents the sections were to be treated with. (Note: Hereafter, all steps, up to counterstaining tissues sections with hematoxylin, were performed in a humidifying chamber.) Tissue sections were then treated with the Protease Plus reagent for 30mins at 40^{o}C. After Protease Plus treatment, tissue sections were rinsed twice in DW. Following the DW rinse, tissue sections were incubated with the appropriate hybridization probe for 2 hrs at 40^{o}C. Excess hybridization probe was washed by incubating tissue sections in 1X Wash Buffer (provided by vendor). Tissue sections were washed by submerging the slide-rack twice in 1X Wash Buffer for 2 mins each at RT. After this, tissue sections were treated sequentially with Hybridize Amp 1 to 6 reagents (provided by vendor). Hybridize Amp 1 and 3 incubation conditions were for 30 mins at 40^{o}C. Hybridize Amp 2 and 4 incubation conditions were for 15 mins at 40^{o}C. Hybridize Amp 5 and 6 incubation conditions were at RT for 30 mins and 15 mins, respectively. Between each Hybridize Amp reagent treatment, tissue sections were washed once in 1X Wash Buffer for 2 mins at RT to remove earlier reagent. Thereafter, tissue sections were incubated in the 3,3'-Diaminobenzamide (DAB) substrate for 10 mins at RT following which excess substrate was washed using 1X Wash Buffer. Tissue sections were counterstained with hematoxylin (#6765002, Thermo Fischer Scientific) for 2 mins at RT and then excess hematoxylin was removed by rinsing the sections in DW. Lastly, tissue sections were dehydrated by sequentially incubating them in 70% and 95% ethanol for 2 mins each and in xylene for 5 mins. For long term preservation, tissue sections were mounted using Xylene Substitute Mountant (#1900233, Thermo Scientific) mounting medium. Results were observed and curated using the Leica DM 2000 microscope.

2.11 Western blotting assay (WB)

Western blotting assay was used to analyze NP and pregnant maternal liver samples. Specifically, CD133, AFP, and EPCAM were analyzed from liver total protein lysates, whereas protein components belonging to the hippo pathway were analyzed from cytoplasmic and nuclear protein lysates.

Hepatic total protein extraction: Total protein lysates were prepared by following the instructions of the T-PER Tissue Protein Extraction kit (#78510, Thermo Fischer Scientific). Each total protein lysate sample was prepared from approximately 100 mg whole liver tissue. Liver tissues were homogenized in 500 µl of chilled T-PER reagent. Protease inhibitors (#78443; Halt™

Protease and Phosphatase Inhibitor Single-Use Cocktail, EDTA-free (100X); Thermo Scientific) was added to the T-PER reagent as per vendor instructions. The homogenates were transferred to 1.5 ml eppendorf tubes and centrifuged at 7000 rpm for 5 mins. Following centrifugation, the supernatant was transferred to a fresh 1.5 ml eppendorf tube while the pellet was discarded. The supernatant served as the total protein lysate.

Hepatic cytoplasmic and nuclear protein extraction: Cytoplasmic and nuclear protein lysates were prepared by following the instructions of the NE-PER Nuclear and Cytoplasmic Extraction Reagents kit (#78833; Thermo Fisher Scientific). The following is a brief description of the extraction protocol. Cytoplasmic protein lysate was prepared by homogenizing approximately 50mg whole liver tissues in a mixture of CER I and CER II solutions, provided by the vendor. Protease inhibitors (#78443; Halt™ Protease and Phosphatase Inhibitor Single-Use Cocktail, EDTA-free (100X); Thermo Scientific) were added to the mixture as per vendor instructions. Tissue homogenates were centrifuged at 14,500 xg for 5 mins and the collected supernatant served as the cytoplasmic protein lysate. Nuclear protein lysate was extracted from the pellet generated after centrifugation of tissue homogenates. Pellets were incubated in NER solution, provided by the vendor, for 40 mins with intermittent vortexing. The pellet-NER solution mixture was centrifuged at 14,500 xg for 10 mins and the collected supernatant served as the nuclear protein lysate.

Measurement of protein concentration and loading sample preparation: The protein concentration of the total, cytoplasmic, and nuclear protein lysates were measured by the Protein Pierce 660 nm method. Briefly, the protein lysates were mixed with the Pierce 660 nm Protein Assay Reagent (#22660, Thermo Fischer Scientific) at a 1:16 dilution ratio and incubated for 5 mins at RT. Protein concentration of the samples were measured using the NanoDrop 2000 Spectrophotometer (Thermo Scientific, Rockford, IL). The total, cytoplasmic, and nuclear protein loading samples were prepared using the respective protein samples, the 4X LDS Loading Buffer (#NP0008, Invitrogen) and β-mercaptoethanol (#BP176-100, Thermo Fischer Scientific).

WB: Appropriate protein samples were loaded onto a precast gel and the component proteins of the samples were separated by Sodium Dodecyl Sulphate - Polyacrylamide Gel Electrophoresis

(SDS-PAGE) at 120V. Total protein and cytoplasmic protein samples were separated using the NuPage™ 4-12% Bis-tris gel (#NP0336BOX, Invitrogen) while nuclear protein samples were separated using the BOLT™ 4-12% Bis-Tris Plus gel (#NW04125BOX, Invitrogen) gel. Running buffer, used for electrophoresis, had the following composition. Next, the proteins were transferred onto a PVDF membrane (#88518, Thermo Fischer Scientific) using the 'wet-transfer method'. Transfer buffer, used for protein transfer, had the following composition. To determine the efficiency of protein transfer, the PVDF membranes were stained with Ponceau-S stain for 2 mins at RT. Excess Ponceau-S stain was removed by rinsing the PVDF membrane in milli-Q water. Membranes were blocked using either 5% non-fat milk or 5% Bovine Serum Albumin (BSA) (#BP1605, Fischer Scientific), depending on primary antibody vendor instructions, for 1 hr at RT with constant shaking. Both blocking solutions were prepared in 1X Tris Buffered Saline-Tween 20 (1X TBST). Following blocking, membranes were incubated overnight with the appropriate primary antibodies at 4^{o}C with constant shaking. Primary antibodies and their working dilutions are listed in Table 2.3. Both primary antibody and secondary antibody working solutions were prepared by diluting the appropriate volume of primary or secondary antibody in their respective blocking solutions. The following day, membranes were washed with 1X TBST and incubated with their respective secondary antibodies for 1 hr at RT with constant shaking. All secondary antibodies used in this study were conjugated to horse-radish peroxidase enzyme. Secondary antibodies and their working dilutions are listed in Table 2.4. Lastly, the membranes were incubated with the SuperSignal™ West Pico PLUS Chemiluminescent Substrate (#34577, Thermo Fischer Scientific) to enable visualization of protein expression patterns. Protein bands were visualized using the IMAGEQUANT LAS4000 Mini (General Electric, NJ).

2.12 Immunohistochemistry (IHC)

IHC was performed using a standard/routine staining protocol. The only exception, wherein the protocol was modified slightly, was while staining for BrdU. The slight modifications for BrdU immunostaining are mentioned following the description of the standard staining protocol. In brief, tissue sections were deparaffinized and rehydrated using xylene and a series of alcohol solutions with decreasing concentration gradient (100%, 95%, 85%, and 70% alcohol). The antigenicity of target proteins was improved by heat-induced epitope retrieval. Tissue sections were boiled in citrate buffer (10 mM citric acid, 0.05% Tween-20, pH=6.0) for ~20 mins and allowed to cool

gradually. Excess peroxidase activity was quenched with 0.3% hydrogen peroxide (H_2O_2). Quenching step was skipped in the case of immunofluorescence staining which employed a fluorophore-tagged secondary antibody (2^{o}Ab). Following the quenching step, tissue sections were blocked with an appropriate 5% serum solution in 1X Dulbecco's Phosphate Buffered Saline (1X DPBS) with calcium (Ca^{2+}) and magnesium (Mg^{2+}) (#114-059-101, Quality Biological). Subsequently, tissue sections were incubated with the appropriate primary antibody (1^{o}Ab) overnight at 4^{o}C. The next day, excess 1^{o}Ab was washed with 1X phosphate buffered saline (1X PBS) and tissues were treated with the appropriate 2^{o}Ab at RT. Detailed description of the 1^o- and 2^o-Abs used are mentioned in Table Nos. 3 and 4, respectively. In the case of biotin-conjugated 2^{o}Abs, following incubation with 2^{o}Ab, tissue sections were treated with avidin-horse radish peroxidase (HRP) conjugated solution and DAB substrate before being counterstained, dehydrated, and mounted. In the case of fluorophore conjugated 2^{o}Ab, tissue sections were mounted directly using Prolong Gold mounting media containing the DAPI counterstain (#P36962, Invitrogen) following 2^{o}Ab treatment.

BrdU is an analog of the nucleotide, thymidine, and is therefore incorporated into the genomic DNA. In order to improve the accessibility of the anti-BrdU antibody to its antigen, the genomic DNA was subjected to gentle hydrolysis using hydrochloric acid (HCl). After quenching, tissue sections were incubated in 1 N HCl for 10 mins at 56^{o}C. Following this, tissue sections were incubated in sodium borate buffer for 30 mins at RT to neutralize the effects of HCl. Next, tissue sections were washed with 1X PBS before being blocked. Thereafter, further processing of tissues was carried out by following standard protocol. Hematoxylin and Eosin (H&E) staining was performed by the Indiana University Histology Core Facility.

Table 3: **List of primary antibodies (1ºAbs), their dilutions, and applications**

Sr No:	Antibody	Catalog No.	Vendor	Dilution	Application
1	BrdU	5292	Cell Signaling	1:100	IHC-P
2	GFP	ab6673	Abcam	1:200	IHC-P
3	AFP	LS-C123534	Lifespan Biosciences	a) 1:400	IHC-P
				b) 1:1000	WB
4	CD133	PAB12663	Abnova	a) 1:3000	IHC-P
				b) 1:1000	WB
5	EPCAM	50591-R002	Sino Biological	a) 1:1500	IHC-P
				b) 1:1000	WB
6	Ki67	RM-9106-S1	Thermo Scientific	1:100	IHC-P
7	Beta-Catenin	610153	BD Transduction	1:100	IHC-P
8	MST1	3682T	Cell Signaling	1:1000	WB
9	Phospho-MST1	3681S	Cell Signaling	1:1000	WB
10	LATS1	3477T	Cell Signaling	1:5000	WB
11	Phospho-LATS1	9157S	Cell Signaling	1:1000	WB
12	MOB1	13730	Cell Signaling	1:1000	WB
13	Phospho-MOB1	8699	Cell Signaling	1:1000	WB
14	YAP1	14074	Cell Signaling	a) 1:200	IHC-P
				b) 1:1000	WB
15	Phospho-YAP1	4911S	Cell Signaling	1:1000	WB
16	TAZ	72804T	Cell Signaling	1:1000	WB
17	Phospho-TAZ	59971S	Cell Signaling	1:1000	WB
18	GAPDH	5174	Cell Signaling	1:1000	WB
19	Arginase1	93668T	Cell Signaling	1:1000	IHC-P
20	E-Cadherin	3195S	Cell Signaling	1:200	IHC-P
21	CYP1A2	A0062	Abclonal	1:200	IHC-P
22	CYP2E1	A2160	Abclonal	1:1000	IHC-P
23	Glu. Synt.	Sc-376767	Abclonal	1:200	IHC-P

Table 4: List of secondary antibodies (2ºAbs), their dilutions, and applications

Sr No:	Name	Catalog No.	Vendor	Dilution	Application
1	Bovine anti-Goat	sc-2378	Santa Cruz	1:20,000	WB
2	Goat anti-Rabbit	170-6515	Bio-Rad	1:20,000	WB
3	Horse anti-Mouse	BA-2000	Vector Laboratories	1:200	IHC-P
4	Donkey anti-Goat	705-065-147	Jackson ImmunoResearch	1:200	IHC-P
5	Goat anti-Rabbit	111-065-144	Jackson ImmunoResearch	1:200	IHC-P
6	Donkey anti-Mouse	715-585-151	Jackson ImmunoResearch	1:200	IHC-P
7	Donkey anti-Goat	705-545147	Jackson ImmunoResearch	1:200	IHC-P
8	Donkey anti-Rabbit	711-545-152	Jackson ImmunoResearch	1:200	IHC-P
9	Donkey anti-Rabbit	711-585-152	Jackson ImmunoResearch	1:200	IHC-P

2.13 Serum collection and liver function test

Liver function test was performed to determine if YAP1 deletion affected the biosynthetic activity of the maternal liver during gestation. Serum samples were collected from Gd18 $YAP1^{flox/flox}$ and $YAP1^{-/-}$ mice that were previously injected with AAV8-TBG-Null and AAV8-TBG-Cre viral vectors respectively. Mice were anesthetized and blood was extracted from the posterior vena cava. Blood samples were allowed stand and coagulate for 30 mins at RT after which serum was separated by means of centrifugation. Serum samples were sent to Eli Lilly and Company, Indianapolis, USA.

2.14 Statistical Analysis

In this study, we used the ‘one-way ANOVA’ test and the ‘Unpaired Student t-test’ (assuming equal variance) to calculate the p-value and to test for significance. Data obtained was considered statistically significant, in comparison to the control group, when p-value < 0.05. The sample size (“n” value) ranged between 3-5 depending on the experiment. The error bars in the bar-graphs represents standard error of mean (S.E.M).

CHAPTER 3. RESULTS

3.1 Maternal organs exhibit differential gravimetric responses during pregnancy

To begin, we carried out a comprehensive analysis of the gravimetric (weight related) response of the maternal liver during gestation in the C57BL/6J mouse strain. Additionally, we also measured the pregnancy-induced weight responses of the maternal spleen, pancreas, kidneys, heart, and lungs. The gravimetric response of maternal organs was measured as a function of total organ weight and organ-to-body weight ratio. After generating timed pregnancies, mice were sacrificed and the total body- and maternal organ-weights were recorded. Pregnancy-induced gravimetric changes were registered by comparing pregnant maternal organs weights to their respective non-pregnant (NP) counterparts.

We found that, among the maternal organs examined, the maternal liver, spleen, and pancreas showed robust and dynamic gravimetric responses to pregnancy, whereas others remained unaffected (Fig. 4). The maternal liver weight increased progressively, up to 1.7 times heavier than the NP state, during the second half of gestation (Fig. 4A). The maternal liver-to-body weight ratios showed similar increases. Prior to parturition, the proportion of maternal liver enlargement and total body weight gain returned to the NP state (Fig. 4A). Both the maternal spleen weight and the maternal spleen-to-body weight ratio increased between gestation days (Gds)-11 to 15 and returned to the pre-pregnancy levels by the end of pregnancy (Fig. 4B). The maternal pancreas weight showed a slight but significant increase on Gd18 in comparison to the NP pancreas, whereas the maternal pancreas-to-body weight ratio remained unchanged (Fig. 4C). Maternal kidneys, heart, and lungs did not respond gravimetrically to pregnancy (Fig4. 4D-F). That explained decreased maternal kidney-to-body weight ratio when bodyweight gained during later stage of gestation (Fig. 4D). The maternal heart weight and the maternal heart-to-body weight ratio gradually increased and decreased respectively without reaching statistical significance, in line with a previous report [28, 29] (Fig. 4E). The maternal lungs were too small to sensitively affect the organ-to-body weight ratios (Fig. 4F). Together, our results demonstrate that only a subset of maternal organs exhibits growth response to pregnancy with distinct growth patterns, suggesting organ-dependent regulatory mechanisms.

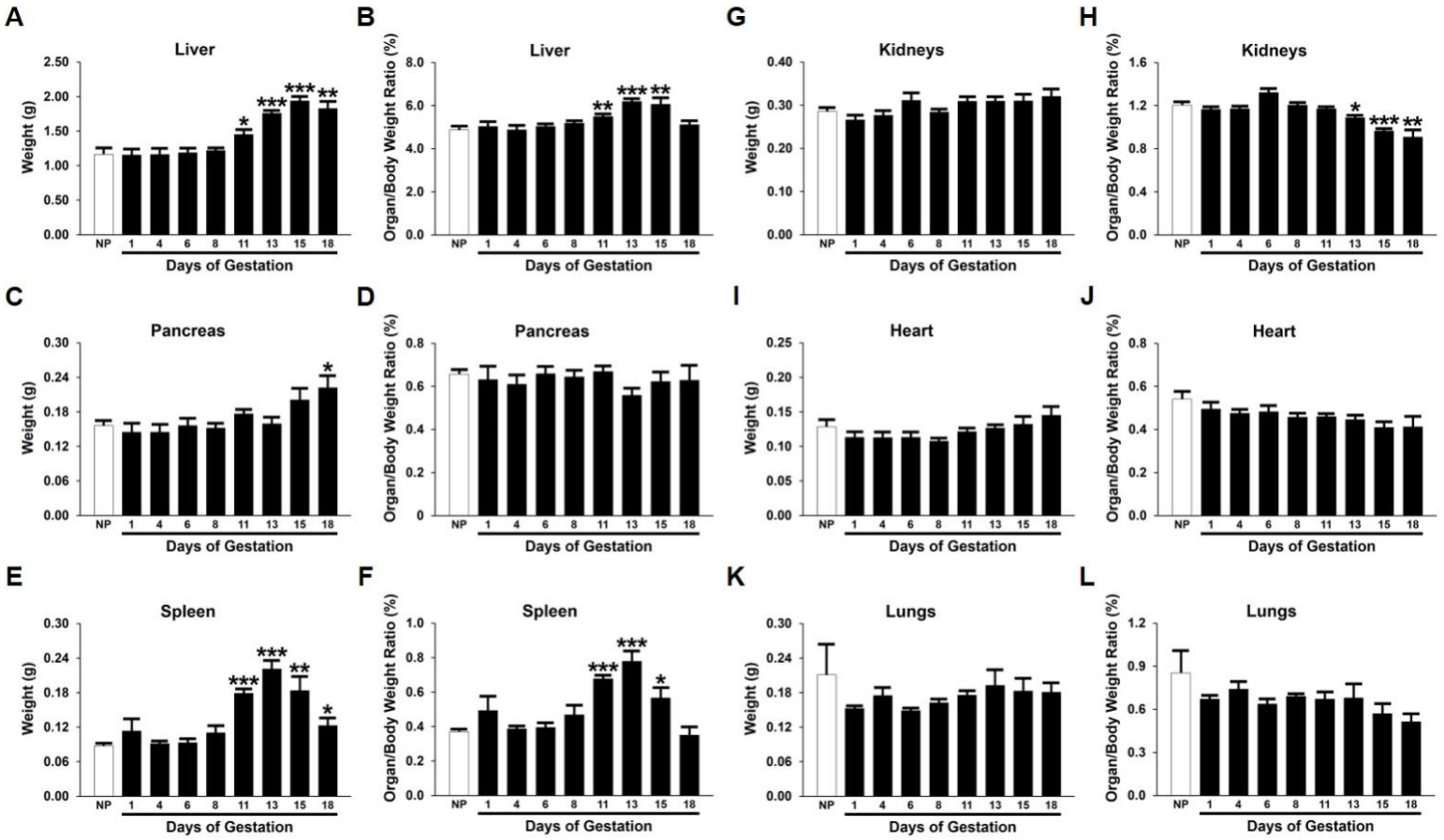

Figure 4: Gravimetric responses of maternal organs during pregnancy.

Timed pregnancies were generated using 3 months-old virgin female and male C57BL/6J mice. Pregnant mice were sacrificed on gestation days indicated above. The total-maternal organ weights and body weights were recorded to measure the pregnancy-induced gravimetric responses. Organs harvested from non-pregnant (NP) female mice served as controls. Shown above are the gravimetric responses of the maternal liver (A), spleen (B), pancreas (C), kidneys (D), heart (E), and lungs (F). Data are expressed as means ± SEM (n=5). * indicates $p < 0.05$; ** $p < 0.01$; *** $p < 0.001$, when compared to the NP state.

3.2 Pregnancy-induced maternal organ growth is accompanied by large-scale cellular DNA synthesis activity

While previous studies have shown that maternal hepatocytes undergo DNA synthesis or S-phase during maternal liver enlargement, the exact number of maternal hepatocytes undergoing the S-phase has not yet been quantified. Furthermore, we also wanted to see if there was a relationship between pregnancy-induced maternal organ enlargement and potential cell proliferation in other maternal organs as well. To determine this, timed pregnancies were generated in C57BL/6J mice. Pregnant C57BL/6J mice were chronically exposed to BrdU from Gd1 up to the day of sample collection. NP mice exposed to the same regime of BrdU for 18 days were used as control. The rate of potential cellular proliferation in NP and pregnant maternal organs was measured by BrdU-immunostaining and quantification of percent change in $BrdU^+$ cells.

We observed that only the maternal organs that exhibited pregnancy-induced gravimetric increases, namely the liver, spleen, and pancreas, displayed a concomitant increase in BrdU-incorporation, indicating S-phase entry and DNA synthesis. In the maternal liver, BrdU-incorporation was seen in the hepatocytes and as pregnancy progressed the percentage of $BrdU^+$ hepatocytes increased progressively in comparison to NP livers and $BrdU^+$ hepatocytes were randomly distributed (Fig. 5A). By the end of pregnancy approximately forty nine percent (~49%) maternal hepatocytes underwent/undergoes DNA synthesis (Fig. 5B). Surprisingly, the maternal pancreas also showed large-scale BrdU-incorporation during pregnancy despite exhibiting only a slight increase in organ weight at the end of gestation (Gd18). BrdU-incorporation in the maternal pancreas increased progressively through gestation and was exhibited by a subpopulation of pancreatic islet cells and acinar cells (Fig. 5C). Compared to NP pancreas, pregnancy led to an approximately thirty-nine (~39%) increase in acinar cell DNA synthesis (Fig. 5D). While the proliferation of maternal pancreatic islet cells during pregnancy has been described previously, our report shows, for the first time, the potential proliferation of the maternal acinar cells. In the maternal spleen, we found that pregnancy led to both, increased BrdU-incorporation and enlargement of the white pulp and red pulp in comparison to the NP spleen. Pregnancy-induced changes in the maternal spleen was estimated by observation and we did not quantify BrdU-incorporation in splenic cells as this was beyond the scope of this report. Since the maternal kidney,

heart, and lung showed no overt differences in BrdU-incorporation during the course of gestation (Fig. 5E), we did not quantify the percentage of $BrdU^+$ cells in the three maternal organs. The above findings indicate that, pregnancy-induced maternal organ enlargement may in-part be an outcome of potential cellular proliferation that is confined to certain organ-specific cellular subtypes.

Figure 5: 5-Bromo-2'-deoxyuridine (BrdU) incorporation in maternal organs.

Timed pregnancies were generated using 3 months-old virgin female and male C57BL/6J mice. Pregnant mice were exposed constantly to BrdU, via drinking water, from gestation day 1 (Gd1) up to the day of sacrifice. Non-pregnant (NP) mice exposed to BrdU for 18 days served as controls. (A) Representative photomicrographs of NP and pregnant maternal livers (Gds-10, 14, & 18) immunostained for BrdU are shown. $BrdU^+$ maternal hepatocytes are stained with dark brown nuclei. (B) Quantification of the percentage of $BrdU^+$ maternal hepatocytes are presented. Data represents mean ±S.E.M (n=3). * indicates $p < 0.05$ when compared to NP livers. (C) Representative photomicrographs of NP and pregnant maternal pancreas (Gds-10, 14, & 18) immunostained for BrdU are shown. $BrdU^+$ maternal acinar cells (indicated by black arrowheads) are stained with dark brown nuclei. (D) Quantification of the percentage of $BrdU^+$ acinar cells in NP and pregnant maternal pancreas. Data represents mean ±S.E.M (n=3). * indicates $p < 0.05$ in comparison to NP mice. (E) BrdU-immunostaining of NP and Gd18 maternal spleen, kidney, heart and lungs. Cells with dark brown stained nuclei are $BrdU^+$. Sample size (n) = 3 mice

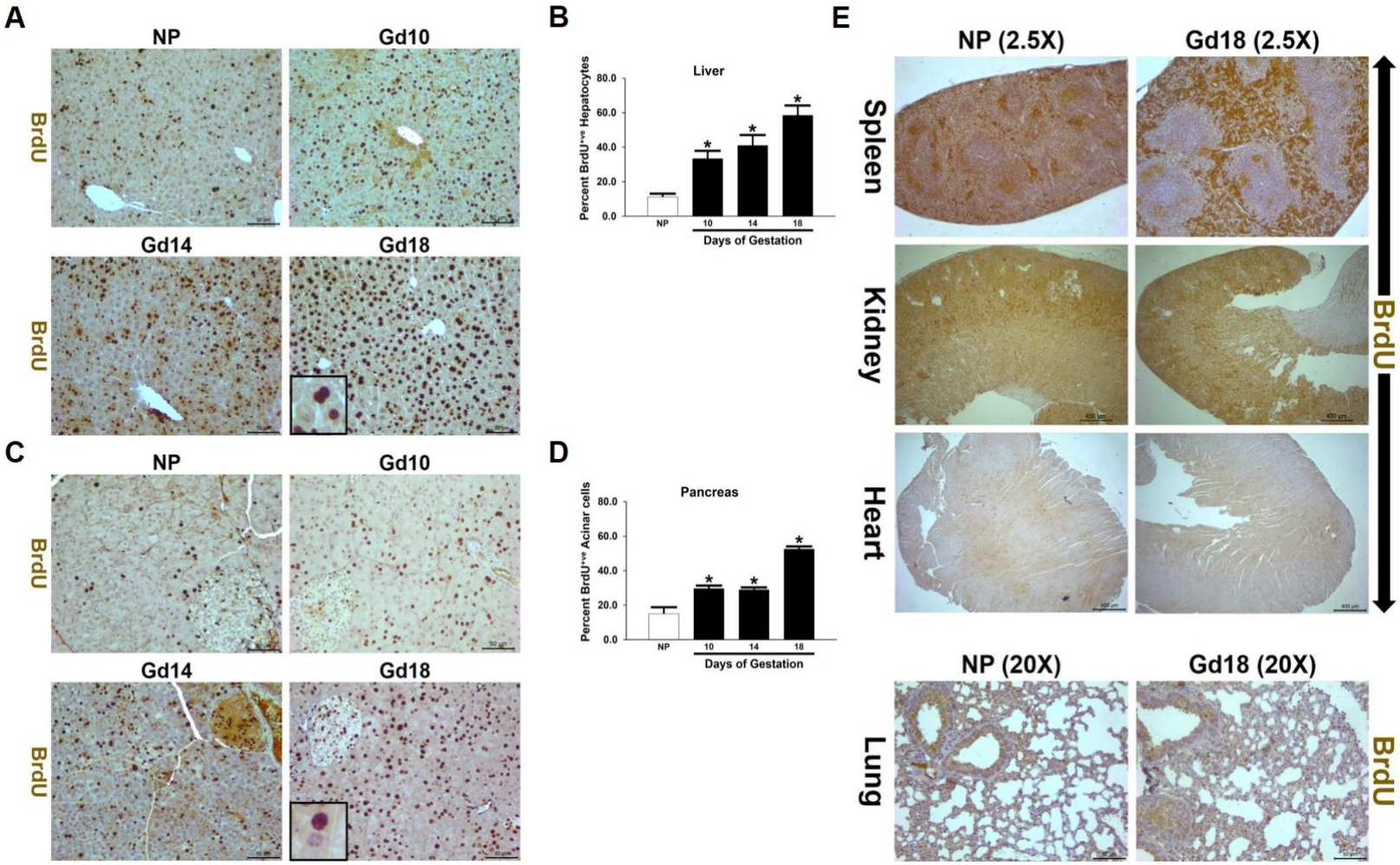
A
NP
Gd10
Gd14
Gd18
BrdU
B
Liver
Percent BrdU+ve Hepatocytes
80.0
60.0
40.0
20.0
0.0
NP
10
14
18
Days of Gestation
C
NP
Gd10
Gd14
Gd18
BrdU
D
Pancreas
Percent BrdU+ve Acinar cells
80.0
60.0
40.0
20.0
0.0
NP
10
14
18
Days of Gestation
E
NP (2.5X)
Gd18 (2.5X)
Spleen
Kidney
Heart
BrdU
NP (20X)
Gd18 (20X)
Lung
BrdU

3.3 During pregnancy, maternal hepatocytes exhibit endoreplication instead of cell division following completion of S-phase

Until recently, it was widely believed that during the process of liver enlargement following 2/3rd PHx, another instance/phenomenon of adult liver enlargement, all hepatocytes completing the S-phase also follow through with the M-phase and undergo cell proliferation. However, a report by Miyaoka et. al showed that only half the hepatocytes undergoing S-phase also follow through with and complete the M-phase while, the remaining hepatocytes undergo endoreplication, that is a state of increased ploidy [59]. In light of this report, we wanted to determine the percentage of hepatocytes undergoing cell division (M-phase) following the completion of S-phase in the pregnant maternal liver.

For this, using NP *RS26*$^{floxstopEYFP/floxstopEYFP}$ mice and the hepatocyte specific AAV8-TBG-Cre viral vector, a small and randomly distributed sub-population of hepatocytes were permanently labelled with EYFP. This sub-population of EYFP^{+} hepatocytes served as a representative population whose proliferative fate could be tracked and measured during the course of gestation. The AAV8-TBG-Cre dosage was optimized such that only individual hepatocytes, in sufficient number, were labelled with EYFP and the cases/instances of two (or more) adjoining hepatocytes being labelled simultaneously was minimal (false positive) (Fig. 6A). One group of pre-labelled mice were then made pregnant and chronically exposed to BrdU from Gd1 to Gd18 while, the other group was kept in the NP condition and exposed to BrdU for 18 days (NP control group). NP and Gd18 maternal livers were collected and co-immunolabelled for EYFP and BrdU to calculate the rate of hepatocyte cell proliferation during pregnancy (Fig. 6A). We hypothesized that if all maternal hepatocytes undergoing the S-phase would complete at least one round of cell division then we should see a significant increase in "mitotic units" in Gd18 maternal livers compared to the NP controls. A "mitotic unit" was comprised of two adjoining EYFP^{+}:BrdU^{+} hepatocytes that represent a pair of daughter cells post cell division (Fig. 6B). Additionally, this observation should also be complimented by an overall increase in paired EYFP^{+} hepatocyte units in Gd18 livers. This additional condition was meant to rule out the effects of false positive "mitotic units" that were a result of two adjoining maternal hepatocytes being simultaneously transfected with the viral vector and becoming EYFP^{+}, rather than from actual cell division.

Before quantifying the extent of maternal hepatocyte hyperplasia during pregnancy we first confirmed that transfecting maternal hepatocytes with the viral vector did not affect their entry into S-phase. To establish this, we quantified the percentage of $EYFP^+$:$BrdU^+$ hepatocytes (out of total EYFP+ hepatocytes) in NP and Gd18 maternal livers and found that viral transfection did not affect S-phase entry. In NP livers ~10% of $EYFP^+$ hepatocytes were $BrdU^+$ whereas in Gd18 maternal livers ~58% $EYFP^+$ hepatocytes were $BrdU^+$ (Fig. 7A), similar to what we observed previously in Section 3.2. Next, we quantified the percentage of "mitotic units" and found that while there was an increase in "mitotic units" between NP and Gd18 maternal livers, the overall percentage (in terms of absolute numbers) of maternal hepatocytes (Gd18) undergoing potential cell division was only ~3.5% (at a maximum) (Fig. 7C). However, to rule out the possibility that the increased "mitotic units" in Gd18 maternal livers was not an outcome of false positive labelling, we quantified the total percentage of paired $EYFP^+$ units in NP and pregnant maternal livers. Our results showed that there was no difference in the percentage of paired $EYFP^+$ hepatocytes between the two states of liver. The overall false positive rate that two hepatocytes were simultaneously transfected with the viral vector was around ~8% in both livers (Fig. 7B). This implies that the increase in "mitotic units" observed earlier was because more false positive pairs of $EYFP^+$ hepatocytes became $BrdU^+$, due to increased S-phase entry in pregnant livers, rather than being a result of cell division. Taken together, our findings strongly suggest that maternal hepatocytes undergoing the S-phase during pregnancy do not undergo cell division. Instead, a sub-population of maternal hepatocytes undergo endoreplication as a mechanism to cope with pregnancy-induced stresses.

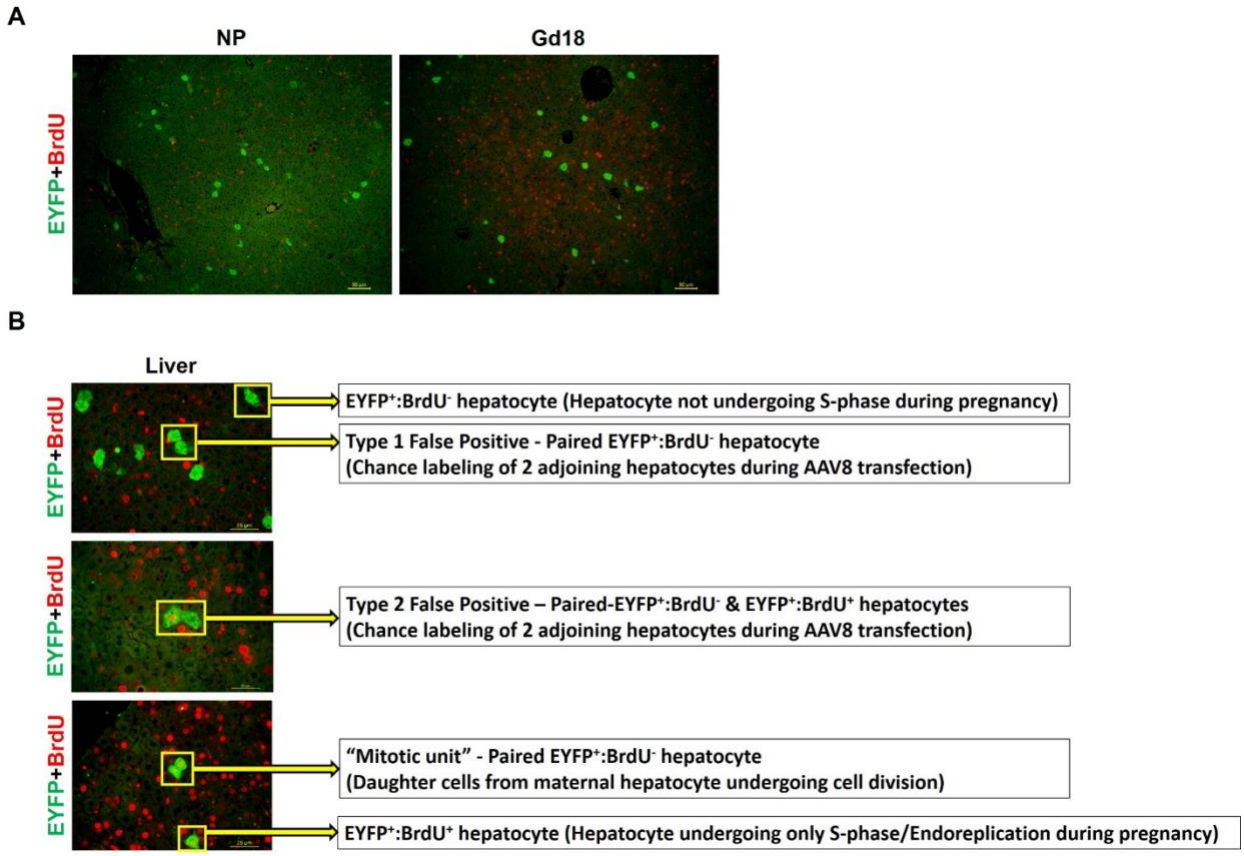

Figure 6: Efficacy of hepatocyte labeling, and different cellular units used to quantify and determine maternal hepatocyte proliferation during pregnancy.

3 months-old virgin Rosa26-EYFP (enhanced yellow fluorescent protein) female mice were injected with the adeno-associated virus 8-thyroxine binding globulin-Cre recombinase (AAV8-TBG-Cre) to permanently label a small representative population of hepatocytes. AAV8-TBG-Cre was administered through hydrodynamic tail vein injection. Following a rest period of one-week, timed pregnancies were generated with one group of AAV8-TBG-Cre mice while the remaining mice were kept in non-pregnant state (NP). Both pregnant and NP groups were chronically exposed to 5-Bromo-2'-deoxyuridine (BrdU), via drinking water, for a duration of 18 gestation days or its equivalent. NP and gestation day 18 (Gd18) livers were collected and co-immunolabelled for EYFP and BrdU to determine percentage of maternal hepatocytes undergoing proliferation after S-phase. (A) Representative photomicrographs of NP and Gd18 maternal livers following hepatocyte labeling and BrdU treatment. Efficacy of hepatocyte labelling, which was a small representative sub-population of individual $EYFP^+$ hepatocytes, can be observed in NP livers. Also, the lack of increase in $EYFP^+$ hepatocytes in Gd18 maternal livers shows the lack of proliferation during pregnancy. (B) Different phenotypes of EYFP-labelled hepatocytes used for quantifying percentage of maternal hepatocytes undergoing hyperplasia during pregnancy. The three ideal hepatocyte phenotypes were as follows: $EYFP^+$:$BrdU^-$ single hepatocytes (hepatocytes not undergoing cell cycle), $EYFP^+$:$BrdU^+$ hepatocytes (hepatocytes undergoing S-phase without M-phase/cell division), adjoining pair of $EYFP^+$:$BrdU^+$ hepatocytes ("Mitotic unit", hepatocytes undergoing cell division post S-phase and form daughter cell pair). In addition to the ideal phenotype, false positive "mitotic unit" phenotypes also occurred and were as follows: two adjoining $EYFP^+$:$BrdU^-$ hepatocytes and two adjoining hepatocytes with $EYFP^+$:$BrdU^-$ and $EYFP^+$:$BrdU^+$ phenotype. False positive "mitotic units" resulted from the chance effect of two adjoining hepatocytes being simultaneously labelled with AAV8 and express EYFP, thus, giving the effect of paired daughter cells.

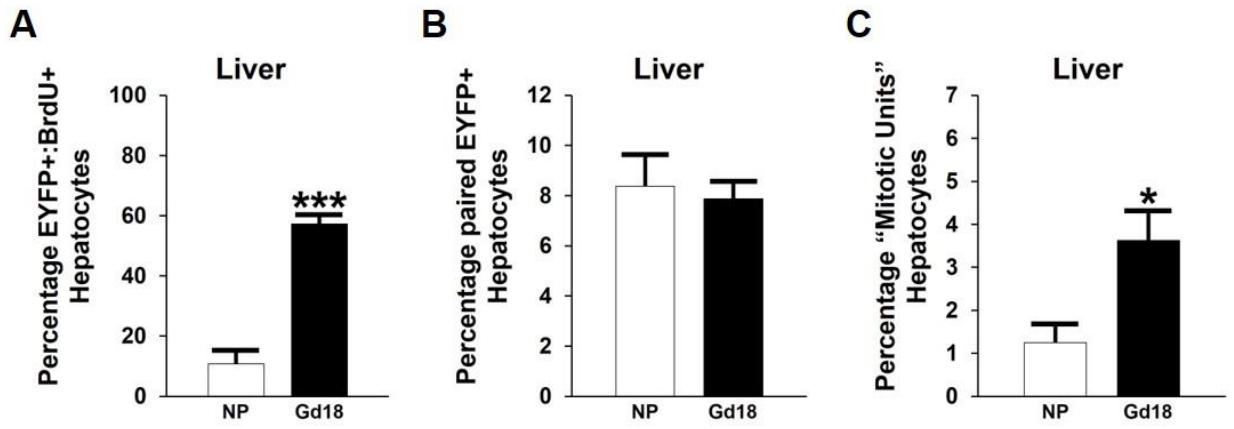

Figure 7: Determining maternal hepatocyte rate of cell division.

Quantification of the percentage of (A) $EYFP^+$:$BrdU^+$ hepatocytes (individual) in the non-pregnant (NP) and gestation day 18 (Gd18) maternal livers. Percentages indicated the proportion of $EYFP^+$ hepatocytes that underwent the S-phase of the cell cycle during a period equivalent (NP state) or equal to 18 days of gestation (Gd18). The parameter was measured to determine whether AAV8 transfection altered the percentage of maternal hepatocytes undergoing the S-phase during gestation. (B) Quantification of the percentage of paired $EYFP^+$ hepatocytes in the NP and Gd18 maternal livers. Paired EYFP+ hepatocytes include false positive units (paired $EYFP^+$:$BrdU^-$ units and pair of $EYFP^+$:$BrdU^+$ and $EFYP^+$:$BrdU^-$ units). Percentages indicated the proportion of two adjacent $EYFP^+$ hepatocytes out of the sub-population of labelled hepatocytes. (C) "Mitotic units" (adjacently located, paired $EYFP^+$:$BrdU^+$ maternal hepatocytes) in NP and Gd18 maternal livers. Percentages indicated the proportion of "mitotic units" out of the subpopulation of $EYFP^+$ hepatocytes. The parameter was used to estimate the percentage of S-phase completing hepatocytes undergoing cell division during pregnancy. Data, in all graphs, indicates mean ±S.E.M (n=3). * indicates $p < 0.05$ and ***$p < 0.001$ compared to the NP state. Abbreviations: EYFP-Enhanced yellow fluorescent protein and BrdU-5-Bromo-2'-deoxyuridine.

3.4 Examination of the proliferative activity of $Axin2^+$ hepatocytes during pregnancy and other physiological conditions

$Axin2^+$ hepatocytes are a sub-population of pericentrally located hepatocytes that are distinguished by their characteristic expression of the AXIN2 protein [22]. A recent report demonstrated that $Axin2^+$ hepatocytes served as the adult "hepatocyte stem cells" as these cells replaced ~35% of pre-existing adult hepatocytes over a duration of one year, under homeostatic conditions [74]. Therefore, we were interested to determine whether $Axin2^+$ hepatocytes repopulated the adult liver during pregnancy and after 2/3rd PHx. To determine fate of adult $AXIN2^+$ hepatocytes during pregnancy and after 2/3rd PHx, we used the bi-transgenic *RS26*$^{floxstopLacZ/floxstopLacZ}$:*Axin2*$^{+/CreERT2}$

mouse strain. This strain enabled us to permanently label Axin2$^+$ hepatocytes and their progeny, resulting from cellular proliferation, with the LacZ reporter.

Before determining the role of Axin2$^+$ hepatocytes following pregnancy and 2/3rd PHx we wanted to establish the occurrence of Axin2$^+$ hepatocytes in adult livers (3-3.5 months-old) under normal homeostatic conditions. For this, male and female mice were administered tamoxifen (100 mg/kg) for five consecutive days and two weeks later the male and female livers were analyzed by LacZ staining (Fig. 8-A & B). We found that Axin2$^+$ hepatocytes were successfully labelled in both male and female livers and as reported earlier, the Axin2$^+$ hepatocytes were located only around the central vein region (Fig. 8-A&B). In this study, the group described above served as the control group and all the results were compared with the observations made in the above group. After establishing the status of Axin2$^+$ hepatocytes under normal conditions we next determined the fate of the cells during the process of pregnancy-induced maternal liver growth. Axin2$^+$ hepatocytes in virgin female mice were pre-labeled by administering tamoxifen once daily for either three (60 mg/kg) or five (100 mg/kg) consecutive days. Following tamoxifen administration, mice were rested for two weeks to facilitate tamoxifen clearance after which timed pregnancies were generated. Post-partum day 2 (Pp2) maternal livers were analyzed by LacZ staining. Our results showed that there was no observable difference in LacZ staining area between the NP (control) female livers and Pp2 maternal livers (Fig. 8E). If Axin2$^+$ hepatocytes underwent significant cell proliferation during pregnancy-induced maternal liver enlargement, we would expect an increase in the area of LacZ staining compared to the control group. However, our results imply that Axin2$^+$ hepatocytes do not undergo cell proliferation during pregnancy.

To discern the fate of Axin2$^+$ hepatocytes following 2/3rd PHx, male and female mice were administered tamoxifen using the same regime and dose as the control group. 2/3rd PHx was performed on pre-labeled male and female mice two-weeks after tamoxifen administration. Livers were analyzed by LacZ staining 25 days post-surgery. We found that the LacZ staining in partially hepatectomized mice (Fig. 8-F & G) was the same as the control group (Fig. 8-A & B). There was no difference in LacZ staining between female and male partially hepatectomized livers (Fig. 8-F & G). This suggested that Axin2$^+$ hepatocytes, regardless of the sex, did not undergo hyperplasia during liver regrowth post 2/3rd PHx.

Since Axin2^{+} hepatocytes failed to repopulate the liver by cell proliferation under both physiological conditions and because our experimental conditions were different from the previous report in terms of the reporter protein (LacZ versus EGFP) and tamoxifen dosage (5 mg/mouse versus 3 mg/mouse), we decided to replicate the findings of the earlier report. Male and female mice were administered tamoxifen to label Axin2^{+} hepatocytes and livers were analyzed one year post labeling. Surprisingly, our results showed that Axin2^{+} hepatocytes did not repopulate 30% of the livers as described previously (Fig. 8-C & D). We found that, once again there was no difference in LacZ staining between control livers, analyzed 14 days after labeling (Fig. 8-A & B), and one-year old livers (Fig. 8-C & D).

Overall, our findings suggest that the processes of pregnancy, 2/3rd PHx, and homeostasis does not stimulate Axin2^{+} hepatocytes to undergo accelerated cell division to repopulate the adult liver.

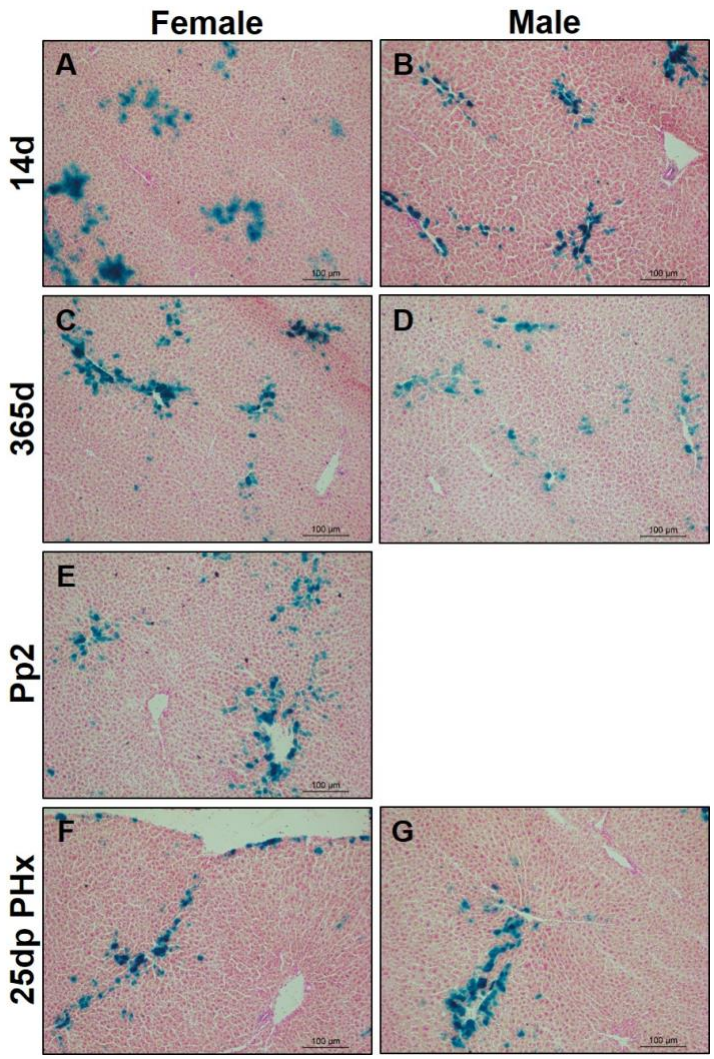

Figure 8: Axin2^{+} hepatocytes did not exhibit expansion by cellular proliferation during pregnancy, 2/3rd partial hepatectomy, and homeostasis.

Homeostasis: Beta-galactosidase (LacZ) staining of female and male livers 14 days (A&B) and 365 days (C&D) post labeling of Axin2^{+} hepatocytes using tamoxifen. Virgin female and male Rosa26$^{+/stopfloxLacZ}$; Axin2$^{+/CreERT2}$ mice, aged 3-3.5 months, were injected tamoxifen (100 mg/kg/mouse) once daily for five consecutive days. Female and male livers were analyzed 14- and 365-days post tamoxifen administration by LacZ staining (n=3). Pregnancy: LacZ staining of post-partum day 2 (Pp2) maternal livers (E). Virgin female Rosa26$^{wt/stopfloxLacZ}$; Axin2$^{wt/CreERT2}$ mice, aged 3-3.5 months, were injected tamoxifen. Timed pregnancies were generated 14 days post tamoxifen administration. Pp2 maternal livers were collected analyzed by LacZ staining (n=2). 2/3rd Partial Hepatectomy (PHx): LacZ staining of female and male livers 25 days post 2/3rd PHx. Mice were administered tamoxifen similar to that mentioned under Homeostasis. 14 days post tamoxifen administration, 2/3rd PHx was performed on female and male mice. Livers from both sexes were analyzed by LacZ staining 25 days post-surgery (n=3). Axin2^{+} hepatocytes are stained blue in color due to the expression of LacZ and are located around the central vein.

3.5 Pregnancy induces dynamic expression of various hepatoblast protein markers in the maternal hepatocytes by post-transcriptional regulation

Preliminary studies revealed that pregnancy induces the expression of CD133, AFP, and EPCAM proteins in the maternal liver during gestation. In the context of the liver, CD133, AFP, and EPCAM are considered as hepatoblast marker proteins expressed during the early embryonic stages of liver development. Hepatoblasts are multi-potent hepatic progenitor cells that eventually give rise to mature hepatocytes and cholangiocytes. Therefore, we wanted to determine the identity of the maternal hepatic cells expressing these markers in-order to determine the potential involvement of the hepatic stem cell compartment in the maternal liver's adaptive response to pregnancy. To do so, we characterized the expression of the *Afp*, *Cd133*, and *Epcam* genes in NP and pregnant maternal livers through gestation. Timed pregnancies were generated using C57BL/6J mice following which NP (control group) and pregnant maternal livers (Gds-1, 4, 6, 8, 11, 13, 15, and 18) were collected from different gestation days. Expression of *Afp*, *CD133*, and *Epcam* genes were characterized by RT-qPCR, ISH, WB, and IHC.

We found that the identity of the hepatic cells that reflected the dynamic expression pattern of CD133, AFP, and EPCAM in the maternal livers during gestation was the hepatocyte. Measurement of the relative mRNA expression of *Cd133*, *Afp*, and *Epcam* showed that among the three markers, only the expression of Cd133 increased during the course of pregnancy. Compared to the NP state, *Cd133* mRNA expression increased progressively and significantly from Gds-6 to 13 following which it returned to NP levels by Gd18 (Fig. 9A). Expression of *Afp* and *Epcam* mRNA either remained the same as the NP level or decreased by a significant extent on specific gestation days. *Afp* mRNA expression was found to decrease on Gds-6 and 18 (Fig. 10A) while, *Epcam* mRNA expression reduced by a significant margin on Gd18 (Fig. 11A). ISH of *Cd133*, *Afp*, and *Epcam* revealed that all three markers were expressed by hepatocytes in both, the NP and pregnant (maternal) livers (Gds-15 and 18). *Cd133* and *Epcam* mRNA (Figs. 9B & 11B, respectively) was expressed by almost all hepatocytes whereas *Afp* mRNA (Fig. 10B) was expressed by a sub-population of hepatocytes. In addition to the hepatocytes, *Cd133* and *Epcam* mRNA (Figs. 9B & 11B, respectively) was also found to be expressed by cholangiocytes, of both NP and pregnant livers, as was expected and reported in other studies. Curiously, in case of the hepatocytes, we found that the mRNA of all three markers were localized within the cell's nuclei,

instead of the cytoplasm. Furthermore, while in the NP state, the mRNA of all three markers was localized in the nuclei (Figs. 9-,10-, & 11-B), on Gds-15 and 18, the transcripts of *Cd133* and *Afp* was found to also be localized in the cytoplasm of a small sub-population of hepatocytes. However, such a phenomenon was not seen in case of *Epcam* transcripts that remained localized in the nuclei, in both conditions (Fig. 11B). To verify the specificity of each probe used for ISH, NP and pregnant liver tissues were simultaneously assayed along with E18 (embryonic day 18) fetal liver and NP heart tissues that were used as positive and negative controls, respectively. As expected, we found that a majority of fetal hepatocytes expressed both Cd133 (Fig. 9B) and Afp mRNAs (Fig. 10B) whereas *Epcam* mRNA was strictly expressed in cells destined to differentiate into cholangiocytes, around the biliary ductal region (Fig. 11B).

The protein expression profile, generated by WB assay of NP and maternal livers, not only confirmed expression of CD133, AFP, and EPCAM at the protein level, but also, further elucidated their expression pattern throughout gestation (Fig. 9C). In the NP livers, EPCAM protein was found to be expressed whereas CD133 and AFP showed either a barely detectable level or no expression, respectively (Fig. 9C). During gestation, CD133 expression was induced from Gd1 and increased gradually to a substantial level by the end of pregnancy (Fig. 9C). Robust expression of AFP was induced from Gd11 that lasted to the end of pregnancy. Contrarily, the expression of EPCAM was found to decrease considerably from Gds-6 to 15 and returned to its NP levels by Gd18 (Fig. 9C). Lastly, results of the immuno-histological characterization of CD133, AFP, and EPCAM further corroborated the above findings. In the NP condition, CD133 was expressed only by cholangiocytes (Fig. 9D). AFP was not expressed by any hepatic cell type (Fig. 10C). And, surprisingly, we found EPCAM to not only be expressed by cholangiocytes, but, also by a subset of hepatocytes around the central vein (CV) (Fig. 11C). Additionally, we also noticed that while EPCAM was localized to the plasma membrane of cholangiocytes, within hepatocytes, the protein was localized in the cytoplasm (Fig. 11C). The expression pattern of EPCAM was surprising because, until now, this protein was only believed to be expressed by cholangiocytes of the liver. In the maternal livers, CD133 was expressed by a large population of hepatocytes and the intensity of protein expression increased from Gd15 to Gd18 (Fig. 9C). Likewise, we observed that AFP was also expressed by a sub-population of hepatocytes in both Gd15 and Gd18 maternal livers (Fig. 10C). The expression of AFP by maternal hepatocytes is another novel finding of this study because, according to literature surveys, it is widely believed that AFP is only expressed by the

developing fetal hepatocytes and not by maternal hepatocytes. And lastly, although EPCAM expression in maternal cholangiocytes remained unaffected during gestation, we noticed a significant decrease in maternal hepatocyte expression on Gd15; followed by a switch in expression from peri-central to the peri-portal hepatocyte subpopulation by the end of gestation (Gd18) (Fig. 11C). This observation was particularly remarkable as it suggests that pregnancy could be a unique physiological process that could permanently alter the spatial (zonal) expression of specific hepatic cell markers.

Taken together, our data shows that pregnancy induces a dynamic expression of CD133, AFP, and EPCAM proteins in the maternal liver. However, contrary to our expectation, the expression of these three factors occurs within the maternal hepatocytes, rather than due to their activation within the hepatic stem cell compartment during pregnancy. Furthermore, our results also show that the maternal hepatocytes regulate the expression of these three specific markers by a unique mechanism that, to the best of our knowledge, has never been seen before in the liver. In the case of *Cd133* and *Afp*, maternal hepatocytes regulate the protein expression of the two factors through the spatiotemporal localization or restriction of their respective transcripts within the hepatocyte nuclei during gestation. While, in the case of *Epcam*, hepatocytes appeared to regulate the expression of this protein marker in a spatiotemporal manner that was dependent on hepatic zonation.

Figure 9: Characterization of *Cd133* gene expression in non-pregnant (NP) and pregnant maternal livers.

Timed pregnancies were generated using 3-3.5 months-old virgin female and male C57BL/6J mice. NP and pregnant maternal livers [gestation days (Gds)-1, 4, 6, 8, 11, 13, 15, & 18] were collected and analyzed using various assays to characterize Cd133 gene expression. (A) RT-qPCR assay measuring the relative *Cd133* mRNA expression in NP and pregnant maternal livers (Gds-1, 4, 6, 8, 11, 13, 15, & 18). The data indicates mean ±S.E.M (n=5). * represents $p < 0.05$ and ** $p < 0.01$, compared to NP livers. (B) Photomicrographs representing *Cd133* mRNA in situ hybridization of NP, pregnant maternal livers (Gds-15 & 18), E18 (embryonic day 18) fetal liver (positive control), and NP heart (negative control). *Cd133* mRNA, indicated by brown colored spots, were observed in the nucleus and cytoplasm of hepatocytes. Scale bar denotes 20 µm. (C) Western blot analysis of NP and pregnant maternal livers (Gds-1, 4, 6, 8, 11, 13, 15, & 18). Loading samples were prepared from total protein lysates. Proteins detected include CD133, AFP, EPCAM, and GAPDH. GAPDH served as the internal loading control. (D) Photomicrographs representing CD133 immunostaining of NP liver, pregnant maternal livers (Gds-15 & 18), and E18 fetal liver (positive control tissue). Hepatocytes with dark brown stained cytoplasm express AFP. Scale bar denotes 25 µm

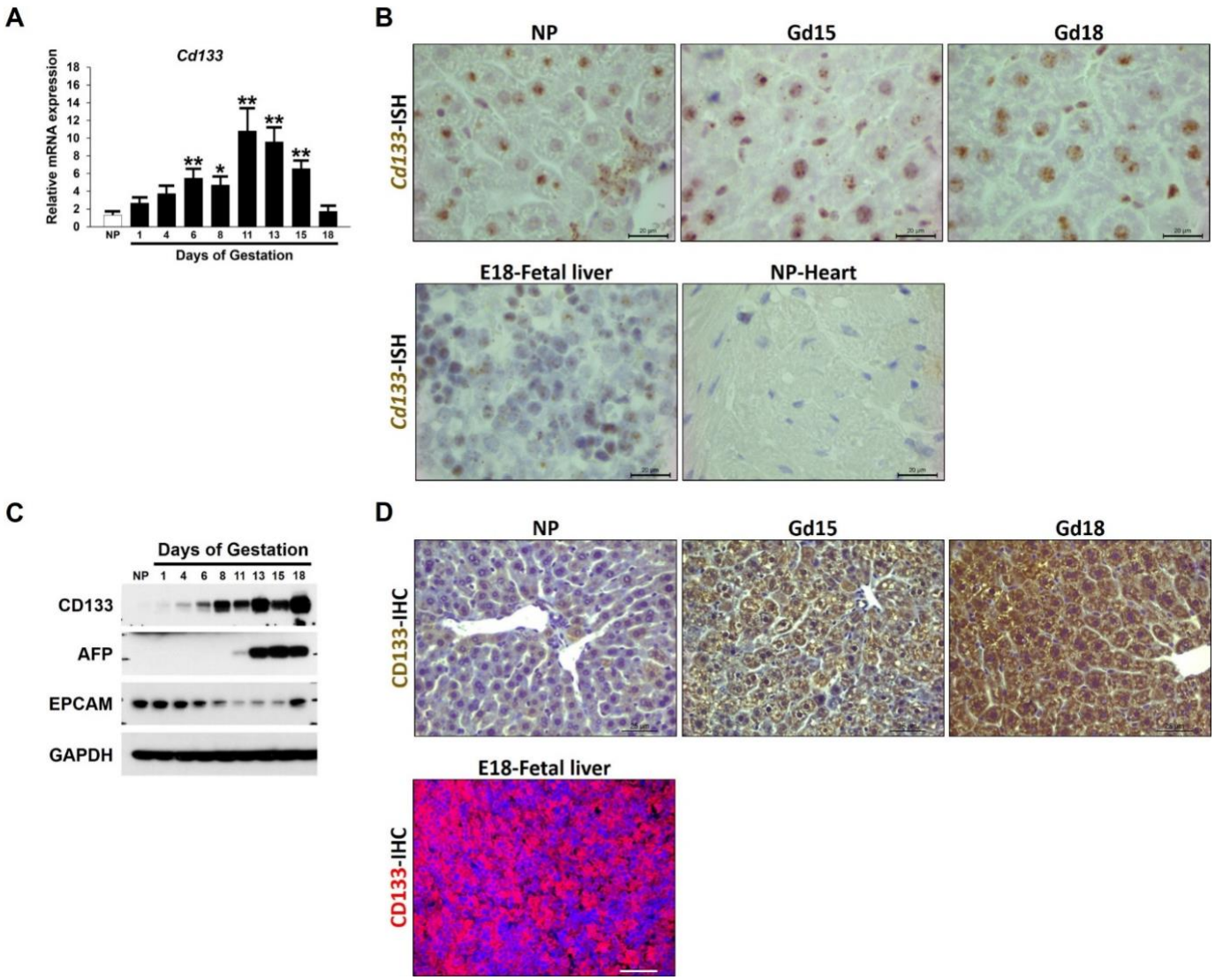
A
Cd133
Relative mRNA expression
Days of Gestation
NP
1
4
6
8
11
13
15
18
B
NP
Gd15
Gd18
Cd133-ISH
E18-Fetal liver
NP-Heart
C
Days of Gestation
CD133
AFP
EPCAM
GAPDH
D
CD133-IHC
E18-Fetal liver

Figure 10: Characterization of *Afp* gene expression in non-pregnant (NP) and pregnant maternal livers.

(A)RT-qPCR assay measuring the relative *Afp* (alpha-fetoprotein) mRNA expression in NP and pregnant (gestation days-1, 4, 6, 8, 11, 13, 15, & 18). The data indicates mean ±S.E.M (n=5). * represents $p < 0.05$ and ** $p < 0.01$, when compared to NP livers. (B) (embryonic day 18) fetal liver (positive control), and NP heart (negative control). *Afp* mRNA, indicated by brown colored spots, were observed in the nucleus and cytoplasm of hepatocytes. Scale bar denotes 20 µm. (C) Photomicrographs representing AFP immunostaining of NP, pregnant maternal livers (Gds-15 & 18), and E18 fetal liver (positive control tissue). Cells with dark brown stained cytoplasm express CD133. Scale bar denotes 25 µm.

A
Afp
Relative mRNA expression
2.5
2.0
1.5
1.0
0.5
0.0
NP
1
4
6
8
11
13
15
18
Days of Gestation
B
NP
Gd15
Gd18
Afp-ISH
E18-Fetal liver
NP-Heart
Afp-ISH
C
NP
Gd15
Gd18
AFP-IHC
E18-Fetal liver
AFP-IHC

Figure 11: Characterization of *Epcam* gene expression in non-pregnant (NP) and pregnant maternal livers.

(A) RT-qPCR assay measuring the relative *Epcam* (epithelial cell adhesion molecule) mRNA expression in NP and pregnant (gestation days-1, 4, 6, 8, 11, 13, 15, & 18). The data indicates mean ±S.E.M (n=5). ** represents $p < 0.01$ and ***$p < 0.001$, compared to NP livers. (B) Photomicrographs representing in situ hybridization probing for *Epcam* mRNA in NP, pregnant maternal livers [gestation days (Gds)-15 & 18], E18 (embryonic day 18) fetal liver (positive control), and NP heart (negative control). *Epcam* mRNA, indicated by brown colored spots, was observed in the nucleus of hepatocytes as well as cholangiocytes/biliary epithelial cells (positive control) around the bile duct. Scale bar denotes 20 µm. (C) Photomicrographs representing EPCAM immunostaining of NP liver, pregnant maternal livers (Gds-15 & 18), and E18 fetal liver (positive control tissue). Cells stained with dark brown color express EPCAM. Scale bar denotes 25 µm. Abbreviations: BD - Bile duct; PT - Portal triad; and CV - Central vein.

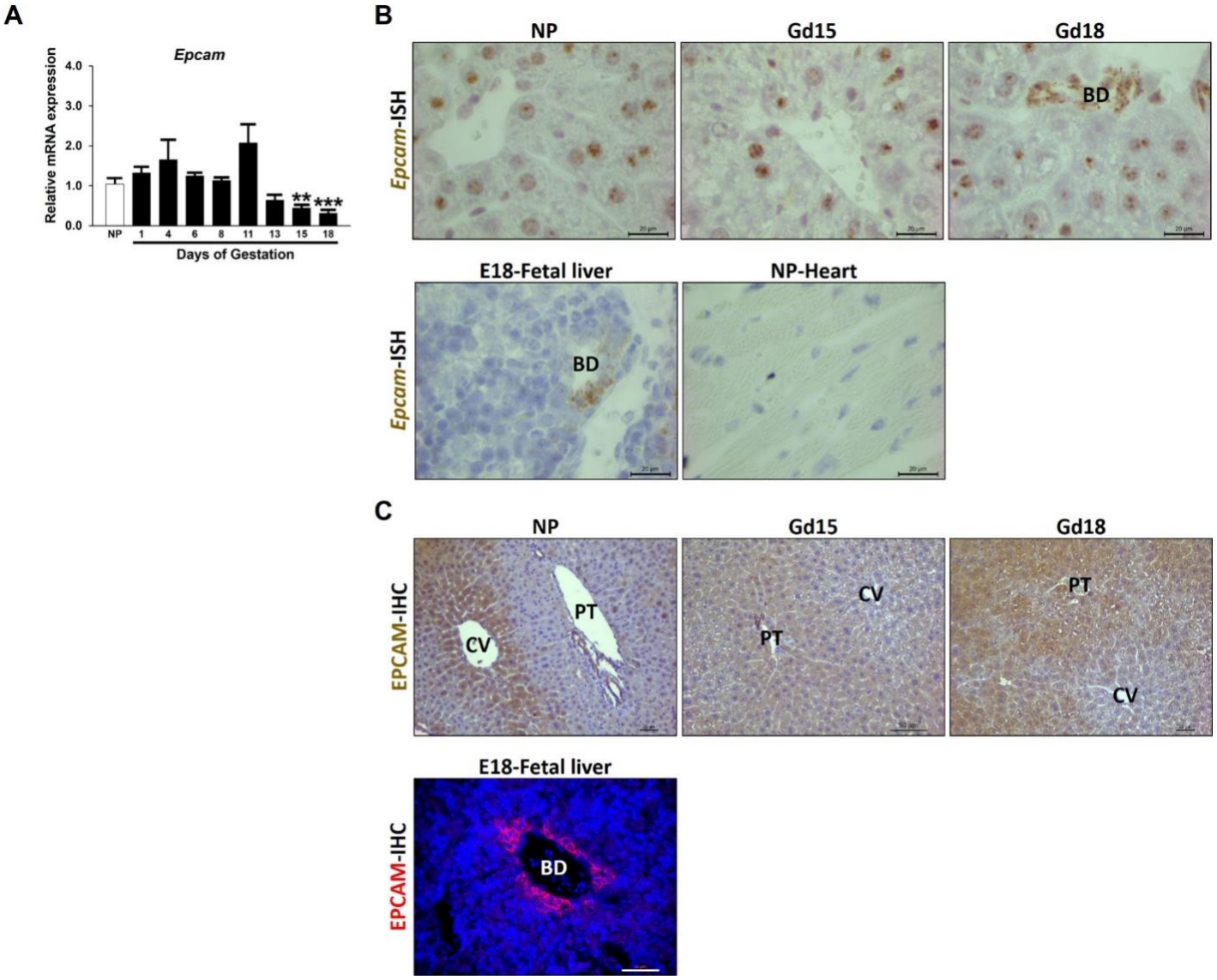
A
Epcam
Relative mRNA expression
4.0
3.0
2.0
1.0
0.0
**
***
NP
1
4
6
8
11
13
15
18
Days of Gestation
B
NP
Gd15
Gd18
Epcam-ISH
BD
E18-Fetal liver
NP-Heart
Epcam-ISH
BD
C
NP
Gd15
Gd18
EPCAM-IHC
CV
PT
CV
PT
PT
CV
E18-Fetal liver
EPCAM-IHC
BD

3.6 Metabolic zonation pattern of maternal livers does not undergo overt and permanent changes during the course of gestation

In the previous section, we observed that, pregnancy resulted in the switching of EPCAM expression from peri-central to peri-portal hepatocytes by the end of gestation. This observation led us to investigate whether pregnancy could also lead to changes in the metabolic zonation patterns of the maternal liver. To investigate the potential pregnancy-induced changes in hepatic metabolic zonation, liver tissues were collected from NP and pregnant (Gds-15 and 18) mice of the C57BL/6J strain and processed for immuno-histochemical analysis. To visualize the potential pregnancy-induced changes in metabolic zonation patterns, liver tissues were immuno-labelled for the well-known hepatic metabolic zonation markers namely, Arginase 1, CYP1A2, CYP2E1, E-Cadherin, and GS.

Our results showed that, for all five markers tested, the overall metabolic zonation pattern of both maternal livers (Gds-15 & 18) were the same as that in NP livers (Fig. 12). The only zonation marker that showed a noticeable, but slight, change in its expression during pregnancy was CYP1A2. The expression patterns of the marker protein described hereafter was applicable to both NP and pregnant conditions. As has been described in various other studies, we found that Arginase1 and CYP2E1 were expressed by both Zone 1 and Zone 2 hepatocytes and absent in Zone 3 hepatocytes. CYP1A2 was expressed by both Zone 3 and Zone 2 hepatocytes albeit, with differing intensities. Zone 3 hepatocytes expressed CYP1A2 more strongly compared to Zone 2 hepatocytes. However, while the zonation pattern of CYP1A2 in all three livers (NP, Gd15, & Gd18) remained the same, we noticed an overall temporary decrease in marker expression within Gd15 maternal livers that reverted to NP levels by Gd18. This suggests that, during gestation, the maternal hepatic CYP1A2 expression level decreases but returns to normal by the end of it. GS was expressed by a specific subpopulation of Zone 3 hepatocytes that immediately surrounded the central vein. And E-cadherin was expressed on the plasma membrane of Zone 1 hepatocytes. Unlike in the case of EPCAM, we found that none of the five metabolic zonation markers underwent a zonal switch in their respective expression.

On the whole, our data suggests that pregnancy does not lead to overt and permanent changes in the metabolic zonation pattern of the maternal liver. Potential changes that could occur in the zonation patterns may be specific and restricted to only a few markers, as was seen previously in the case of EPCAM. This implies that the maternal liver tries to maintain most of its metabolic functions while simultaneously undergoing physiological adaptations to cope with the demands of pregnancy.

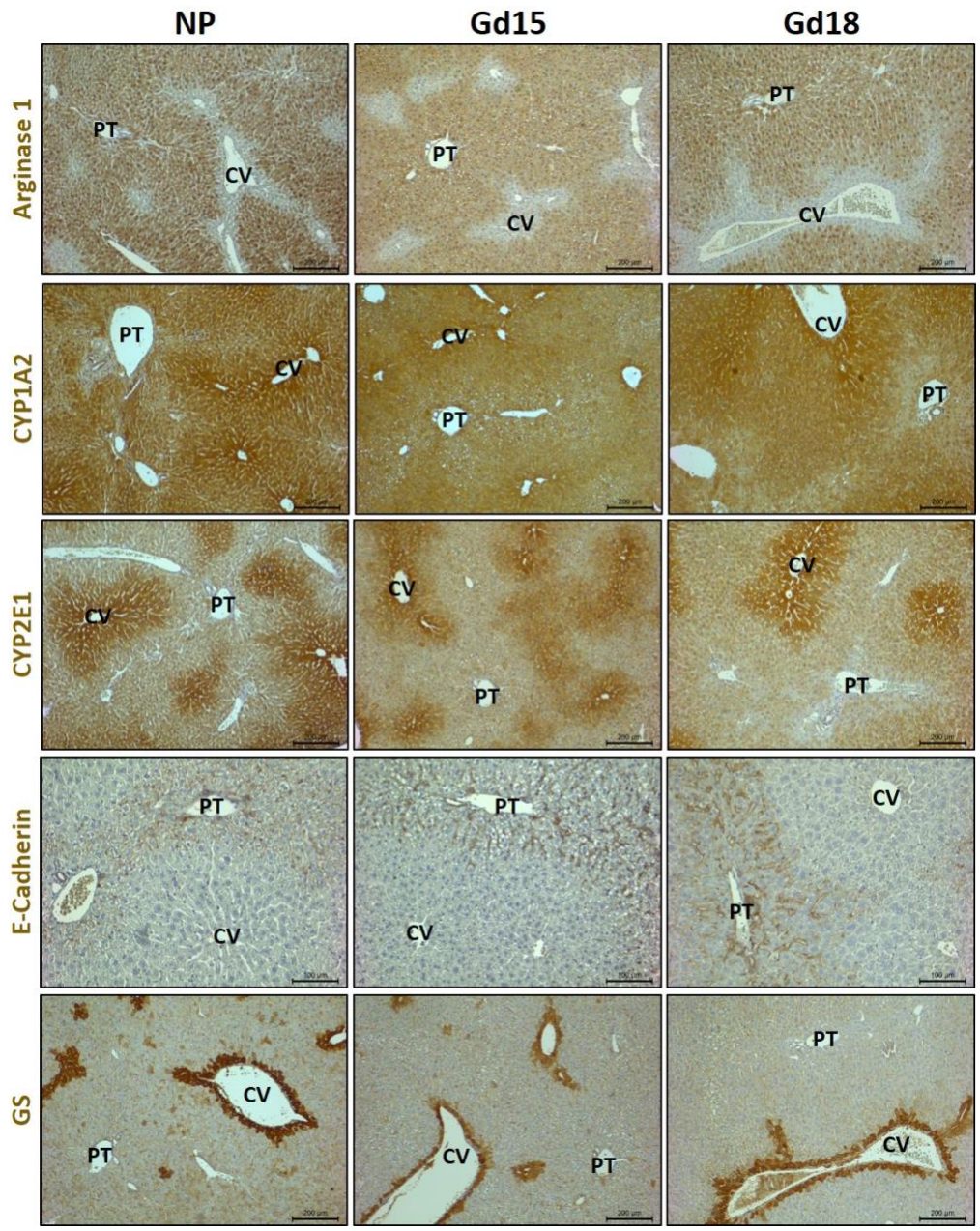

Figure 12: Changes in the maternal hepatic metabolic zonation patterns during gestation.

Non-pregnant and pregnant maternal livers [gestation days (Gds)-15 & 18] were collected after generating timed pregnancies using 3-3.5 months-old virgin female and male C57BL/6J mice. Liver tissue samples were processed for immuno-histological analysis. Pregnancy-induced changes in metabolic zonation patterns were elucidated by immuno-labeling liver tissue samples with five representative zonation marker proteins namely, Arginase 1, CYP1A2, CYP2E1, E-Cadherin, and Glutamine synthetase (GS). Shown above are representative photomicrographs of NP, Gd15, and Gd18 livers stained with the aforementioned markers. Abbreviations: PT - Portal triad and CV - Central vein.

3.7 Activity status of hippo pathway remains unchanged during pregnancy-induced maternal liver growth

The hippo pathway is an important signal transduction pathway that is known to regulate organ growth. Therefore, we wanted to determine if the hippo pathway played a role in controlling pregnancy-induced maternal liver growth. To determine the activity status of the hippo pathway in the maternal liver throughout gestation, we used the C57BL/6J mouse strain. NP and pregnant maternal livers (Gds-8, 15, and 18) were assayed by WB and RT-qPCR. WB assay was used to determine the activation or inactivation of various protein components of the hippo pathway. RT-qPCR was used to determine the activation of canonical target genes of YAP1 namely, *Ctgf* and *Notch2*.

Our results indicated that the overall activity status of the different cytoplasmic and nuclear components of the hippo pathway remained the same as that in NP livers and did not change throughout gestation (Fig. 13). In the case of the cytoplasmic components, WB analysis and quantification of relative protein expression showed that the levels of phospho-MST1 (pMST1), (total) LATS1, pLATS1, (total) TAZ, and pTAZ remained unchanged between NP and pregnant maternal livers (Gds-8, 15, and 18) (Fig. 13-A, B, C, & E). The relative protein expressions of (total) MST1, (total) YAP1, and pYAP1 decreased significantly by about ~quarter-fold (~0.25X) only on Gd18, in comparison to the NP state (Fig. 13-A, B & D). However, since the phosphorylated/total (p/t) protein ratios of MST1, LATS1, YAP1, and TAZ remained unchanged between the NP and pregnant liver states (Fig. 13-B to E), this suggested that the overall activity status of the cytoplasmic components of hippo pathway was unaffected during pregnancy. Analysis of the hippo pathway nuclear components further validated the above results. The relative protein expression of nuclear YAP1 and TAZ, compared to NP livers, remained unchanged throughout gestation (Fig. 14-A, B, & C). Measurement of the relative transcript levels of *Ctgf* and *Notch2* in the NP and pregnant maternal livers (Gds-1, 4, 6, 8, 11, 13, 15, and 18) revealed that the expression of both YAP1 target genes remained mostly unaffected throughout the course of gestation. The *Ctgf* transcript levels during the course of gestation remained the same as the NP state (Fig. 14D). *Notch2* mRNA levels for the first half of pregnancy remained the same as the NP levels but decreased significantly during the second half of pregnancy (Fig. 14E).

Taken together, our data shows that the activation status of the hippo pathway and YAP1 in the maternal liver is unaffected during the process of pregnancy-induced maternal liver enlargement. This strongly suggests that the hippo pathway is not involved in regulating pregnancy-induced maternal liver growth via the pathway's canonically established mechanism.

Figure 13: **Activation status of the cytoplasmic components of hippo pathway.**

Timed pregnancies were generated using 3-3.5 months-old virgin female and male C57BL/6J mice. Non-pregnant (NP) and pregnant maternal livers [gestation days (Gds)-11, 15, & 18] were collected and cytoplasmic protein extracts/lysates were prepared. (A) Western blotting analysis of the cytoplasmic components of hippo pathway. Western blotting was performed using the cytoplasmic protein extracts to analyze expression of proteins mentioned above. Sample size (n) was 3 per group. GAPDH served as the internal loading control. (B-E) Quantification of relative protein expression of cytoplasmic components of the hippo pathway. (Panel B) Relative protein expression of total mammalian STE20 family kinase 1 (MST1), phospho-MST1 (pMST1), and ratio of phospho-/total-MST1 (p/t-MST1), during gestation. (Panel C) Relative protein expression of total large tumor suppressor kinase 1 (LATS1), phospho-LATS1 (pLATS1), and ratio of phospho-/total-LATS1 (p/t-LATS1). Serine 909 (S909) represents the phosphorylation site of pLATS1. (Panel D) Relative protein expression of total yes-associated protein 1 (YAP1), phospho-YAP1 (pYAP1), and ratio of phospho-/total-YAP1 (p/t-YAP1), during gestation. Serine 127 (S127) represents the phosphorylation site of pYAP1. (Panel E) Relative protein expression of total tafazzin (TAZ), phospho-TAZ (pTAZ), and ratio of phospho-/total-TAZ (p/t-TAZ), during gestation. Quantification was done using ImageJ software. Relative fold change was calculated after normalizing samples to GAPDH. Data, in above graphs, indicate mean ±S.E.M (n=3). * represents $p < 0.05$ compared to NP livers.

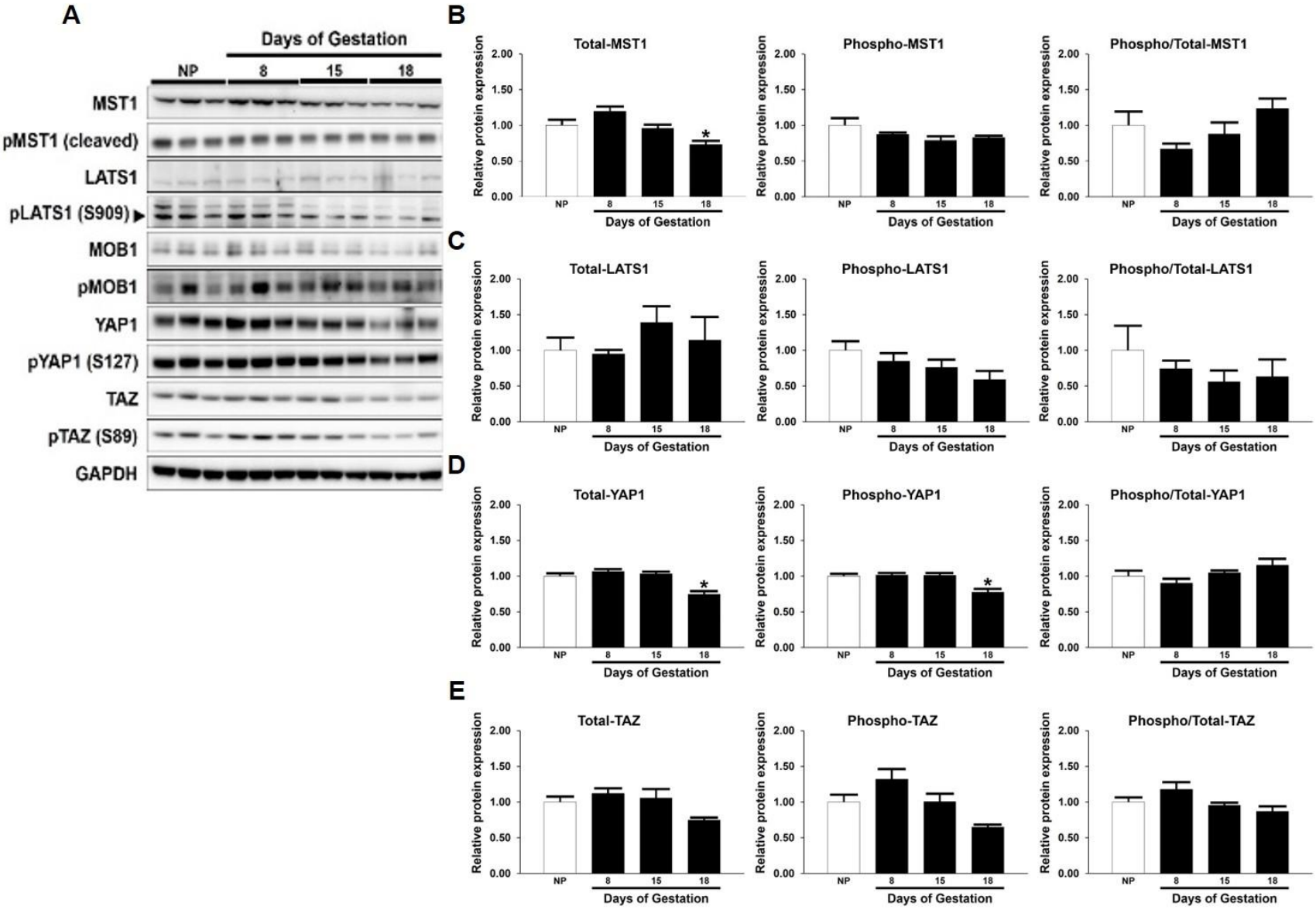
A
Days of Gestation
NP
8
15
18
MST1
pMST1 (cleaved)
LATS1
pLATS1 (S909)
MOB1
pMOB1
YAP1
pYAP1 (S127)
TAZ
pTAZ (S89)
GAPDH
B
Total-MST1
Phospho-MST1
Phospho/Total-MST1
C
Total-LATS1
Phospho-LATS1
Phospho/Total-LATS1
D
Total-YAP1
Phospho-YAP1
Phospho/Total-YAP1
E
Total-TAZ
Phospho-TAZ
Phospho/Total-TAZ
Relative protein expression
2.00
1.50
1.00
0.50
0.00
NP
8
15
18
Days of Gestation
*

Figure 14: Activation status of nuclear components of the hippo pathway.

3-3.5 months-old C57BL/6J mice were used to generate timed pregnancies. Non-pregnant (NP) and pregnant maternal livers [gestation days (Gds)-11, 15, & 18] were collected and nuclear protein lysates were prepared. (A) Western blotting analysis of the nuclear components of the hippo pathway. The nuclear-yes-associated protein 1 (YAP1) and tafazzin (TAZ) levels were measured during gestation to determine the cytoplasmic-to-nuclear translocation of the two hippo pathway effectors. Total nuclear protein was stained using ponceau S stain and served as internal loading control. Sample size (n) was 3 per group. (B & C) Quantification of relative protein expression of nuclear-YAP1 and TAZ during pregnancy. Quantification was done using ImageJ software. Relative fold change was calculated after normalizing samples to total nuclear protein. Data indicates mean ±S.E.M (n=3). Relative YAP1 expression was compared to NP livers. (D & E) Measuring the activation of hippo pathway target genes. The relative mRNA expression of (D) connective tissue growth factor (*Ctgf*) and (E) *Notch2* were measured in the maternal livers throughout gestation. Total mRNA was extracted from NP and pregnant maternal livers (Gds-1, 4, 6, 8, 11, 13, 15, & 18), of the C57BL/6J mouse strain, in order to perform RT-qPCR assay. *Ctgf* and *Notch2* are well known target genes of the hippo pathway. Data represents the mean ±S.E.M (n=5). * denotes $p < 0.05$; ** $p < 0.01$; *** $p < 0.001$, in comparison to the NP condition.

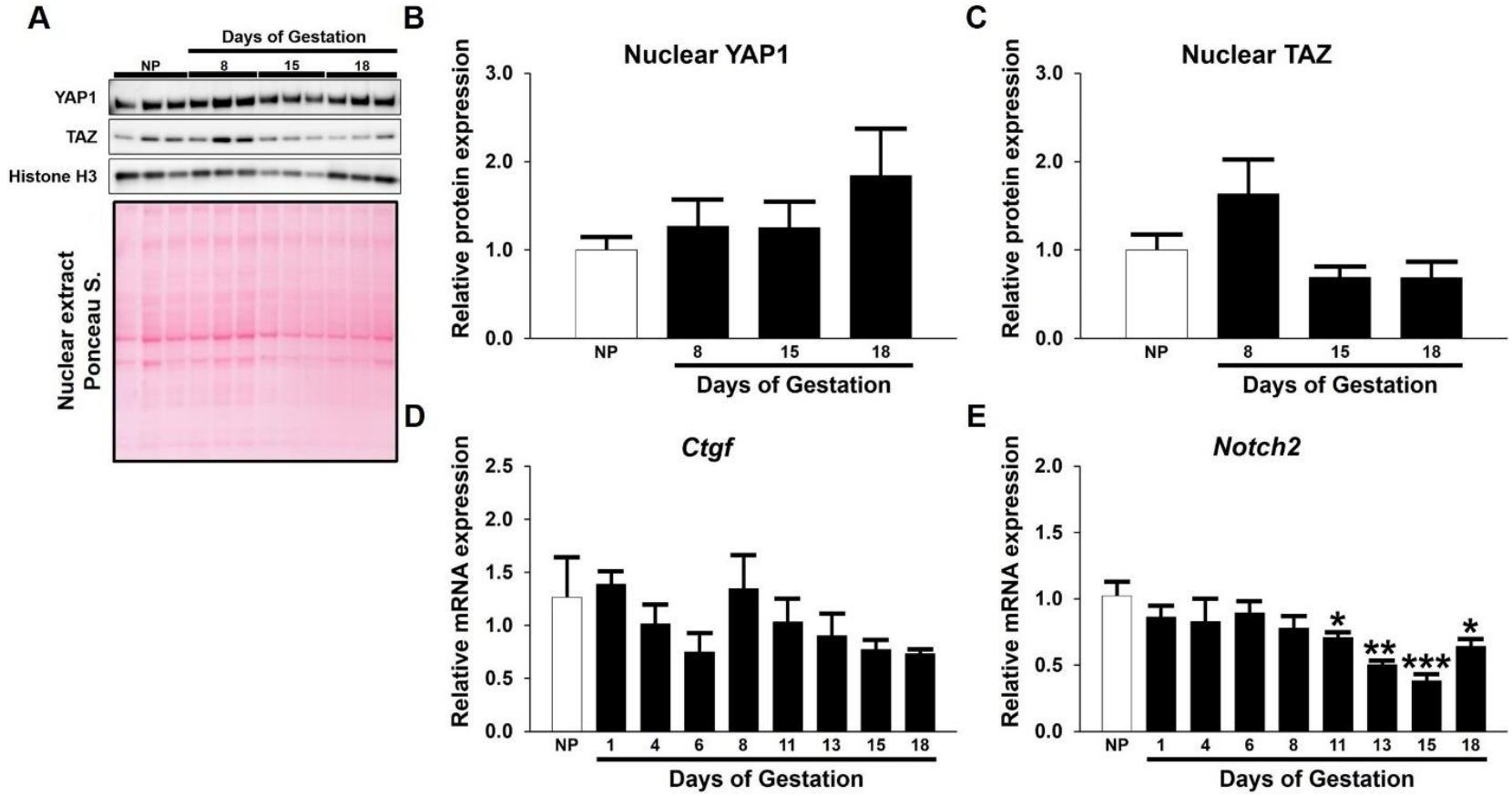
A
Days of Gestation
NP
8
15
18
YAP1
TAZ
Histone H3
Nuclear extract
Ponceau S.
B
Nuclear YAP1
Relative protein expression
3.0
2.0
1.0
0.0
NP
8
15
18
Days of Gestation
C
Nuclear TAZ
Relative protein expression
3.0
2.0
1.0
0.0
NP
8
15
18
Days of Gestation
D
Ctgf
Relative mRNA expression
2.5
2.0
1.5
1.0
0.5
0.0
NP
1
4
6
8
11
13
15
18
Days of Gestation
E
Notch2
Relative mRNA expression
2.0
1.5
1.0
0.5
0.0
*
**
***
*
NP
1
4
6
8
11
13
15
18
Days of Gestation

3.8 Effects of maternal hepatocyte specific YAP1 deletion on various aspects of pregnancy-induced maternal liver adaptations and physiology

3.8.1 Mid-gestational maternal hepatocyte specific YAP1 deletion does not affect pregnancy-induced maternal liver enlargement

Contrary to our expectations, our findings strongly suggest that the hippo pathway, and specifically YAP1, does not play a canonical role in regulating maternal liver enlargement during gestation. To further validate this finding, we decided to study the effects of maternal hepatocyte specific YAP1 knockout (KO) on pregnancy-induced maternal liver growth. Maternal hepatocyte specific YAP1 deletion was achieved by using the *Yap1*$^{flox/flox}$ mouse strain in combination with the hepatocyte specific AAV8-TBG-Cre vector. Timed pregnancies were generated using *Yap1*$^{flox/flox}$ mice and pregnant mice were injected with either the AAV8-TBG-null (*Yap1*$^{f/f}$ control group) or AAV8-TBG-Cre (*Yap1*$^{-/-}$ KO group) on Gd7. Pregnant mice from both groups were sacrificed on Gd18 and various analysis were performed to establish the effects of YAP1 deletion on maternal liver growth.

Before studying the effects of YAP1 deletion on maternal liver growth, we first confirmed the successful deletion of *Yap1* gene from maternal hepatocytes. For this, we first measured and compared the *Yap1* gene transcript levels in *Yap1*$^{f/f}$ and *Yap1*$^{-/-}$ maternal livers (Gd18) (Fig. 15A). We found there was a significant reduction in the *Yap1* transcript levels in the *Yap1*$^{-/-}$ maternal livers compared to the *Yap1*$^{f/f}$ controls. Next, to establish maternal hepatocyte specific YAP1 protein deletion we performed WB and IHC assays using *Yap1*$^{f/f}$ and *Yap1*$^{-/-}$ maternal livers (Gd18). WB analysis showed that YAP1 protein levels decreased significantly in *Yap1*$^{-/-}$ maternal livers (Fig. 17E) and IHC analysis confirmed that YAP1 protein was specifically deleted from *Yap1*$^{-/-}$ maternal hepatocytes (Fig. 15B). We also noted that maternal BECs, around the PT, continued to express YAP1 in both groups of mice (Fig. 15B). H&E staining of maternal livers from the two groups was done to assess the development of overt histopathologies in the maternal livers due to viral transfection and YAP1 deletion but, our results indicated no observable defects in the maternal livers of both groups (Fig. 15C). After verifying the successful deletion of YAP1

from maternal hepatocytes we also wanted to confirm that this treatment did not cause any overt or unexpected changes to the maternal liver and the progression of pregnancy. To detect anomalies in pregnancy we measured the rate of abortion as well as the average fetal and placental weights in the *Yap1*$^{f/f}$ and *Yap1*$^{-/-}$ groups of mice. We found that not only were there no cases of abortions (Fig. 15D) but there were also no changes in the average-fetus and placental weights between the control and YAP1 KO groups (Fig. 15E).

After confirming the successful deletion of YAP1 from maternal hepatocytes, we next analyzed the effects of YAP1 deletion on pregnancy-induced maternal liver growth (Fig. 16). To analyze this, we first compared the total maternal liver weight as well as the liver-to-body weight ratio of Gd18 maternal livers collected from *Yap1*$^{f/f}$ and *Yap1*$^{-/-}$ mice. We observed that there was no difference in both the parameters between the control and YAP1 KO groups (Fig. 16-A & B). This finding further suggested that the hippo-YAP1 pathway does not have a role in the process of pregnancy-induced maternal liver growth. Additionally, to test if hepatocyte specific YAP1 deletion indirectly affected the weight response of other maternal organs during pregnancy, we measured the Gd18 gravimetric responses of various maternal organs from control and YAP1 KO mice. We found that maternal hepatocyte YAP1 deletion had no effect on the gravimetric responses of other maternal organs as well (Fig. 16-C to J). Recently it was shown that the hippo-YAP pathway could induce organ growth by means of cellular hypertrophy, as was seen in the case of cardiomyocyte hypertrophy [199]. Therefore, we measured the maternal hepatocyte cell density in *Yap1*$^{f/f}$ and *Yap1*$^{-/-}$ maternal livers to determine the effects of YAP1 deletion on maternal hepatocyte hypertrophy during pregnancy (Fig. 16K). However, here also we found no difference in the maternal hepatocyte density between *Yap1*$^{f/f}$ control- and *Yap1*$^{-/-}$ KO-livers. Since YAP1 is a pro-proliferation factor and maintains a cell in active cell-cycle, we wanted to determine if YAP1 deletion in the maternal liver affected the number of maternal hepatocytes actively participating in the cell-cycle on Gd18. Quantification of Ki67 positive maternal hepatocytes in *Yap1*$^{f/f}$ control and *Yap1*$^{-/-}$ KO maternal livers showed no significant change between the two groups (Fig. 16L).

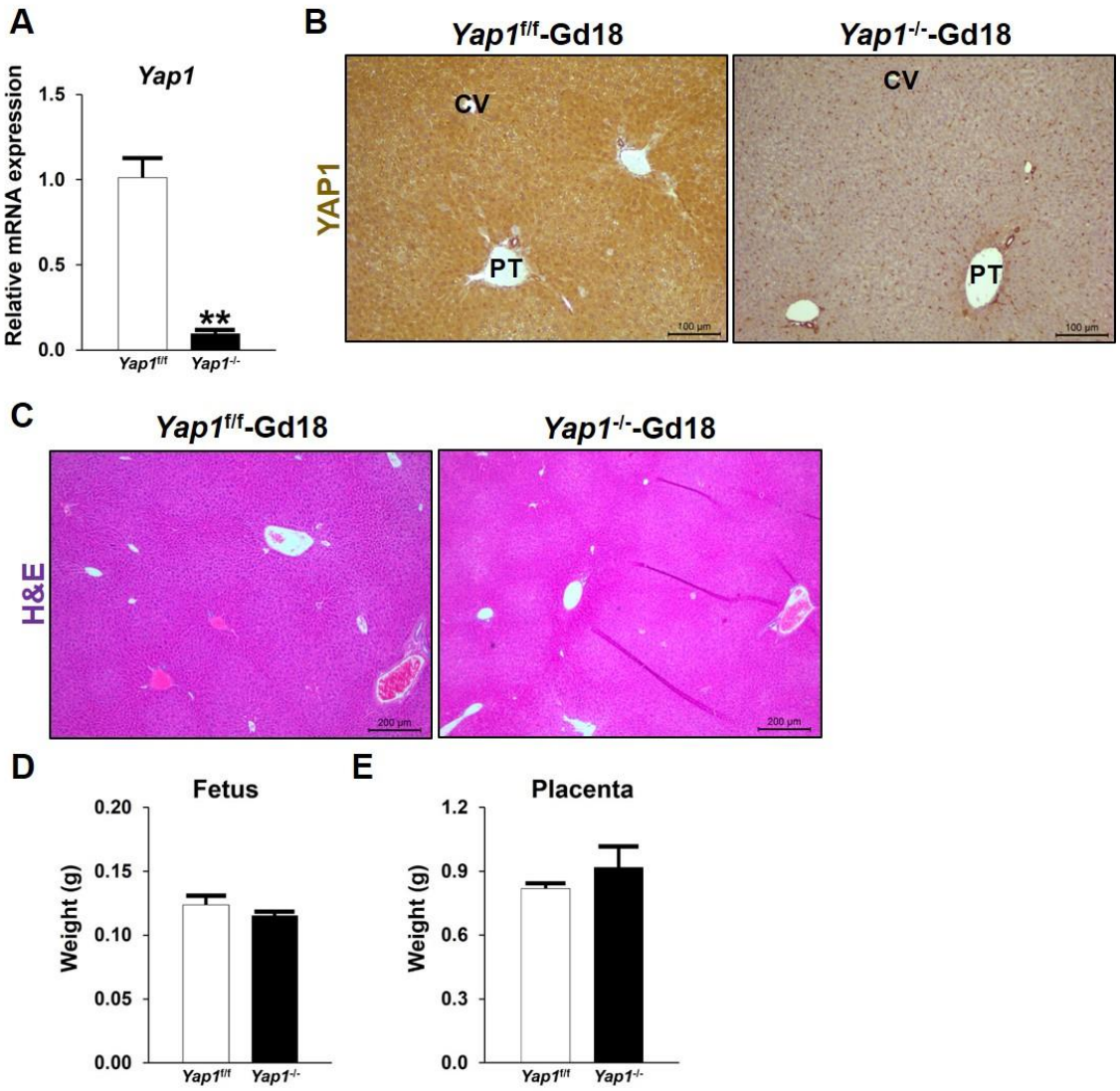

Figure 15: Validation of maternal hepatocyte specific *Yap1* gene deletion.

Timed pregnancies were generated in 3 months-old virgin female *Yap1*$^{flox/flox}$ mice. On gestation day 7 (Gd7) one group of mice (*Yap1*$^{-/-}$) were administered with the AAV8-TBG-Cre viral vector, to delete *Yap1* in maternal hepatocytes, while the other group administered the AAV8-TBG-Null vector served as the control group (*Yap1*$^{f/f}$). Gd18 maternal livers were collected from both group of mice and analyzed using different assays to establish successful maternal hepatocyte specific *Yap1* deletion. (A) *Yap1* mRNA expression was measured in Gd18 maternal livers of *Yap1*$^{f/f}$ (control) and *Yap1*$^{-/-}$ (Yap1 knockout) mice. *Yap1* mRNA expression was measured by performing RT-qPCR assay. Total mRNA extracts were prepared from *Yap1*$^{f/f}$ and *Yap1*$^{-/-}$ maternal livers. Data represents mean relative mRNA expression ±S.E.M with sample size (n) = 3 mice per group. ** indicates $p < 0.01$ compared to the control group (*Yap1*$^{f/f}$). (B) Representative photomicrographs of *Yap1*$^{f/f}$ and *Yap1*$^{-/-}$ maternal livers (Gd18) immuno-stained for YAP1 protein. Hepatic cells expressing YAP1 are stained brown in color. Sample size (n) was 3 per group. (C) Representative photomicrographs of hematoxylin and eosin (H&E) stained *Yap1*$^{f/f}$ and *Yap1*$^{-/-}$ maternal livers (Gd18). H&E staining was performed to detect histopathologies in the maternal livers due to *Yap1* deletion. The average fetus (D) and placenta (E) weights were measured in the *Yap1*$^{f/f}$ (control) and *Yap1*$^{-/-}$ (Yap1 knockout) groups to determine aberration in pregnancy due to *Yap1* deletion. Data represents mean weight ± S.E.M (n=3). Abbreviations: PT - Portal triad and CV - Central vein.

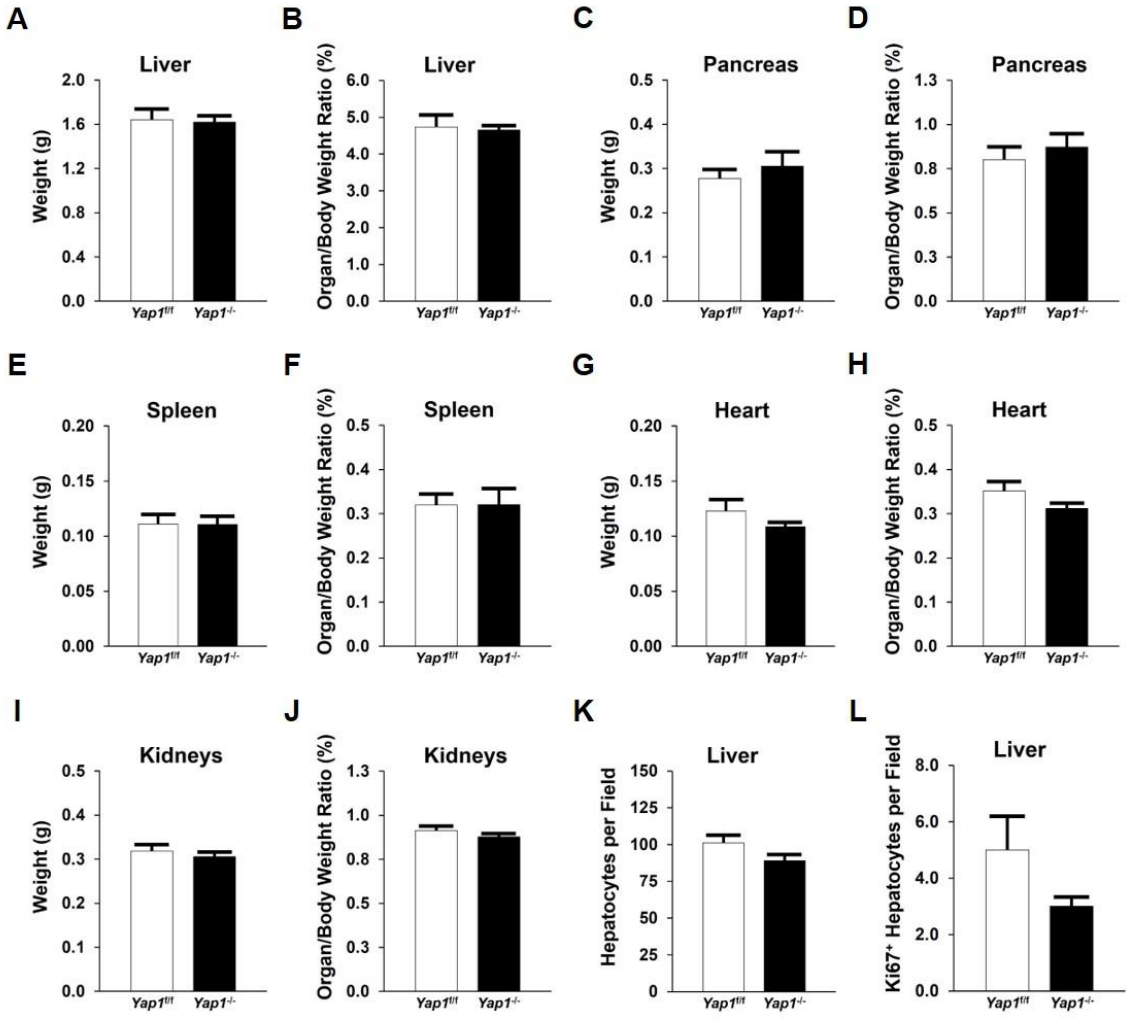

Figure 16: Effect of maternal hepatocyte specific *Yap1* gene deletion on pregnancy-induced maternal organ growth.

To determine the effect of *Yap1* deletion on maternal organ growth we collected various maternal organs, mentioned above, from gestation day 18 (Gd18) *Yap1*$^{f/f}$ (control) and *Yap1*$^{-/-}$ (*Yap1* knockout) mice. Bar graphs shown above represent the total organ weight and organ-to-body ratio of the maternal-liver (A&B), spleen (C&D), pancreas (E&F), kidneys (G&H), and heart (I&J). Data represents mean ±S.E.M (n=3). (K) Quantification of average maternal hepatocytes per field of view. FFPE *Yap1*$^{f/f}$ and *Yap1*$^{-/-}$ maternal liver sections were immunostained for β-catenin protein to quantify number of hepatocytes per field. (L) Quantification of Ki67^{+} maternal hepatocytes per field of view. *Yap1*$^{f/f}$ and *Yap1*$^{-/-}$ maternal liver sections were immunostained for Ki67 protein to quantify number of Ki67^{+} hepatocytes per field. Data represents mean ±S.E.M (n=3).

3.8.2 Maternal hepatocyte specific YAP1 deletion leads to inhibition of CD133 expression without affecting AFP and EPCAM expression.

Based on literature surveys, one important biological significance that was common between YAP [200-204], CD133 [205, 206], AFP, and EPCAM [157, 207-209] is that all four factors are prominent marker proteins in different types of cancers. Furthermore, reports that looked at the relation between cancers characterized by high levels of YAP expression and the expression of CD133, AFP, or EPCAM found that YAP overexpression eventually led to an increase in CD133, AFP, or EPCAM expression, respectively. This correlation suggests that YAP could be involved in regulating the expression of the other three markers. Due to this correlation between the expression of YAP and the three other protein markers, we were interested to determine the effects of YAP1 deletion on the expression of CD133 [210, 211], AFP [212], and EPCAM in maternal hepatocytes during pregnancy. For this, RT-qPCR, WB, and IHC analyses were performed using *Yap1*$^{f/f}$ and *Yap1*$^{-/-}$ Gd18 maternal livers.

Overall, our results showed that among the three developmental factors (CD133, AFP, and EPCAM), the deletion of YAP1 from maternal hepatocytes during gestation led to changes in the expression of the *Cd133* and *Afp* genes (Fig. 17). However, while *Afp* gene expression was altered specifically at the transcript level, *Cd133* gene expression was altered at the protein level. At the transcript level, the relative expression of *Cd133* and *Epcam* mRNA in *Yap1*$^{-/-}$ maternal livers remained consistent with the *Yap1*$^{f/f}$ control group (Fig. 17-A & C). And although we noticed a reduction in *Cd133* mRNA level in *Yap1*$^{-/-}$ maternal livers, this decrease did not reach the threshold of statistical significance (Fig. 17A). On the other hand, the relative expression of *Afp* mRNA increased significantly by a 0.5-fold difference in *Yap1*$^{-/-}$ maternal livers compared to their *Yap1*$^{f/f}$ counterparts (Fig. 17B). At the protein expression level, we found that while the expression of AFP and EPCAM remained unchanged between *Yap1*$^{f/f}$ and *Yap1*$^{-/-}$ maternal livers, the CD133 protein expression decreased significantly in *Yap1*$^{-/-}$ maternal livers (Fig. 17-D, F, G, & H). The results of protein expression by WB assay were further corroborated by IHC analysis. In the case of CD133 immunostaining, we noticed an observable decrease in CD133 expression within the maternal hepatocytes of *Yap1*$^{-/-}$ livers, whereas most maternal hepatocytes in *Yap1*$^{f/f}$ livers continued to express CD133 (Fig. 17I). AFP immuno-staining showed presence of AFP in a small sub-population of maternal hepatocytes within both *Yap1*$^{f/f}$ and *Yap1*$^{-/-}$ Gd18 livers (Fig. 17I). And

lastly, EPCAM immuno-staining showed that regardless of the presence or absence of YAP1, the sub-population of hepatocytes around the PT continued to express EPCAM (Fig. 17I).

In conclusion, our findings show that during the course of gestation, YAP1 plays a central role in the regulation of the expression of *Afp*, specifically at the transcript level, and CD133 at the protein level. Additionally, the observation that maternal hepatocyte specific YAP1 deletion leads to direct alterations in expression of *Cd133* and *Afp* gene products further validates the finding that CD133 and AFP are indeed expressed by maternal hepatocytes during pregnancy.

Figure 17 : Effects of maternal hepatocyte specific *Yap1* gene deletion on expression of YAP1, CD133, AFP, and EPCAM.

Gestation day 18 (Gd18) maternal livers were collected from *Yap1*$^{f/f}$ (control) and *Yap1*$^{-/-}$ (YAP1 knockout) mice. Total mRNA and total protein extracts were prepared from Gd18 maternal livers collected from both groups of mice. RT-qPCR assay was performed using total mRNA extracts and the relative mRNA expression of *Cd133* (A), Alpha-fetoprotein (*Afp*) (B), and Epithelial cell adhesion molecule (*Epcam*) (C) was measured in *Yap1*$^{f/f}$ and *Yap1*$^{-/-}$ maternal livers. Data represents mean ±S.E.M (n=3; *$p < 0.05$; **$p < 0.01$; ***$p < 0.001$). (D) Western blotting analysis was performed using total protein extracts to measure the protein expression of YAP1, CD133, AFP, EPCAM, and GAPDH. GAPDH was used as the internal loading control. Sample size (n) = 3 mice per group. The relative protein expression of YAP1 (E), CD133 (F), AFP (G), and EPCAM (H) was quantified to determine protein expression fold change as a result of *Yap1* deletion in *Yap1*$^{f/f}$ (control) and *Yap1*$^{-/-}$ (*Yap1* knockout) maternal livers (Gd18). Quantification was done using ImageJ software. Relative fold change was measured after normalizing samples to GAPDH. (I) Panel showing representative photomicrographs of *Yap1*$^{f/f}$ and *Yap1*$^{-/-}$ Gd18 maternal livers immuno-stained for CD133, AFP, and EPCAM. Hepatic cells expressing the three target proteins are stained brown in color. Results show that amongst the three protein markers, maternal hepatocyte specific YAP1 deletion only affected CD133 expression whereas AFP and EPCAM expression showed no significant changes between *Yap1*$^{f/f}$ and *Yap1*$^{-/-}$ groups. Sample size (n) = 3 per group. Abbreviations: CV - Central vein and PT - Portal triad.

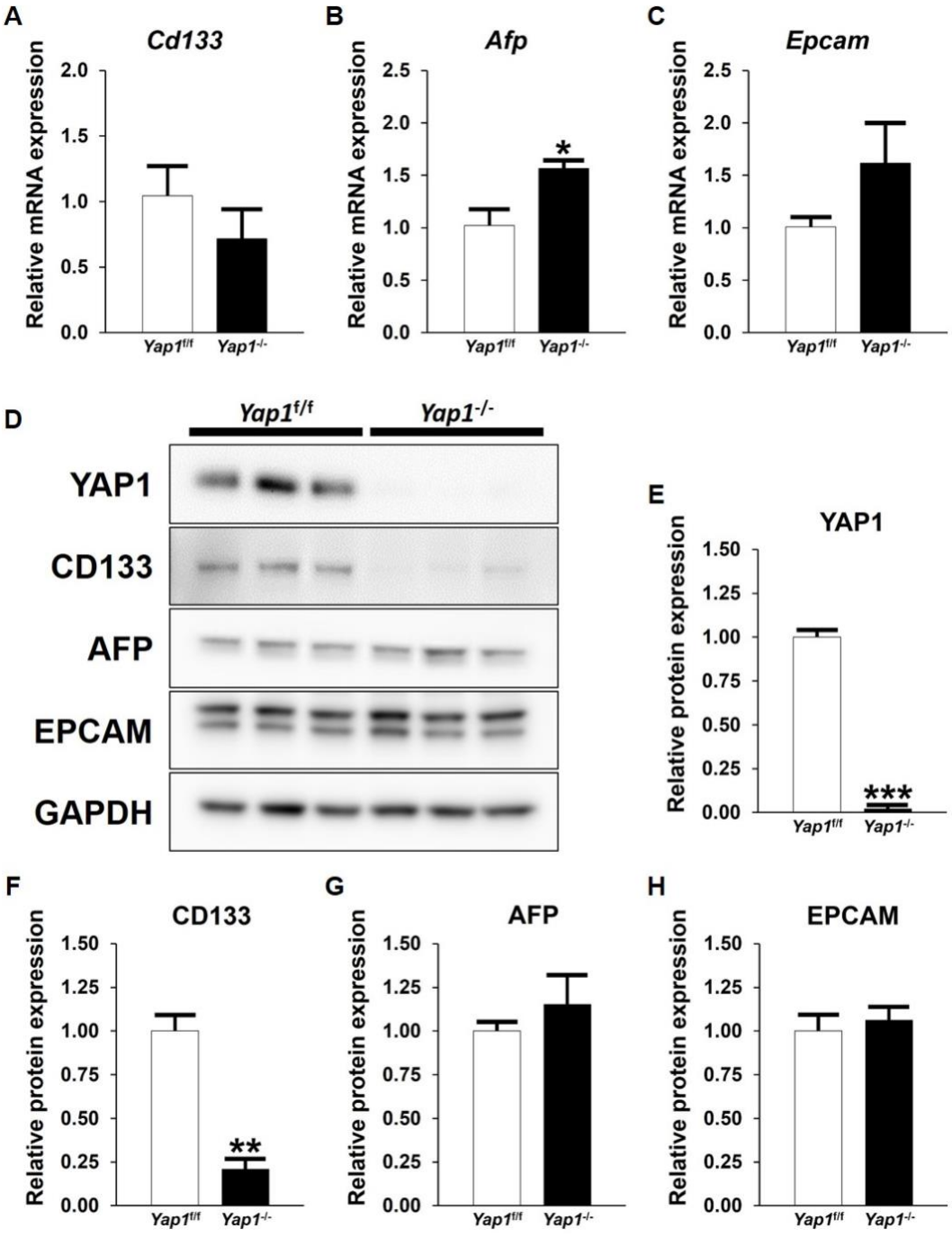
A
Cd133
Relative mRNA expression
2.0
1.5
1.0
0.5
0.0
Yap1f/f
Yap1-/-
B
Afp
Relative mRNA expression
2.5
2.0
1.5
1.0
0.5
0.0
*
Yap1f/f
Yap1-/-
C
Epcam
Relative mRNA expression
2.5
2.0
1.5
1.0
0.5
0.0
Yap1f/f
Yap1-/-
D
Yap1f/f
Yap1-/-
YAP1
CD133
AFP
EPCAM
GAPDH
E
YAP1
Relative protein expression
1.50
1.25
1.00
0.75
0.50
0.25
0.00
***
Yap1f/f
Yap1-/-
F
CD133
Relative protein expression
1.50
1.25
1.00
0.75
0.50
0.25
0.00
**
Yap1f/f
Yap1-/-
G
AFP
Relative protein expression
1.50
1.25
1.00
0.75
0.50
0.25
0.00
Yap1f/f
Yap1-/-
H
EPCAM
Relative protein expression
1.50
1.25
1.00
0.75
0.50
0.25
0.00
Yap1f/f
Yap1-/-

Figure 17 continued.

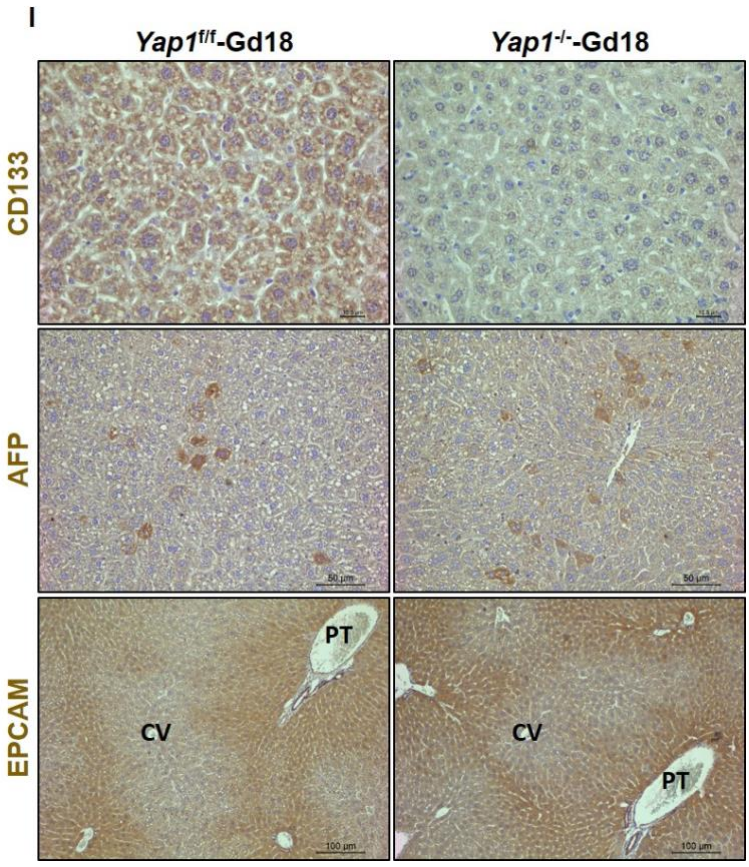

3.8.3 Mid-gestational maternal hepatocyte specific YAP1 deletion does not affect the maternal hepatic metabolic zonation patterns

Recent studies have indicated that the hippo pathway could play an important role in the development and maintenance of hepatic metabolic zonation [22, 173, 186, 213]. For example, a report by Fitamant et. al demonstrated that the genetic ablation of YAP, along with MST-1 and 2, in adult mouse hepatocytes leads to significant changes in the metabolic zonation patterns of GS and ornithine aminotransferase (OAT) [197]. In light of these findings, we were curious determine to whether the maternal hepatocyte specific YAP1 deletion could lead to changes in the metabolic zonation patterns of the maternal liver, particularly during the context of gestation. To determine this, Gd18 maternal livers were collected from *Yap1*$^{f/f}$ and *Yap1*$^{-/-}$ mice and immunolabelled for

the five representative metabolic zonation markers that were used earlier namely, Arginase1, CYP1A2, CYP2E1, E-Cadherin, and GS.

However, we found that the metabolic zonation pattern of all five zonation markers was the same in both Gd18 maternal livers that were collected from *Yap1*$^{f/f}$ and *Yap1*$^{-/-}$ groups of mice (Fig. 18). The immuno-staining patterns, that in turn represented the metabolic zonation of the maternal livers, appeared to be the same between *Yap1*$^{f/f}$ and *Yap1*$^{-/-}$ maternal livers (Gd18) and no observable differences could be seen (Fig. 18). Additionally, we also compared the metabolic zonation pattern of *Yap1*$^{f/f}$ and *Yap1*$^{-/-}$ maternal livers (Fig. 18) with that of Gd18 maternal livers harvested from C57BL/6J mice (Fig. 12) in order to rule out the possibility of potential changes to the metabolic zonation that could have been introduced due to transfection of maternal hepatocytes with the AAV8 viral vector. Our comparison showed that the metabolic zonation patterns of all three groups of mice were identical suggesting that transfection of maternal hepatocytes with AAV8 did not cause changes in metabolic zonation.

Therefore, in conclusion, our findings suggest that the deletion of YAP1 from maternal hepatocytes during the course of gestation does not affect the maternal hepatic metabolic zonation.

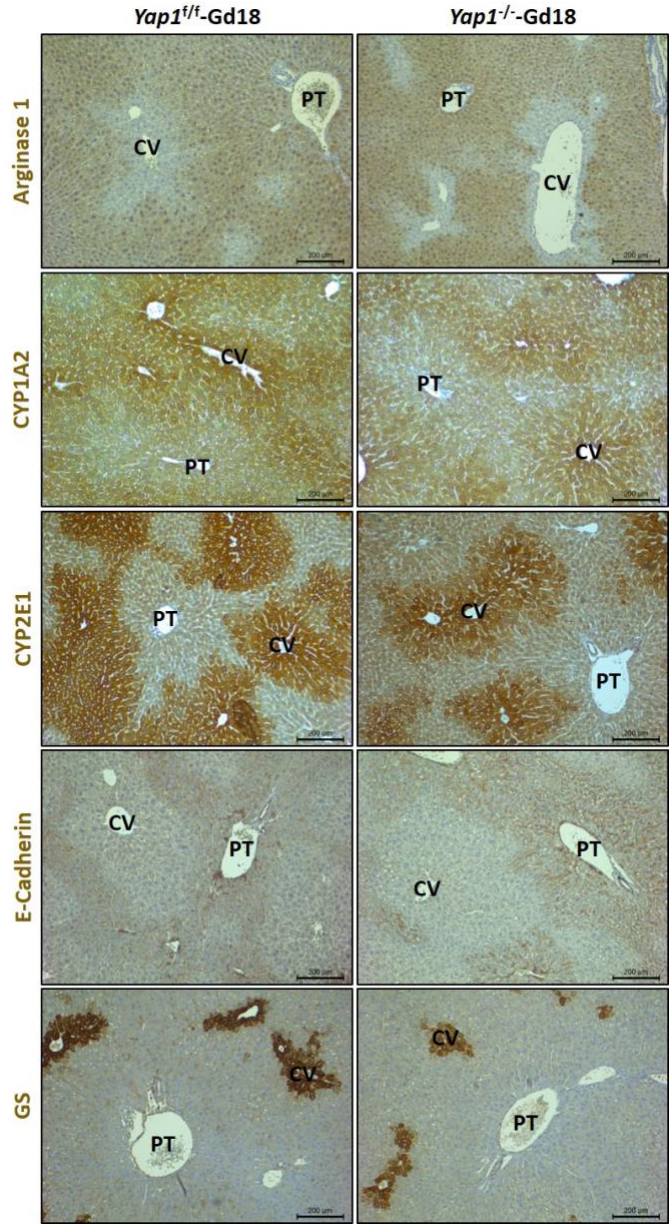

Figure 18: Effects of mid-gestational maternal hepatocyte specific YAP1 deletion on the maternal hepatic metabolic zonation.

Gestation day 18 (Gd18) maternal livers were collected from *Yap1*$^{f/f}$ and *Yap1*$^{-/-}$ mice. Formalin fixed paraffin embedded maternal liver sections were prepared for performing immuno-histological assay. Gd18 *Yap1*$^{f/f}$ and *Yap1*$^{-/-}$ maternal livers were immuno-stained for five representative metabolic zonation markers indicated above. Shown above are representative photomicrographs of *Yap1*$^{f/f}$ and *Yap1*$^{-/-}$ maternal livers immuno-labelled for Arginase 1, CYP1A2, CYP2E1, E-Cadherin, and Glutamine synthetase (GS) zonation markers. Note that cells expressing the respective markers are stained brown in color. Sample size (n) = 3. Abbreviations: PT - Portal triad and CV - Central vein.

3.8.4 Effects of YAP1 mid-gestational maternal hepatocyte specific YAP1 deletion on the biosynthetic metabolic processes of the maternal liver

Lastly, very little is known about the role of the hippo pathway and YAP in the regulation of the biosynthetic metabolic processes of the liver. Therefore, in this vein, we wanted to analyze the effects of maternal hepatocyte specific YAP1 deletion on the biosynthetic processes of the maternal liver, especially within the context of pregnancy. To analyze this, we performed the liver function test using Gd18 maternal serum that was collected from *Yap1*$^{f/f}$ (control) and *Yap1*$^{-/-}$ (YAP1 KO) groups of mice. The liver function test is a commonly used clinical assay that involves measuring the serum concentrations of various metabolites synthesized by the liver in order to gauge the general health of the organ. The eight metabolites included, alkaline phosphatase (ALP), alanine aminotransferase (ALT), aspartate aminotransferase (AST), albumin (ALB), globulin (Glb), cholesterol (Chol), triglyceride (Trig), and glucose (Glu).

We observed that, among the eight hepatic metabolites, the mid-gestational maternal hepatocyte specific YAP1 deletion led to changes in the concentrations of ALP and Chol (Fig. 19). The maternal serum concentrations of the remaining hepatic metabolites including, ALT, AST, ALB, Glb, Trig, and Glu remained the same between the *Yap1*$^{f/f}$ and *Yap1*$^{-/-}$ groups (Fig. 19-B, C, D, E, G, & H). The concentration of ALP increased from 57 IU/L in *Yap1*$^{f/f}$ mice to 70 IU/L in *Yap1*$^{-/-}$ mice (Fig. 19A) whereas, on the other hand, the Chol concentration decreased slightly from 53 IU/L in *Yap1*$^{f/f}$ mice to 47 IU/L in the YAP1 KO group (Fig. 19F). Therefore, our results imply that the hippo pathway and in-particular YAP1 plays a crucial role in regulating the biosynthesis of ALP and Chol.

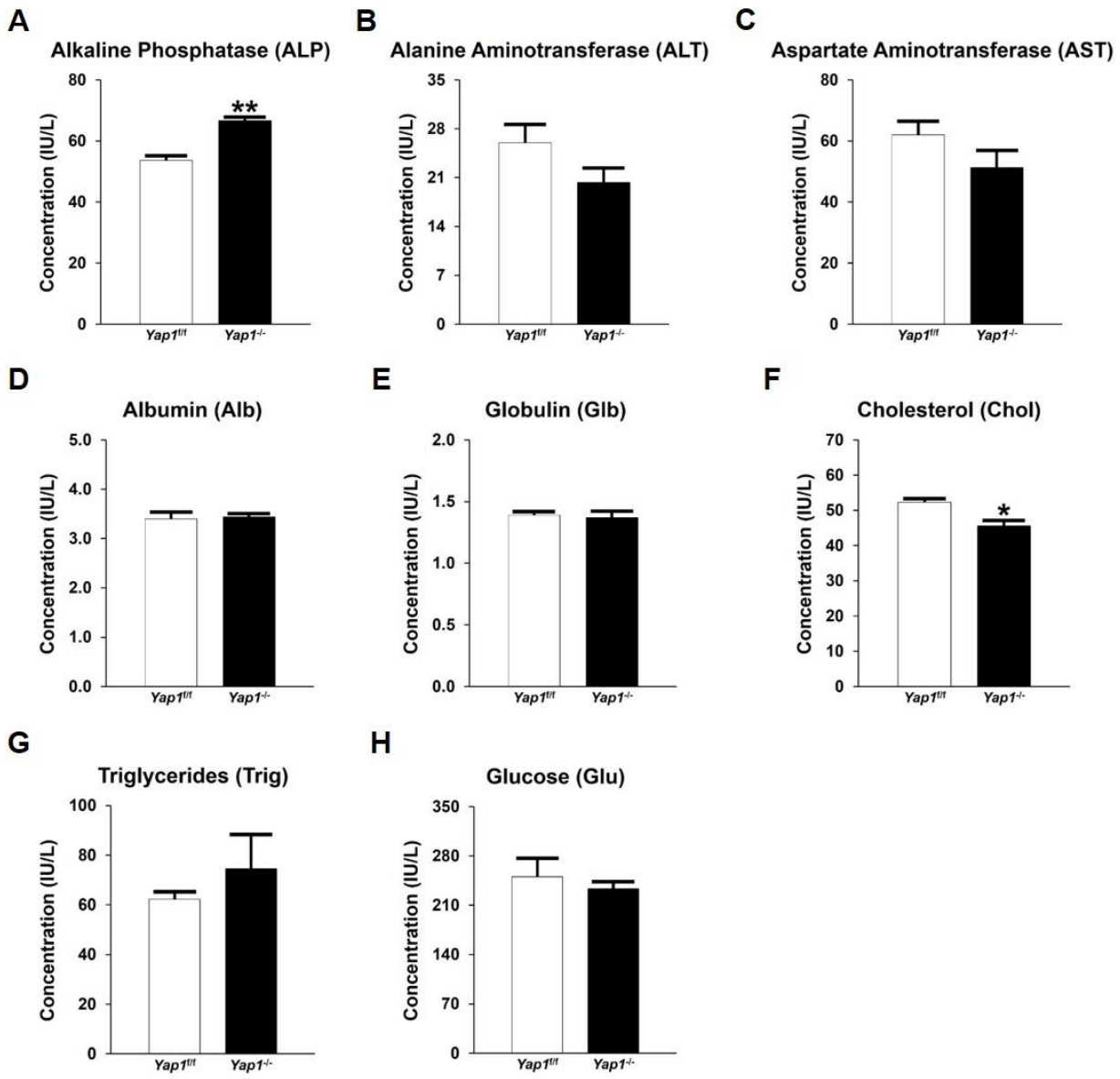

Figure 19: Effects of maternal hepatocyte specific *Yap1* gene deletion on liver function test.

The maternal serum was collected from gestation day 18 (Gd18) *Yap1*$^{f/f}$ (control) and *Yap1*$^{-/-}$ (*Yap1* knockout) mice to determine the effects of deletion of *Yap1* from maternal hepatocytes during pregnancy. The serum concentrations of (A) alkaline phosphatase (ALP), (B) alanine aminotransferase (ALT), (C) aspartate aminotransferase (AST), (D) albumin (ALB), (E) globulin (Glb), (F) cholesterol (Chol), (G) triglycerides (Trig), and (H) glucose (Glu) were measured from Gd18 *Yap1*$^{f/f}$ and *Yap1*$^{-/-}$ samples. Data represents mean ±SEM (n=3). * indicates $p < 0.05$ and ** $p < 0.01$, compared to *Yap1*$^{f/f}$ controls.

CHAPTER 4. DISCUSSION

The analysis of pregnancy-dependent maternal organ growth showed us that, amongst the maternal organs analyzed, only a subset of organs, namely, the liver, spleen, and pancreas exhibited weight increases during gestation (Fig. 4). The weight increases in all three organs occurred during the second half of pregnancy. Furthermore, while the maternal pancreas showed only a slight increase in organ weight at the end of pregnancy, the maternal liver and spleen exhibited robust increase in both total organ weight and organ-to-body weight ratio (Fig. 4). This distinct organ-dependent size adjustments most likely reflects the differential functional demands specific to each maternal organ. Our results pertaining to pregnancy-induced maternal organ weight changes were mostly consistent with previous studies and with other strains of mice. The only maternal organ from which our results might potentially differ would be the maternal heart. An earlier report by Eghbali et. al found that the maternal heart weight on Gd19 was slightly higher compared to its counterpart in the NP state [28, 29]. However, our results showed that, while the maternal heart weight showed an increasing trend, its weight increase by Gd17 did not reach statistical significance. This could suggest that the size of the maternal heart during gestation increases by a significant degree between Gds-17 and 19 when compared to the NP state.

Our attempt to establish a relation between potential cellular hyperplasia and maternal organ growth showed a direct correlation between the two aspects (Fig. 5). All three maternal organs that undergo pregnancy-induced enlargement also incorporated a significant amount of BrdU, which suggested the potential role of cell proliferation driving the growth of the respective organs. Remaining maternal organs namely, the kidney, heart, and lungs that did not exhibit organ growth also did not show an overt difference in BrdU incorporation between the NP and pregnant states (Fig. 5). While we established that maternal hepatocytes incorporating BrdU most probably do not undergo hyperplasia, the proliferative fate of cells in the maternal pancreas and spleen remains to be determined. One of our novel findings is that we, for the first time, show robust DNA synthesis activity of acinar cells during pregnancy (Fig. 5). Similar to maternal hepatocytes, approximately 39% of acinar cells also enter S-phase by the end of pregnancy. However, the signaling mechanism that initiates these substantial events still remains to be determined.

We provided evidence suggesting that maternal hepatocytes most likely undergo endoreplication in response to pregnancy (Figs. 6 & 7). A report by Milona et. al proposed that maternal hepatocytes get suspended at G2 phase and our data in this report supports this proposal [32]. Of note, during 2/3rd partial hepatectomy-induced liver regeneration, among the approximately 66% of cycling hepatocytes, only one-half progress through the entire cell cycle and eventually divide, whereas the other half undergo endoreplication simply to increase their ploidy number [59]. Here we uncovered such a massive endoreplication activity in maternal hepatocytes. Several lines of evidence from multiple studies indicate that various organisms employ endoreplication as a mechanism of achieving rapid organ growth, especially under heavy stress or conditions inhibiting cell proliferation. Several groups have well established that maternal hepatocytes show hypertrophy [32, 33, 42]. Putting together all these findings, we believe that maternal hepatocytes follow both hypertrophy and endoreplication pathways to simultaneously increase cell size and DNA content. By doing so, maternal hepatocytes are able to expand their metabolic capacity in a cost-effective way in order to minimally interfere with fetal development. Because cell division consumes a large quantity of cellular resources and energy, maternal hepatocytes avoid increasing their number to accommodate pregnancy. We think that this is the major biological significance underlying this unique behaver of maternal hepatocytes. In the future studies, it would be interesting to determine if maternal hepatocyte hypertrophy occurred in all hepatocytes or was limited to only hepatocytes undergoing endoreplication. In addition, we need to take more approaches including flow cytometry to further test our theory. Furthermore, it would also be highly useful to determine the exact molecular mechanisms that orchestrate maternal hepatocyte endoreplication during pregnancy. Currently, endoreplication has been shown to be regulated by three signaling pathways namely, notch pathway, mTOR pathway, and EGFR/RAS/MAPK pathway, in a context dependent manner[47, 63-66]. However, among the three signaling mechanisms, a previous report from our lab found that the mTOR signaling pathway was activated in the maternal livers, during the course of pregnancy. The levels of p-AKT1, p-mTOR, p-p70S6K, and p-4E-BP1, various activated components of the mTOR pathway, increased significantly during the second half of pregnancy[43]. As this coincides with the entry of maternal hepatocytes into the S-phase, this makes it highly likely that the mTOR pathway may be a key regulator of pregnancy-induced maternal hepatocyte endoreplication and hypertophy. It was also found that the levels of another key indicator of endoreplication, that is CycE, remained constantly elevated throughout

gestation [42]. The increased presence of CycE in maternal livers could further explain the progressively increasing pattern of maternal hepatocyte BrdU incorporation. However, the protein expression profile of the mitotic cyclin, CycB, is not yet known. Elevated levels of CycE along with a lack of expression of M-phase cyclin, CycB, would further validate endoreplication of maternal hepatocytes. Mammalian achaete scute homolog 2 (MASH2) protein, also known as achaete scute like homolog (ASCL), is a negative regulator or endoreplication[214]. Studies from our lab have shown that maternal hepatic ASCL1 expression (a homolog of MASH2) increases progressively and closely follows the progression of maternal hepatocyte S-phase entry[31]. Therefore, we suspect that ASCL1 may be important in modulating the number of endoreplication cycles taking place within the maternal hepatocytes and perhaps their timely exit from the cell cycle. Therefore, based on the above findings, we strongly suspect the role of the mTOR pathway in orchestrating pregnancy-induced maternal hepatocyte endoreplication as well as hypertrophy. But further validation is still required. Understanding the molecular mechanisms of maternal hepatocyte endoreplication could have potential applications towards strategies and protein targets to block cell cycle progression and carcinogenesis in the liver.

Our studies revealed endoreplication as a unique cellular mechanism driving pregnancy-induced maternal liver growth. Liver regrowth after 1/3rd PHx is induced solely by hepatocyte hypertrophy without hyperplasia [59]. Liver regrowth after 2/3rd PHx results from a combination of hepatocyte hyperplasia and endoreplication [59]. Here we showed that maternal liver growth response is only mediated by hepatocyte endoreplication, providing an ideal *in vivo* model system to investigate cell endocycle.

We demonstrated that Axin2^{+} hepatocytes do not expand in response to pregnancy and liver resection and do not contribute to liver homeostatic turnover (Fig. 8). Wang et al. proposed that Axin2^{+} cells behave like liver stem cells, repopulating the liver over one year period under homeostatic conditions [74]. Our findings are against this proposal. It is to be noted that the experimental conditions in our studies differed from theirs in three aspects: the reporter protein, tamoxifen dosage, and the age of mice. We used LacZ, instead of GFP, as a reporter. Excessive LacZ could affect the behavior of Axin2^{+} hepatocytes. We also used lower dose of tamoxifen and older mice. However, these concerns are unlikely to be significant because our results are consistent with two other recent reports. The findings of both reports essentially show that Axin2^{+} hepatocytes mostly maintained their own population by self-replication over the course of one-

year under homeostatic conditions and following 2/3rd PHx [215-217]. Our group examined the activity of $Axin2^+$ cells additionally during gestation. Taken together, the stem cell-like nature of $Axin2^+$ hepatocytes appear to be questionable and needs to be further clarified.

Most excitingly, we for the first time discovered that adult hepatocytes possess heterogeneous developmental phenotypes at mRNA and protein level, and pregnancy modulates this property of maternal hepatocytes (Figs. 9, 10, & 11). During development, fetal hepatocytes express both mRNAs and proteins of hepatoblast marker genes *Cd133* [87-91], *Afp* [92-97], and *Epcam* [98, 100-104]. Surprisingly, at the mRNA level, most adult hepatocytes conserve these developmental phenotypes; at the protein level, hepatocytes do not express CD133 and AFP, but restrict EPCAM expression in Zone 3. It is well known that hepatocytes exhibit heterogeneous metabolic phenotypes. Here we reveal their distinct developmental phenotypes in adults. At his juncture, the biological significance of this new feature of adult hepatocytes is not clear and needs to be further investigated. Furthermore, we identified pregnancy as a potent regulator of this phenomenon. During gestation, maternal hepatocytes changed these phenotypes largely conserved at mRNA level to both mRNA and protein level, leading to phenotypic resembling between maternal and fetal hepatocytes. This suggests that a factor stimulating fetal hepatocyte development may simultaneously induce similar phenotypic changes in maternal hepatocytes. Moreover, we found that these pregnancy-induced phenotypic alterations of maternal hepatocytes are mediated via the nuclear-cytoplasmic mRNA translocation for *Cd133* and *Afp*, and a zone-dependent mechanism for *Epcam*. It is really intriguing why maternal hepatocytes respond to pregnancy in this way.

We also uncovered for the first time that maternal hepatocytes produce AFP (Fig. 10). AFP is a fetal plasma glycoprotein that is primarily synthesized by the developing fetal hepatocytes and, to a lesser extent, by the cells of the yolk sac. Its presence in the maternal serum is due to its exchange between the fetal and maternal blood during gestation. Clinically, it used to monitor the health of the developing fetus as well as the pregnancy. Abnormally high levels of AFP in the maternal serum are considered as a potential indicator of various fetal defects or fetal diseases such as hemorrhage in fetal compartment, intrauterine death and resorption, anencephaly, and spina bifida. Our finding revealed maternal liver as another source of AFP, implying that abnormally high AFP levels could also be a consequence of maternal liver pathology. There is a possibility that our observation could be restricted to only rodents, and it would be important to verify this finding in

humans. But obtaining human maternal liver samples is challenging because biopsying of maternal livers is not a routine clinical practice.

In our studies, we evaluated the effects of YAP1 on different aspects of maternal liver physiology (Figs. 16 to 19). Surprisingly, we found that pregnancy-induced maternal liver growth is not mediated by the canonical mechanism of hippo-YAP (TAZ) pathway (Figs. 13, 14, & 16). We made this conclusion based on three pieces of evidence. The first is that the activities of hippo pathway components in maternal liver are not affected by pregnancy (Fig. 13). The second is that maternal hepatic YAP and TAZ is not activated throughout the course of gestation (Figs. 13 & 14). The third is that the mid-gestational knockout of YAP1 specifically in maternal hepatocytes did not influence maternal liver growth (Fig. 16). YAP1 is a well-known and probably the most potent stimulator of hepatocyte proliferation liver growth [174, 218-221]. Therefore, these findings further support our earlier conclusion that maternal hepatocytes do not undergo cell division. Moreover, recent reports have shown that YAP participates in regulating liver metabolic zonation. The deletion of YAP from hepatocytes led to an increase in the number of Zone 3 hepatocytes expressing GS, a well-established Zone 3 marker enzyme [197]. In our setting, by comprehensive examination of liver zonation markers including GS, we found that the loss of function of *Yap1* gene did not alter metabolic zonation of maternal livers. Our data indicates that the maternal liver maintains its metabolic landscape via a different mechanism. Strikingly, we identified YAP1 as a key regulator of CD133 protein expression in maternal hepatocytes. The absence of YAP1 in these cells did not affect their Cd133 mRNA expression but substantially diminished their CD133 protein expression. Thus, YAP1 is required for the posttranscriptional expression of this protein. This finding demonstrated a mechanism partially controlling the developmental phenotypes of maternal hepatocytes. YAP1 is reported to regulate lipid metabolism [193-196]. Activation of YAP1 in hepatocytes causes fatty liver. Here we observed deceased cholesterol concentrations in maternal circulation due to the absence of YAP1 in maternal hepatocytes, in line with this report. The finding warrants further studies to elucidate how YAP1 regulates lipid metabolism during pregnancy.

In summary, we demonstrate several novel aspects of the physiology of maternal livers. As pregnancy progresses, maternal hepatocytes increase their metabolic capacity via hypertrophy/endoreplication independent of hippo pathway, change their phenotypes partially by YAP1, and maintain their functional zonation. These findings allow us to gain significant insights

into how maternal livers adapts to pregnancy and provide some clues to understand pregnancy-associated diseases.

REFERENCES

1. Luza, S.C. and H.C. Speisky, *Liver copper storage and transport during development: implications for cytotoxicity.* Am J Clin Nutr, 1996. **63**(5): p. 812s-20s.
2. Smallwood, R.A., et al., *Liver-copper levels in liver disease: studies using neutron activation analysis.* Lancet, 1968. **2**(7582): p. 1310-3.
3. Hutson, S.M., et al., *Regulation of albumin synthesis by hormones and amino acids in primary cultures of rat hepatocytes.* Am J Physiol, 1987. **252**(3 Pt 1): p. E291-8.
4. Nayak, N.C. and I. Mital, *The dynamics of alpha-fetoprotein and albumin synthesis in human and rat liver during normal ontogeny.* Am J Pathol, 1977. **86**(2): p. 359-74.
5. Adamek, A. and A. Kasprzak, *Insulin-Like Growth Factor (IGF) System in Liver Diseases.* Int J Mol Sci, 2018. **19**(5).
6. Matsusaka, T., et al., *Liver angiotensinogen is the primary source of renal angiotensin II.* J Am Soc Nephrol, 2012. **23**(7): p. 1181-9.
7. Shimada, Y., et al., *Production of thrombopoietin (TPO) by rat hepatocytes and hepatoma cell lines.* Exp Hematol, 1995. **23**(13): p. 1388-96.
8. Weibel, E.R., et al., *Correlated morphometric and biochemical studies on the liver cell. I. Morphometric model, stereologic methods, and normal morphometric data for rat liver.* J Cell Biol, 1969. **42**(1): p. 68-91.
9. Blouin, A., R.P. Bolender, and E.R. Weibel, *Distribution of organelles and membranes between hepatocytes and nonhepatocytes in the rat liver parenchyma. A stereological study.* J Cell Biol, 1977. **72**(2): p. 441-55.
10. Benedetti, A., et al., *A morphometric study of the epithelium lining the rat intrahepatic biliary tree.* J Hepatol, 1996. **24**(3): p. 335-42.
11. Alpini, G., et al., *Molecular and functional heterogeneity of cholangiocytes from rat liver after bile duct ligation.* Am J Physiol, 1997. **272**(2 Pt 1): p. G289-97.
12. Huang, B.Q., et al., *Isolation and characterization of cholangiocyte primary cilia.* Am J Physiol Gastrointest Liver Physiol, 2006. **291**(3): p. G500-9.
13. Bonnardel, J., et al., *Stellate Cells, Hepatocytes, and Endothelial Cells Imprint the Kupffer Cell Identity on Monocytes Colonizing the Liver Macrophage Niche.* Immunity, 2019. **51**(4): p. 638-654.e9.
14. Wisse, E., et al., *The liver sieve: considerations concerning the structure and function of endothelial fenestrae, the sinusoidal wall and the space of Disse.* Hepatology, 1985. **5**(4): p. 683-92.
15. Wack, K.E., et al., *Sinusoidal ultrastructure evaluated during the revascularization of regenerating rat liver.* Hepatology, 2001. **33**(2): p. 363-78.
16. Parker, G.A. and C.A. Picut, *Liver immunobiology.* Toxicol Pathol, 2005. **33**(1): p. 52-62.
17. Friedman, S.L., *Hepatic stellate cells: protean, multifunctional, and enigmatic cells of the liver.* Physiol Rev, 2008. **88**(1): p. 125-72.

18. Frevert, U., et al., *Intravital observation of Plasmodium berghei sporozoite infection of the liver.* PLoS Biol, 2005. **3**(6): p. e192.

19. van Grunsven, L.A., *3D in vitro models of liver fibrosis.* Adv Drug Deliv Rev, 2017. **121**: p. 133-146.

20. Gebhardt, R., *Metabolic zonation of the liver: regulation and implications for liver function.* Pharmacol Ther, 1992. **53**(3): p. 275-354.

21. Jungermann, K. and N. Katz, *Functional specialization of different hepatocyte populations.* Physiol Rev, 1989. **69**(3): p. 708-64.

22. Benhamouche, S., et al., *Apc tumor suppressor gene is the "zonation-keeper" of mouse liver.* Dev Cell, 2006. **10**(6): p. 759-70.

23. Kusminski, C.M. and P.E. Scherer, *New zoning laws enforced by glucagon.* Proc Natl Acad Sci U S A, 2018. **115**(17): p. 4308-4310.

24. Shingo, T., et al., *Pregnancy-stimulated neurogenesis in the adult female forebrain mediated by prolactin.* Science, 2003. **299**(5603): p. 117-20.

25. Karnik, S.K., et al., *Menin controls growth of pancreatic beta-cells in pregnant mice and promotes gestational diabetes mellitus.* Science, 2007. **318**(5851): p. 806-9.

26. Parsons, J.A., T.C. Brelje, and R.L. Sorenson, *Adaptation of islets of Langerhans to pregnancy: increased islet cell proliferation and insulin secretion correlates with the onset of placental lactogen secretion.* Endocrinology, 1992. **130**(3): p. 1459-66.

27. Scaglia, L., F.E. Smith, and S. Bonner-Weir, *Apoptosis contributes to the involution of beta cell mass in the post partum rat pancreas.* Endocrinology, 1995. **136**(12): p. 5461-8.

28. Eghbali, M., et al., *Molecular and functional signature of heart hypertrophy during pregnancy.* Circ Res, 2005. **96**(11): p. 1208-16.

29. Redondo-Angulo, I., et al., *C/EBPβ is required in pregnancy-induced cardiac hypertrophy.* Int J Cardiol, 2016. **202**: p. 819-28.

30. Bustamante, J.J., G. Dai, and M.J. Soares, *Pregnancy and lactation modulate maternal splenic growth and development of the erythroid lineage in the rat and mouse.* Reprod Fertil Dev, 2008. **20**(2): p. 303-10.

31. Bustamante, J.J., et al., *Gene profiling of maternal hepatic adaptations to pregnancy.* Liver Int, 2010. **30**(3): p. 406-15.

32. Milona, A., et al., *The normal mechanisms of pregnancy-induced liver growth are not maintained in mice lacking the bile acid sensor Fxr.* Am J Physiol Gastrointest Liver Physiol, 2010. **298**(2): p. G151-8.

33. Price, L.R., et al., *Transcriptome-wide analysis suggests that temporal changes in the relative contributions of hyperplasia, hypertrophy and apoptosis underlie liver growth in pregnant mice.* Biol Reprod, 2017. **97**(5): p. 762-771.

34. Hoekzema, E., et al., *Pregnancy leads to long-lasting changes in human brain structure.* Nat Neurosci, 2017. **20**(2): p. 287-296.

35. Butler, A.E., et al., *Adaptive changes in pancreatic beta cell fractional area and beta cell turnover in human pregnancy.* Diabetologia, 2010. **53**(10): p. 2167-76.

36. Van Assche, F.A., L. Aerts, and F. De Prins, *A morphological study of the endocrine pancreas in human pregnancy.* Br J Obstet Gynaecol, 1978. **85**(11): p. 818-20.

37. Schannwell, C.M., et al., *Left ventricular hypertrophy and diastolic dysfunction in healthy pregnant women.* Cardiology, 2002. **97**(2): p. 73-8.

38. Maymon, R., et al., *Normal sonographic values of maternal spleen size throughout pregnancy.* Ultrasound Med Biol, 2006. **32**(12): p. 1827-31.

39. Chesley, L.C., *Plasma and red cell volumes during pregnancy.* Am J Obstet Gynecol, 1972. **112**(3): p. 440-50.

40. Pritchard, J.A., *CHANGES IN THE BLOOD VOLUME DURING PREGNANCY AND DELIVERY.* Anesthesiology, 1965. **26**: p. 393-9.

41. Kennaway, E. and N. Kennaway, *The Ascorbic Acid Content of the Liver in Pregnant Mice.* Cancer Research, 1944. **4**(11): p. 704-706.

42. Dai, G., et al., *Maternal hepatic growth response to pregnancy in the mouse.* Exp Biol Med (Maywood), 2011. **236**(11): p. 1322-32.

43. Zou, Y., et al., *Nrf2 participates in regulating maternal hepatic adaptations to pregnancy.* Journal of Cell Science, 2013. **126**(7): p. 1618.

44. Wang, M.J., et al., *Hepatocyte polyploidization and its association with pathophysiological processes.* Cell Death Dis, 2017. **8**(5): p. e2805.

45. Lee, H.O., J.M. Davidson, and R.J. Duronio, *Endoreplication: polyploidy with purpose.* Genes Dev, 2009. **23**(21): p. 2461-77.

46. Shu, Z., S. Row, and W.M. Deng, *Endoreplication: The Good, the Bad, and the Ugly.* Trends Cell Biol, 2018. **28**(6): p. 465-474.

47. Deng, W.M., C. Althauser, and H. Ruohola-Baker, *Notch-Delta signaling induces a transition from mitotic cell cycle to endocycle in Drosophila follicle cells.* Development, 2001. **128**(23): p. 4737-46.

48. Lee, L.A. and T.L. Orr-Weaver, *Regulation of cell cycles in Drosophila development: intrinsic and extrinsic cues.* Annu Rev Genet, 2003. **37**: p. 545-78.

49. Schaeffer, V., et al., *Notch-dependent Fizzy-related/Hec1/Cdh1 expression is required for the mitotic-to-endocycle transition in Drosophila follicle cells.* Curr Biol, 2004. **14**(7): p. 630-6.

50. Follette, P.J., R.J. Duronio, and P.H. O'Farrell, *Fluctuations in cyclin E levels are required for multiple rounds of endocycle S phase in Drosophila.* Curr Biol, 1998. **8**(4): p. 235-8.

51. Park, S.Y. and M. Asano, *The origin recognition complex is dispensable for endoreplication in Drosophila.* Proc Natl Acad Sci U S A, 2008. **105**(34): p. 12343-8.

52. Weiss, A., et al., *Continuous Cyclin E expression inhibits progression through endoreduplication cycles in Drosophila.* Curr Biol, 1998. **8**(4): p. 239-42.

53. Grafi, G. and B.A. Larkins, *Endoreduplication in maize endosperm: involvement of m phase--promoting factor inhibition and induction of s phase--related kinases.* Science, 1995. **269**(5228): p. 1262-4.

54. Leiva-Neto, J.T., et al., *A dominant negative mutant of cyclin-dependent kinase A reduces endoreduplication but not cell size or gene expression in maize endosperm.* Plant Cell, 2004. **16**(7): p. 1854-69.

55. Schweizer, L., et al., *Dynamics of maize endosperm development and DNA endoreduplication.* Proc Natl Acad Sci U S A, 1995. **92**(15): p. 7070-4.

56. Nagata, Y., Y. Muro, and K. Todokoro, *Thrombopoietin-induced polyploidization of bone marrow megakaryocytes is due to a unique regulatory mechanism in late mitosis.* J Cell Biol, 1997. **139**(2): p. 449-57.

57. Ravid, K., et al., *Roads to polyploidy: the megakaryocyte example.* J Cell Physiol, 2002. **190**(1): p. 7-20.

58. Parisi, T., et al., *Cyclins E1 and E2 are required for endoreplication in placental trophoblast giant cells.* Embo j, 2003. **22**(18): p. 4794-803.

59. Miyaoka, Y., et al., *Hypertrophy and unconventional cell division of hepatocytes underlie liver regeneration.* Curr Biol, 2012. **22**(13): p. 1166-75.

60. Hassel, C., et al., *Induction of endocycles represses apoptosis independently of differentiation and predisposes cells to genome instability.* Development, 2014. **141**(1): p. 112-23.

61. Duncan, A.W., et al., *Frequent aneuploidy among normal human hepatocytes.* Gastroenterology, 2012. **142**(1): p. 25-8.

62. Fox, D.T., J.G. Gall, and A.C. Spradling, *Error-prone polyploid mitosis during normal Drosophila development.* Genes Dev, 2010. **24**(20): p. 2294-302.

63. Jordan, K.C., et al., *Notch signaling through tramtrack bypasses the mitosis promoting activity of the JNK pathway in the mitotic-to-endocycle transition of Drosophila follicle cells.* BMC Dev Biol, 2006. **6**: p. 16.

64. López-Schier, H. and D. St Johnston, *Delta signaling from the germ line controls the proliferation and differentiation of the somatic follicle cells during Drosophila oogenesis.* Genes Dev, 2001. **15**(11): p. 1393-405.

65. Edgar, B.A., N. Zielke, and C. Gutierrez, *Endocycles: a recurrent evolutionary innovation for post-mitotic cell growth.* Nat Rev Mol Cell Biol, 2014. **15**(3): p. 197-210.

66. Xiang, J., et al., *EGFR-dependent TOR-independent endocycles support Drosophila gut epithelial regeneration.* Nat Commun, 2017. **8**: p. 15125.

67. Moberg, K.H., et al., *Archipelago regulates Cyclin E levels in Drosophila and is mutated in human cancer cell lines.* Nature, 2001. **413**(6853): p. 311-6.

68. Duronio, R.J., P.C. Bonnette, and P.H. O'Farrell, *Mutations of the Drosophila dDP, dE2F, and cyclin E genes reveal distinct roles for the E2F-DP transcription factor and cyclin E during the G1-S transition.* Mol Cell Biol, 1998. **18**(1): p. 141-51.

69. Duronio, R.J. and P.H. O'Farrell, *Developmental control of the G1 to S transition in Drosophila: cyclin Eis a limiting downstream target of E2F.* Genes Dev, 1995. **9**(12): p. 1456-68.

70. Duronio, R.J., et al., *The transcription factor E2F is required for S phase during Drosophila embryogenesis.* Genes Dev, 1995. **9**(12): p. 1445-55.

71. Hattori, N., et al., *Periodic expression of the cyclin-dependent kinase inhibitor p57(Kip2) in trophoblast giant cells defines a G2-like gap phase of the endocycle.* Mol Biol Cell, 2000. **11**(3): p. 1037-45.

72. Ullah, Z., et al., *Differentiation of trophoblast stem cells into giant cells is triggered by p57/Kip2 inhibition of CDK1 activity.* Genes Dev, 2008. **22**(21): p. 3024-36.

73. Huch, M., et al., *In vitro expansion of single Lgr5+ liver stem cells induced by Wnt-driven regeneration.* Nature, 2013. **494**(7436): p. 247-50.

74. Wang, B., et al., *Self-renewing diploid Axin2(+) cells fuel homeostatic renewal of the liver.* Nature, 2015. **524**(7564): p. 180-5.

75. Burke, Z.D., et al., *Liver zonation occurs through a beta-catenin-dependent, c-Myc-independent mechanism.* Gastroenterology, 2009. **136**(7): p. 2316-2324.e1-3.

76. Hart, M.J., et al., *Downregulation of beta-catenin by human Axin and its association with the APC tumor suppressor, beta-catenin and GSK3 beta.* Curr Biol, 1998. **8**(10): p. 573-81.

77. Jho, E.H., et al., *Wnt/beta-catenin/Tcf signaling induces the transcription of Axin2, a negative regulator of the signaling pathway.* Mol Cell Biol, 2002. **22**(4): p. 1172-83.

78. Kishida, M., et al., *Axin prevents Wnt-3a-induced accumulation of beta-catenin.* Oncogene, 1999. **18**(4): p. 979-85.

79. Kishida, S., et al., *Axin, a negative regulator of the wnt signaling pathway, directly interacts with adenomatous polyposis coli and regulates the stabilization of beta-catenin.* J Biol Chem, 1998. **273**(18): p. 10823-6.

80. Lim, X., et al., *Interfollicular epidermal stem cells self-renew via autocrine Wnt signaling.* Science, 2013. **342**(6163): p. 1226-30.

81. van Amerongen, R., A.N. Bowman, and R. Nusse, *Developmental stage and time dictate the fate of Wnt/β-catenin-responsive stem cells in the mammary gland.* Cell Stem Cell, 2012. **11**(3): p. 387-400.

82. Suzuki, A., et al., *Tbx3 controls the fate of hepatic progenitor cells in liver development by suppressing p19ARF expression.* Development, 2008. **135**(9): p. 1589-95.

83. Bossard, P. and K.S. Zaret, *Repressive and restrictive mesodermal interactions with gut endoderm: possible relation to Meckel's Diverticulum.* Development, 2000. **127**(22): p. 4915-23.

84. Gordillo, M., T. Evans, and V. Gouon-Evans, *Orchestrating liver development.* Development, 2015. **142**(12): p. 2094-108.

85. Gualdi, R., et al., *Hepatic specification of the gut endoderm in vitro: cell signaling and transcriptional control.* Genes Dev, 1996. **10**(13): p. 1670-82.

86. Shin, D. and S.P. Monga, *Cellular and molecular basis of liver development.* Compr Physiol, 2013. **3**(2): p. 799-815.

87. Collins, A.T., et al., *Prospective identification of tumorigenic prostate cancer stem cells.* Cancer Res, 2005. **65**(23): p. 10946-51.

88. O'Brien, C.A., et al., *A human colon cancer cell capable of initiating tumour growth in immunodeficient mice.* Nature, 2007. **445**(7123): p. 106-10.

89. Rountree, C.B., et al., *A CD133-expressing murine liver oval cell population with bilineage potential.* Stem Cells, 2007. **25**(10): p. 2419-29.

90. Rountree, C.B., et al., *Expansion of CD133-expressing liver cancer stem cells in liver-specific phosphatase and tensin homolog deleted on chromosome 10-deleted mice.* Stem Cells, 2009. **27**(2): p. 290-9.

91. Chaudhari, P., et al., *Expression kinetics of hepatic progenitor markers in cellular models of human liver development recapitulating hepatocyte and biliary cell fate commitment.* Exp Biol Med (Maywood), 2016. **241**(15): p. 1653-62.

92. Farinati, F., et al., *Diagnostic and prognostic role of alpha-fetoprotein in hepatocellular carcinoma: both or neither?* Am J Gastroenterol, 2006. **101**(3): p. 524-32.

93. Hua, M., et al., *Molecular mechanisms regulating the establishment of hepatocyte polarity during human hepatic progenitor cell differentiation into a functional hepatocyte-like phenotype.* J Cell Sci, 2012. **125**(Pt 23): p. 5800-10.

94. Saxena, R. and N. Theise, *Canals of Hering: recent insights and current knowledge.* Semin Liver Dis, 2004. **24**(1): p. 43-8.

95. Shiojiri, N., *Enzymo- and immunocytochemical analyses of the differentiation of liver cells in the prenatal mouse.* J Embryol Exp Morphol, 1981. **62**: p. 139-52.

96. Spear, B.T., et al., *Transcriptional control in the mammalian liver: liver development, perinatal repression, and zonal gene regulation.* Cell Mol Life Sci, 2006. **63**(24): p. 2922-38.

97. Wang, P., et al., *Promoter-defined isolation and identification of hepatic progenitor cells from the human fetal liver.* Histochem Cell Biol, 2008. **130**(2): p. 375-85.

98. González, B., et al., *EpCAM is involved in maintenance of the murine embryonic stem cell phenotype.* Stem Cells, 2009. **27**(8): p. 1782-91.

99. Maetzel, D., et al., *Nuclear signalling by tumour-associated antigen EpCAM.* Nat Cell Biol, 2009. **11**(2): p. 162-71.

100. Münz, M., et al., *The carcinoma-associated antigen EpCAM upregulates c-myc and induces cell proliferation.* Oncogene, 2004. **23**(34): p. 5748-58.

101. Schmelzer, E., et al., *Human hepatic stem cells from fetal and postnatal donors.* J Exp Med, 2007. **204**(8): p. 1973-87.

102. Yoon, S.M., et al., *Epithelial cell adhesion molecule (EpCAM) marks hepatocytes newly derived from stem/progenitor cells in humans.* Hepatology, 2011. **53**(3): p. 964-73.

103. Yovchev, M.I., et al., *Identification of adult hepatic progenitor cells capable of repopulating injured rat liver.* Hepatology, 2008. **47**(2): p. 636-47.

104. Zhang, L., et al., *The stem cell niche of human livers: symmetry between development and regeneration.* Hepatology, 2008. **48**(5): p. 1598-607.

105. Weigmann, A., et al., *Prominin, a novel microvilli-specific polytopic membrane protein of the apical surface of epithelial cells, is targeted to plasmalemmal protrusions of non-epithelial cells.* Proc Natl Acad Sci U S A, 1997. **94**(23): p. 12425-30.

106. Fargeas, C.A., D. Corbeil, and W.B. Huttner, *AC133 antigen, CD133, prominin-1, prominin-2, etc.: prominin family gene products in need of a rational nomenclature.* Stem Cells, 2003. **21**(4): p. 506-8.

107. Uchida, N., et al., *Direct isolation of human central nervous system stem cells.* Proc Natl Acad Sci U S A, 2000. **97**(26): p. 14720-5.

108. Corbeil, D., et al., *The human AC133 hematopoietic stem cell antigen is also expressed in epithelial cells and targeted to plasma membrane protrusions.* J Biol Chem, 2000. **275**(8): p. 5512-20.

109. Torrente, Y., et al., *Human circulating AC133(+) stem cells restore dystrophin expression and ameliorate function in dystrophic skeletal muscle.* J Clin Invest, 2004. **114**(2): p. 182-95.

110. Shmelkov, S.V., et al., *CD133 expression is not restricted to stem cells, and both CD133+ and CD133- metastatic colon cancer cells initiate tumors.* J Clin Invest, 2008. **118**(6): p. 2111-20.

111. Li, Z., *CD133: a stem cell biomarker and beyond.* Exp Hematol Oncol, 2013. **2**(1): p. 17.

112. Shmelkov, S.V., et al., *AC133/CD133/Prominin-1.* Int J Biochem Cell Biol, 2005. **37**(4): p. 715-9.

113. Bhatia, M., *AC133 expression in human stem cells.* Leukemia, 2001. **15**(11): p. 1685-8.

114. Maw, M.A., et al., *A frameshift mutation in prominin (mouse)-like 1 causes human retinal degeneration.* Hum Mol Genet, 2000. **9**(1): p. 27-34.

115. Miraglia, S., et al., *A novel five-transmembrane hematopoietic stem cell antigen: isolation, characterization, and molecular cloning.* Blood, 1997. **90**(12): p. 5013-21.

116. Corbeil, D., et al., *Prominin-1: a distinct cholesterol-binding membrane protein and the organisation of the apical plasma membrane of epithelial cells.* Subcell Biochem, 2010. **51**: p. 399-423.

117. Bourseau-Guilmain, E., et al., *The importance of the stem cell marker prominin-1/CD133 in the uptake of transferrin and in iron metabolism in human colon cancer Caco-2 cells.* PLoS One, 2011. **6**(9): p. e25515.

118. Chen, H., et al., *CD133/prominin-1-mediated autophagy and glucose uptake beneficial for hepatoma cell survival.* PLoS One, 2013. **8**(2): p. e56878.

119. Kwee, S.A., et al., *Choline kinase alpha and hexokinase-2 protein expression in hepatocellular carcinoma: association with survival.* PLoS One, 2012. **7**(10): p. e46591.

120. Lyshchik, A., et al., *Expression of glucose transporter-1, hexokinase-II, proliferating cell nuclear antigen and survival of patients with pancreatic cancer.* Cancer Invest, 2007. **25**(3): p. 154-62.

121. McLeod, J.F. and N.E. Cooke, *The vitamin D-binding protein, alpha-fetoprotein, albumin multigene family: detection of transcripts in multiple tissues.* J Biol Chem, 1989. **264**(36): p. 21760-9.

122. Luft, A.J. and F.L. Lorscheider, *Structural analysis of human and bovine alpha-fetoprotein by electron microscopy, image processing, and circular dichroism.* Biochemistry, 1983. **22**(25): p. 5978-81.

123. Yang, F., et al., *Evolutionary and structural relationships among the group-specific component, albumin and alpha-fetoprotein.* Nucleic Acids Res, 1985. **13**(22): p. 8007-17.

124. Petropoulos, C., et al., *alpha-Fetoprotein and albumin mRNA levels in liver regeneration and carcinogenesis.* J Biol Chem, 1983. **258**(8): p. 4901-6.

125. Petropoulos, C.J., et al., *Cell lineages in liver carcinogenesis: possible clues from studies of the distribution of alpha-fetoprotein RNA sequences in cell populations isolated from normal, regenerating, and preneoplastic rat livers.* Cancer Res, 1985. **45**(11 Pt 2): p. 5762-8.

126. Wan, Y.J. and J.Y. Chou, *Expression of the alpha-fetoprotein gene in adult rat liver.* Arch Biochem Biophys, 1989. **270**(1): p. 267-76.

127. Lemire, J.M. and N. Fausto, *Multiple alpha-fetoprotein RNAs in adult rat liver: cell type-specific expression and differential regulation.* Cancer Res, 1991. **51**(17): p. 4656-64.

128. Mizejewski, G.J., *Alpha-fetoprotein structure and function: relevance to isoforms, epitopes, and conformational variants.* Exp Biol Med (Maywood), 2001. **226**(5): p. 377-408.

129. Nikolić, J.A., et al., *Serum alpha-fetoprotein levels and microheterogeneity in patients with different liver diseases.* J Hepatol, 1990. **11**(2): p. 252-6.

130. Song, H., et al., *Mammalian Mst1 and Mst2 kinases play essential roles in organ size control and tumor suppression.* Proc Natl Acad Sci U S A, 2010. **107**(4): p. 1431-6.

131. Zhou, Y.M., et al., *Clinicopathologic characteristics of intrahepatic cholangiocarcinoma in patients with positive serum a-fetoprotein.* World J Gastroenterol, 2008. **14**(14): p. 2251-4.

132. Varshney, A., et al., *Alpha-fetoprotein as a prognostic marker in acute liver failure: a pilot study.* Trop Doct, 2017. **47**(3): p. 202-205.

133. Aoyagi, Y., T. Ikenaka, and F. Ichida, *alpha-Fetoprotein as a carrier protein in plasma and its bilirubin-binding ability.* Cancer Res, 1979. **39**(9): p. 3571-4.

134. Benassayag, C., et al., *High affinity of nonesterified polyunsaturated fatty acids for rat alpha-fetoprotein (AFP).* Oncodev Biol Med, 1980. **1**(1): p. 27-36.

135. Hong, H., et al., *Rat α-Fetoprotein binding affinities of a large set of structurally diverse chemicals elucidated the relationships between structures and binding affinities.* Chem Res Toxicol, 2012. **25**(11): p. 2553-66.

136. Uriel, J., et al., *Alpha-fetoprotein: the major high-affinity estrogen binder in rat uterine cytosols.* Proc Natl Acad Sci U S A, 1976. **73**(5): p. 1452-6.

137. Wu, J.T., S.M. Monir-Vaghefi, and F. Clayton, *Human alpha-fetoprotein and albumin: differences in zinc binding.* Clin Physiol Biochem, 1987. **5**(2): p. 85-94.

138. Wang, X.W. and B. Xu, *Stimulation of tumor-cell growth by alpha-fetoprotein.* Int J Cancer, 1998. **75**(4): p. 596-9.

139. Butterfield, L.H., et al., *Generation of human T-cell responses to an HLA-A2.1-restricted peptide epitope derived from alpha-fetoprotein.* Cancer Res, 1999. **59**(13): p. 3134-42.

140. Mizejewski, G.J., *The phylogeny of alpha-fetoprotein in vertebrates: survey of biochemical and physiological data.* Crit Rev Eukaryot Gene Expr, 1995. **5**(3-4): p. 281-316.

141. Mizejewski, G.J., *alpha-fetoprotein as a biologic response modifier: relevance to domain and subdomain structure.* Proc Soc Exp Biol Med, 1997. **215**(4): p. 333-62.

142. Feldman, N.B., et al., *Antitumor activity of alpha-fetoprotein conjugate with doxorubicin in vitro and in vivo.* Biochemistry (Mosc), 2000. **65**(8): p. 967-71.

143. Ohkawa, K., et al., *Selective in vitro and in vivo growth inhibition against human yolk sac tumor cell lines by purified antibody against human alpha-fetoprotein conjugated with mitomycin C via human serum albumin.* Cancer Immunol Immunother, 1986. **23**(2): p. 81-6.

144. Severin, S.E., et al., *Alpha-fetoprotein-mediated targeting of anti-cancer drugs to tumor cells in vitro.* Biochem Mol Biol Int, 1995. **37**(2): p. 385-92.

145. Tomasi, T.B., Jr., *Structure and function of alpha-fetoprotein.* Annu Rev Med, 1977. **28**: p. 453-65.

146. Yachnin, S., *The clinical significance of human alpha-fetoprotein.* Ann Clin Lab Sci, 1978. **8**(2): p. 84-90.

147. Soltani, K., *Alpha-fetoprotein: a review.* J Invest Dermatol, 1979. **72**(5): p. 211-3.

148. Linnenbach, A.J., et al., *Sequence investigation of the major gastrointestinal tumor-associated antigen gene family, GA733.* Proc Natl Acad Sci U S A, 1989. **86**(1): p. 27-31.

149. Schnell, U., V. Cirulli, and B.N. Giepmans, *EpCAM: structure and function in health and disease.* Biochim Biophys Acta, 2013. **1828**(8): p. 1989-2001.

150. Szala, S., et al., *Molecular cloning of cDNA for the human tumor-associated antigen CO-029 and identification of related transmembrane antigens.* Proc Natl Acad Sci U S A, 1990. **87**(17): p. 6833-7.

151. Strnad, J., et al., *Molecular cloning and characterization of a human adenocarcinoma/epithelial cell surface antigen complementary DNA.* Cancer Res, 1989. **49**(2): p. 314-7.

152. Schön, M.P., et al., *Biochemical and immunological characterization of the human carcinoma-associated antigen MH 99/KS 1/4.* Int J Cancer, 1993. **55**(6): p. 988-95.

153. Thampoe, I.J., J.S. Ng, and K.O. Lloyd, *Biochemical analysis of a human epithelial surface antigen: differential cell expression and processing.* Arch Biochem Biophys, 1988. **267**(1): p. 342-52.

154. Balzar, M., et al., *The biology of the 17-1A antigen (Ep-CAM).* J Mol Med (Berl), 1999. **77**(10): p. 699-712.

155. Ng, V.Y., et al., *Characterization of epithelial cell adhesion molecule as a surface marker on undifferentiated human embryonic stem cells.* Stem Cells, 2010. **28**(1): p. 29-35.

156. Sundberg, M., et al., *CD marker expression profiles of human embryonic stem cells and their neural derivatives, determined using flow-cytometric analysis, reveal a novel CD marker for exclusion of pluripotent stem cells.* Stem Cell Res, 2009. **2**(2): p. 113-24.

157. Momburg, F., et al., *Immunohistochemical study of the expression of a Mr 34,000 human epithelium-specific surface glycoprotein in normal and malignant tissues.* Cancer Res, 1987. **47**(11): p. 2883-91.

158. Stingl, J., et al., *Characterization of bipotent mammary epithelial progenitor cells in normal adult human breast tissue.* Breast Cancer Res Treat, 2001. **67**(2): p. 93-109.

159. Borkowski, T.A., et al., *Expression of gp40, the murine homologue of human epithelial cell adhesion molecule (Ep-CAM), by murine dendritic cells.* Eur J Immunol, 1996. **26**(1): p. 110-4.

160. Nelson, A.J., et al., *The murine homolog of human Ep-CAM, a homotypic adhesion molecule, is expressed by thymocytes and thymic epithelial cells.* Eur J Immunol, 1996. **26**(2): p. 401-8.

161. Chen, G., et al., *EpCAM is essential for maintenance of the small intestinal epithelium architecture via regulation of the expression and localization of proteins that compose adherens junctions.* Int J Mol Med, 2021. **47**(2): p. 621-632.

162. Litvinov, S.V., et al., *Epithelial cell adhesion molecule (Ep-CAM) modulates cell-cell interactions mediated by classic cadherins.* J Cell Biol, 1997. **139**(5): p. 1337-48.

163. Litvinov, S.V., et al., *Ep-CAM: a human epithelial antigen is a homophilic cell-cell adhesion molecule.* J Cell Biol, 1994. **125**(2): p. 437-46.

164. Chaves-Pérez, A., et al., *EpCAM regulates cell cycle progression via control of cyclin D1 expression.* Oncogene, 2013. **32**(5): p. 641-50.

165. Osta, W.A., et al., *EpCAM is overexpressed in breast cancer and is a potential target for breast cancer gene therapy.* Cancer Res, 2004. **64**(16): p. 5818-24.

166. Wenqi, D., et al., *EpCAM is overexpressed in gastric cancer and its downregulation suppresses proliferation of gastric cancer.* J Cancer Res Clin Oncol, 2009. **135**(9): p. 1277-85.

167. Münz, M., R. Zeidler, and O. Gires, *The tumour-associated antigen EpCAM upregulates the fatty acid binding protein E-FABP.* Cancer Lett, 2005. **225**(1): p. 151-7.

168. Justice, R.W., et al., *The Drosophila tumor suppressor gene warts encodes a homolog of human myotonic dystrophy kinase and is required for the control of cell shape and proliferation.* Genes Dev, 1995. **9**(5): p. 534-46.

169. Xu, T., et al., *Identifying tumor suppressors in genetic mosaics: the Drosophila lats gene encodes a putative protein kinase.* Development, 1995. **121**(4): p. 1053-63.

170. Lee, H., et al., *The Hippo Pathway Is Essential for Maintenance of Apicobasal Polarity in the Growing Intestine of Caenorhabditis elegans.* Genetics, 2019. **213**(2): p. 501-515.

171. Graves, J.D., et al., *Caspase-mediated activation and induction of apoptosis by the mammalian Ste20-like kinase Mst1.* Embo j, 1998. **17**(8): p. 2224-34.

172. Lee, K.K. and S. Yonehara, *Phosphorylation and dimerization regulate nucleocytoplasmic shuttling of mammalian STE20-like kinase (MST).* J Biol Chem, 2002. **277**(14): p. 12351-8.

173. Lu, L., et al., *Hippo signaling is a potent in vivo growth and tumor suppressor pathway in the mammalian liver.* Proc Natl Acad Sci U S A, 2010. **107**(4): p. 1437-42.

174. Zhou, D., et al., *Mst1 and Mst2 maintain hepatocyte quiescence and suppress hepatocellular carcinoma development through inactivation of the Yap1 oncogene.* Cancer Cell, 2009. **16**(5): p. 425-38.

175. Bae, S.J., et al., *SAV1 promotes Hippo kinase activation through antagonizing the PP2A phosphatase STRIPAK.* Elife, 2017. **6**.

176. Callus, B.A., A.M. Verhagen, and D.L. Vaux, *Association of mammalian sterile twenty kinases, Mst1 and Mst2, with hSalvador via C-terminal coiled-coil domains, leads to its stabilization and phosphorylation.* Febs j, 2006. **273**(18): p. 4264-76.

177. Lee, J.H., et al., *A crucial role of WW45 in developing epithelial tissues in the mouse.* Embo j, 2008. **27**(8): p. 1231-42.

178. Chan, E.H., et al., *The Ste20-like kinase Mst2 activates the human large tumor suppressor kinase Lats1.* Oncogene, 2005. **24**(12): p. 2076-86.

179. Chow, A., Y. Hao, and X. Yang, *Molecular characterization of human homologs of yeast MOB1.* Int J Cancer, 2010. **126**(9): p. 2079-89.

180. Praskova, M., F. Xia, and J. Avruch, *MOBKL1A/MOBKL1B phosphorylation by MST1 and MST2 inhibits cell proliferation.* Curr Biol, 2008. **18**(5): p. 311-21.

181. Zhao, B., et al., *Inactivation of YAP oncoprotein by the Hippo pathway is involved in cell contact inhibition and tissue growth control.* Genes Dev, 2007. **21**(21): p. 2747-61.

182. Goulev, Y., et al., *SCALLOPED interacts with YORKIE, the nuclear effector of the hippo tumor-suppressor pathway in Drosophila.* Curr Biol, 2008. **18**(6): p. 435-41.

183. Wu, S., et al., *The TEAD/TEF family protein Scalloped mediates transcriptional output of the Hippo growth-regulatory pathway.* Dev Cell, 2008. **14**(3): p. 388-98.

184. Zhao, B., et al., *Both TEAD-binding and WW domains are required for the growth stimulation and oncogenic transformation activity of yes-associated protein.* Cancer Res, 2009. **69**(3): p. 1089-98.

185. Zhao, B., et al., *TEAD mediates YAP-dependent gene induction and growth control.* Genes Dev, 2008. **22**(14): p. 1962-71.

186. Yimlamai, D., et al., *Hippo pathway activity influences liver cell fate.* Cell, 2014. **157**(6): p. 1324-1338.

187. Heallen, T., et al., *Hippo pathway inhibits Wnt signaling to restrain cardiomyocyte proliferation and heart size.* Science, 2011. **332**(6028): p. 458-61.

188. von Gise, A., et al., *YAP1, the nuclear target of Hippo signaling, stimulates heart growth through cardiomyocyte proliferation but not hypertrophy.* Proc Natl Acad Sci U S A, 2012. **109**(7): p. 2394-9.

189. Yimlamai, D., B.H. Fowl, and F.D. Camargo, *Emerging evidence on the role of the Hippo/YAP pathway in liver physiology and cancer.* J Hepatol, 2015. **63**(6): p. 1491-501.

190. Lavado, A., et al., *Tumor suppressor Nf2 limits expansion of the neural progenitor pool by inhibiting Yap/Taz transcriptional coactivators.* Development, 2013. **140**(16): p. 3323-34.

191. Zhang, H., et al., *Negative regulation of Yap during neuronal differentiation.* Dev Biol, 2012. **361**(1): p. 103-15.

192. Elbediwy, A., et al., *Integrin signalling regulates YAP and TAZ to control skin homeostasis.* Development, 2016. **143**(10): p. 1674-87.

193. Aylon, Y., et al., *The LATS2 tumor suppressor inhibits SREBP and suppresses hepatic cholesterol accumulation.* Genes Dev, 2016. **30**(7): p. 786-97.

194. Koo, J.H. and K.L. Guan, *Interplay between YAP/TAZ and Metabolism.* Cell Metab, 2018. **28**(2): p. 196-206.

195. Rudnick, D.A. and N.O. Davidson, *Functional Relationships between Lipid Metabolism and Liver Regeneration.* Int J Hepatol, 2012. **2012**: p. 549241.

196. Sakakura, Y., et al., *Sterol regulatory element-binding proteins induce an entire pathway of cholesterol synthesis.* Biochem Biophys Res Commun, 2001. **286**(1): p. 176-83.

197. Fitamant, J., et al., *YAP Inhibition Restores Hepatocyte Differentiation in Advanced HCC, Leading to Tumor Regression.* Cell Rep, 2015. **10**(10): p. 1692-1707.

198. Mo, J.S., H.W. Park, and K.L. Guan, *The Hippo signaling pathway in stem cell biology and cancer.* EMBO Rep, 2014. **15**(6): p. 642-56.

199. Gholipour, M. and A. Tabrizi, *The role of Hippo signaling pathway in physiological cardiac hypertrophy.* Bioimpacts, 2020. **10**(4): p. 251-257.

200. Han, S.X., et al., *Expression and clinical significance of YAP, TAZ, and AREG in hepatocellular carcinoma.* J Immunol Res, 2014. **2014**: p. 261365.

201. Kim, G.J., H. Kim, and Y.N. Park, *Increased expression of Yes-associated protein 1 in hepatocellular carcinoma with stemness and combined hepatocellular-cholangiocarcinoma.* PLoS One, 2013. **8**(9): p. e75449.

202. Xu, M.Z., et al., *Yes-associated protein is an independent prognostic marker in hepatocellular carcinoma.* Cancer, 2009. **115**(19): p. 4576-85.

203. Yang, S., et al., *Active YAP promotes pancreatic cancer cell motility, invasion and tumorigenesis in a mitotic phosphorylation-dependent manner through LPAR3.* Oncotarget, 2015. **6**(34): p. 36019-31.

204. Zhang, W., et al., *Downstream of mutant KRAS, the transcription regulator YAP is essential for neoplastic progression to pancreatic ductal adenocarcinoma.* Sci Signal, 2014. **7**(324): p. ra42.

205. Chen, Y.L., et al., *The effects of the location of cancer stem cell marker CD133 on the prognosis of hepatocellular carcinoma patients.* BMC Cancer, 2017. **17**(1): p. 474.

206. Singh, S.K., et al., *Identification of human brain tumour initiating cells.* Nature, 2004. **432**(7015): p. 396-401.

207. Kroepil, F., et al., *High EpCAM expression is linked to proliferation and lauren classification in gastric cancer.* BMC Res Notes, 2013. **6**: p. 253.

208. Pan, M., et al., *EpCAM ectodomain EpEX is a ligand of EGFR that counteracts EGF-mediated epithelial-mesenchymal transition through modulation of phospho-ERK1/2 in head and neck cancers.* PLoS Biol, 2018. **16**(9): p. e2006624.

209. Went, P.T., et al., *Frequent EpCam protein expression in human carcinomas.* Hum Pathol, 2004. **35**(1): p. 122-8.

210. Jiang, N., et al., *YAP1 regulates prostate cancer stem cell-like characteristics to promote castration resistant growth.* Oncotarget, 2017. **8**(70): p. 115054-115067.

211. Yang, K., et al., *Evaluation of Hippo Pathway and CD133 in Radiation Resistance in Small-Cell Lung Cancer.* J Oncol, 2021. **2021**: p. 8842554.

212. Wang, Y.P. and D.X. Tang, *Expression of Yes-associated protein in liver cancer and its correlation with clinicopathological features and prognosis of liver cancer patients.* Int J Clin Exp Med, 2015. **8**(1): p. 1080-6.

213. Patel, S.H., F.D. Camargo, and D. Yimlamai, *Hippo Signaling in the Liver Regulates Organ Size, Cell Fate, and Carcinogenesis.* Gastroenterology, 2017. **152**(3): p. 533-545.

214. Nakayama, H., et al., *Developmental restriction of Mash-2 expression in trophoblast correlates with potential activation of the notch-2 pathway.* Dev Genet, 1997. **21**(1): p. 21-30.

215. Ang, C.H., et al., *Lgr5(+) pericentral hepatocytes are self-maintained in normal liver regeneration and susceptible to hepatocarcinogenesis.* Proc Natl Acad Sci U S A, 2019. **116**(39): p. 19530-19540.

216. Planas-Paz, L., et al., *The RSPO-LGR4/5-ZNRF3/RNF43 module controls liver zonation and size.* Nat Cell Biol, 2016. **18**(5): p. 467-79.

217. Sun, T., et al., *AXIN2(+) Pericentral Hepatocytes Have Limited Contributions to Liver Homeostasis and Regeneration.* Cell Stem Cell, 2020. **26**(1): p. 97-107.e6.

218. Dong, J., et al., *Elucidation of a universal size-control mechanism in Drosophila and mammals.* Cell, 2007. **130**(6): p. 1120-33.

219. Li, H., et al., *Deregulation of Hippo kinase signalling in human hepatic malignancies.* Liver Int, 2012. **32**(1): p. 38-47.

220. Perra, A., et al., *YAP activation is an early event and a potential therapeutic target in liver cancer development.* J Hepatol, 2014. **61**(5): p. 1088-96.

221. Zender, L., et al., *Identification and validation of oncogenes in liver cancer using an integrative oncogenomic approach.* Cell, 2006. **125**(7): p. 1253-67.